The Development of a Nucleic Acid-Directed Switch and Proximity Dependent Protein Assays Using Electrochemical Techniques

by

Katarena Isabella Ford

A dissertation submitted to the Graduate Faculty of
Auburn University
in partial fulfillment of the
requirements for the Degree of
Doctor of Philosophy

Auburn, Alabama
December 15, 2018

Keywords: Proximity effect, Immunoassay, Electrochemical detection, Obesity

Approved by

Christopher J. Easley, C. Harry Knowles Professor of Chemistry & Biochemistry
Curtis Shannon, Andrew T. Hunt Professor and Chairman of Chemistry and Biochemistry
Holly Ellis, William P. Molette Professor of Chemistry & Biochemistry
Wei Zhan, Associate Professor of Chemistry & Biochemistry

Abstract

The analysis of nucleic acids (NA), has increased demand for point-of-care systems, such as rapid preventive health care, forensic applications, etc. Thus inspired, a vast amount of biosensor platforms for the detection of nucleic acids. These platforms are typically recognized via optical readouts such as fluorescence, molecular beacons, polymerase chain reaction (PCR), colorimetric analysis, and more. Although these methods are sensitive and effective, the instrumental availability and reagent consumption can make the overall experience challenging. Electrochemical sensors have received considerable attention due to their rapid response, affordability, minute structure, and remarkable sensitivity. This dissertation focuses on the development of DNA-based electrochemical methods toward an effective drop-and-read quantification of various biomarkers, such as small DNA, RNA, and proteins.

Chapter 1 introduces background research, focusing on diabetes and obesity, functional tissue (adipose tissue) and miRNA, immunoassay development using both tube assay methodologies and conventional electrochemical DNA-based biomarker detection.

In chapter 2 we take advantage of important concepts such as the proximity effect to develop proximity ligation assay (PLA) for the adipose-secreted protein, adiponectin; this protein is important indicator for diabetes, obesity, and metabolic syndrome. PLA is a DNA-based immunoassay, which utilizes polymerase chain reaction (PCR) to amplify overall signal. With this assay, we gained insight to the complexity and significance of adiponectin.

Chapter 3 led us on a different path, to utilize electrochemical detection methods to detect PLA products as a non-optical method. We conducted an important study to evaluate the distance dependence of the placement of our redox-tagged DNA strand with respect to the electrode surface via square wave voltammetry (SWV). This focused on the understanding of surface hybridization, and its effects on electrochemical kinetics which offered a different outlook on interpreting SWV signal and the efficiency of SWV frequency, which is useful for any electrochemical DNA-based sensor.

In chapter 4, we designed an electrochemical nucleic acid quantification method labeled as the electrochemical bistable switch sensor (E-BSS). This novel assay is based on a nucleic acid hybridized-driven system that incorporates strand displacement mechanisms for short oligonucleotides (~22 nt). DNA and RNA, specifically miRNA was successfully detected and quantified in complex matrices. In addition to reduce sample volume (2 µL), we used polydimethylsiloxane (PDMS) electrochemical cells fabricated from 3D-printed polylactic acid molds. This electrochemical system paves the way for future proximity-driven protein assays that could potentially take advantage of our bistable switch-based strand displacement reactions.

Chapter 5 reintroduces the electrochemical proximity assay (ECPA) which is a sensitive protein detection method developed in Dr. Shannon and Dr. Easley's' lab. We have completed studies that can support the development and quantification of biologically relevant molecules. We discuss the importance of ECPA sensing complex which is currently made of six components undergoing non-covalent binding (DNA hybridization and antigen-antibody interactions). The main focus in this chapter is to reduce the current of the background signal and

to reduce the components of the system to a 4-part complex. This, in turn, should create a signal-OFF based assay that is proportional to the target concentration due to the molecular weight change.

Acknowledgments

I would like to start off by saying thank you to Dr. Christopher J. Easley for his guidance, support, and believing in my abilities. Also, I would like to thank him for introducing me to a new form and outlook of chemistry. I will carry this experience throughout my journey in life. To my committee members, Drs. Zhan, Shannon, and Ellis, thank you for your time, availability, and efforts during my time here at Auburn University. Thanks go to my past and present lab mates, Dr. Joonyul Kim, Dr. Cheryl DeJournette, Dr. Jessica Brooks, Dr. Jean Negou, Dr. Xiangpeng Li, Mark Holtan, Niamat Khuda, for your guidance, conversations, and simply for being great colleagues. An added special thanks goes to my senior graduate student who trained me on many aspects of this thesis work, Dr. Subramanian Somasundaram. I really appreciate Dr. Juan Hu's continuous help and support, without you I would have lost my marbles many moons ago, you have become a life-long friend. Best of luck to the other and new coming members in Dr. Easley's laboratory.

I would like to give a special thanks to my university reader Dr. Overtoun Jenda, the NSF LSAMP Bridge to Doctorate Fellowship Program, and the President's Graduate Opportunity Program (PGOP) for providing additional funding for my duration in the Department of Chemistry and Biochemistry. Dr. Kimberly Mulligan thank you for your encouragement and support over the years. I would like to express my deepest gratitude to the National Organization for the Professional Advancement of Black Chemists and Chemical Engineers and the Black Graduate and Professional Student Association for providing tremendous support throughout my studies.

Their encouragement and understanding made this work possible. To my friends in the department and in the community, thank you, you made my time here well-spent. I owe gratitude for all my success and accomplishments to my mother, Angi King, and grandmother, Isabella King, and my sister, Mikayla King. Without them, I would not have even considered graduate school or strived to achieve my goals and dreams.

Lastly, but definitely my first priority, God granted me the serenity to accept the things that I could not change; He gave me the courage to change the things I could; and wisdom to know the difference. Without this prayer and His guidance, I would not have made it through graduate school.

Amen.

Table of Contents

List of Figures

List of Tables

Chapter 1

Introduction

1.1 Endocrine Hormones

The endocrine system is a series of glands that secrete signals (hormones) that arrange a wide variety of bodily functions. These hormone molecules participate in feedback control of many processes within the body, thereby regulating internal systems.[1] There are a number of processes that the endocrine system helps to control, such as growth and development, metabolism, homeostasis, and responses to stimulus events that require a functional reaction, such as stress. The hormones are distributed throughout the body via the blood stream. Akin to the nervous system, the endocrine system is one of the body's main communicators, but instead of using the nerves to send information, the endocrine system utilizes blood vessels to deliver hormones to cells and tissues. The glands of the endocrine system include the hypothalamus, pineal gland, pituitary gland, thyroid, parathyroid, thymus, adrenal, pancreas, ovaries, testes, and more recently the adipose tissue.[2] These glands produce different types of hormones that stimulate a specific response in other cells, tissues, and/or organs[3].

In our laboratory, we are focused on the pancreatic and adipose tissues. Although it was not originally listed as an endocrine tissue, recent research has shown that adipose tissue is not just an inert storage depository for lipids but is, in fact, a major endocrine organ that plays a crucial role in controlling the body's energy via endocrine, metabolic, and inflammatory signals.[4]

The adipocyte, which the unit cell found in adipose tissue, has been proven to secrete a number of proteins. These secretory proteins have been named adipocytokines[4]. The pancreas is also distinct, because this organ can serve as both an endocrine and exocrine gland. Its main function, however, is within the endocrine system to keep the body's blood glucose in balance.[3] The major hormones secreted from the pancreas are insulin and glucagon, and they both regulate blood sugar levels.[5] Insulin signaling is also dominant throughout the body and has a strong effect on the function of adipose tissue.

1.1.1 Metabolic Syndrome

Metabolic diseases are disorders that disturb standard functions of the metabolism on a cellular level, which includes the process of extracting energy from food. There are many enzymes that participate in numerous co-dependent metabolic pathways that carry out the processes. Metabolic diseases have the capability to affect cells' abilities to complete vital biochemical reactions, particularly those that involve transportation hormones, carbohydrates, fatty acids, etc.[6] This led researchers to coin the term "metabolic syndrome" to describe a group of conditions such as increased blood pressure, high blood sugar, extra body fat, and high triglyceride levels. Metabolic syndrome can cause an increased risk that heart disease, stroke, diabetes, and obesity will occur in a patient over time[5]. Over the years, the concept of metabolic syndrome has been reinforced by reoccurrences of disrupted glucose metabolism, increased abdominal fat distribution, dyslipidemia, and hypertension in association with subsequent development of type 2 diabetes mellitus and cardiovascular disease, [7]. The World Health Organization (WHO) definition of the metabolic syndrome includes a body mass index (BMI) greater than 30 kg/m^2 [8]. One of the main causes of these disorders is considered to be insulin

resistance in peripheral tissues such as muscle or adipose tissue. Figure 1.1 shows a proposed model of metabolic syndrome and its components.

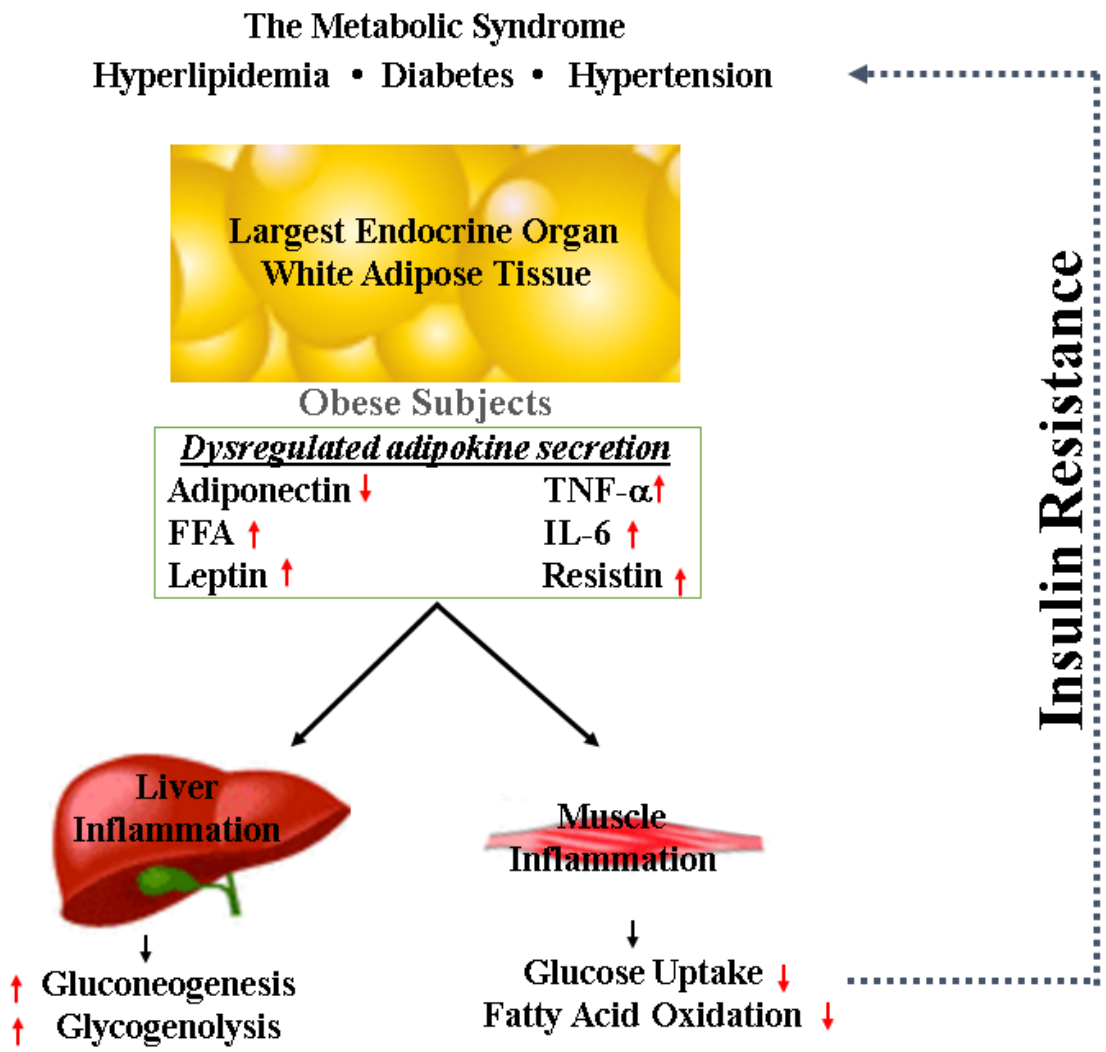

Figure 1.1: Concept of Metabolic Syndrome

1.1.2 Diabetes Mellitus

Diabetes mellitus is a disease state associated with metabolic syndrome; there are two types: Type 1 diabetes (T1D) and type 2 diabetes (T2D). T1D, also known as juvenile diabetes, is an autoimmune disease where the body's immune system attacks the cells that produce insulin (pancreatic β-cells). This can result in either no insulin or a very low amount of insulin being produced. Along with other nutrient signals following a meal, digestion of starches chiefly ends with a 6 carbon sugar, glucose, which stimulates insulin secretion from pancreatic β-cells. This insulin directs peripheral tissues to absorb consumed nutrients. Most people with type 1 diabetes mellitus must take exogenous insulin injections on a daily basis. Although this treatment is effective in a patient for decades, it is laborious and undesirable, thus the search for a more effective cure for the disease is ongoing. Recent advances in medicine, such as closed-loop insulin pumps, have promised to better treat the symptoms of the disease, [9]. Additionally, researchers continue to pursue pancreatic islet transplants as a possible long-term cure.

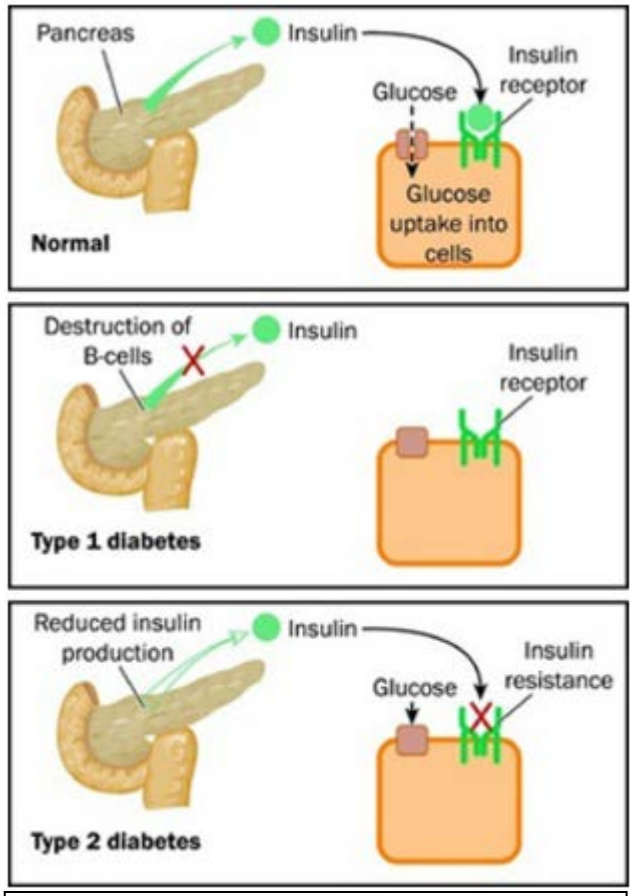

Figure 1.2: Depiction of Diabetes Mellitus with effects of insulin.[1] ***http://www.endocrineweb.com/endocrinology/overview-pancreas***

Type 2 diabetes mellitus is the most common type of diabetes. It has been described by the American diabetes association (ADA) as a "confusing entity"[10]. T2D is usually associated with insulin resistance and does not generally require insulin treatment for survival. Insulin resistance occurs when the action of insulin on its receptors in the muscle, liver, and fat begins to degrade. After rapid postprandial increases in blood sugar levels, insulin resistance can cause pancreatic islets to secrete more insulin than normally required, leading to hyperinsulinemia. Blood glucose levels will continue to rise, since insulin action on its receptors is reduced, leading to hyperglycemia and its damaging side effects. Also, type 2 diabetes has major ties with obesity, alongside insulin resistance. Usually, losing and maintaining a proper weight and BMI can reverse insulin resistance, and most patients' symptoms of diabetes can become dormant.

As of 2015, diabetes affected an estimated 415 million people worldwide and 44.3 million in North America and the Caribbean. The ADA has estimated the total medical costs of diabetes in America; by 2012, the cost had risen to an average of $245 billion[11]. From **Figure 1.3**, which shows the prevalence of diabetes broken down worldwide, it seems the disease has become more pronounced in the Western Pacific and South East Asia[12].

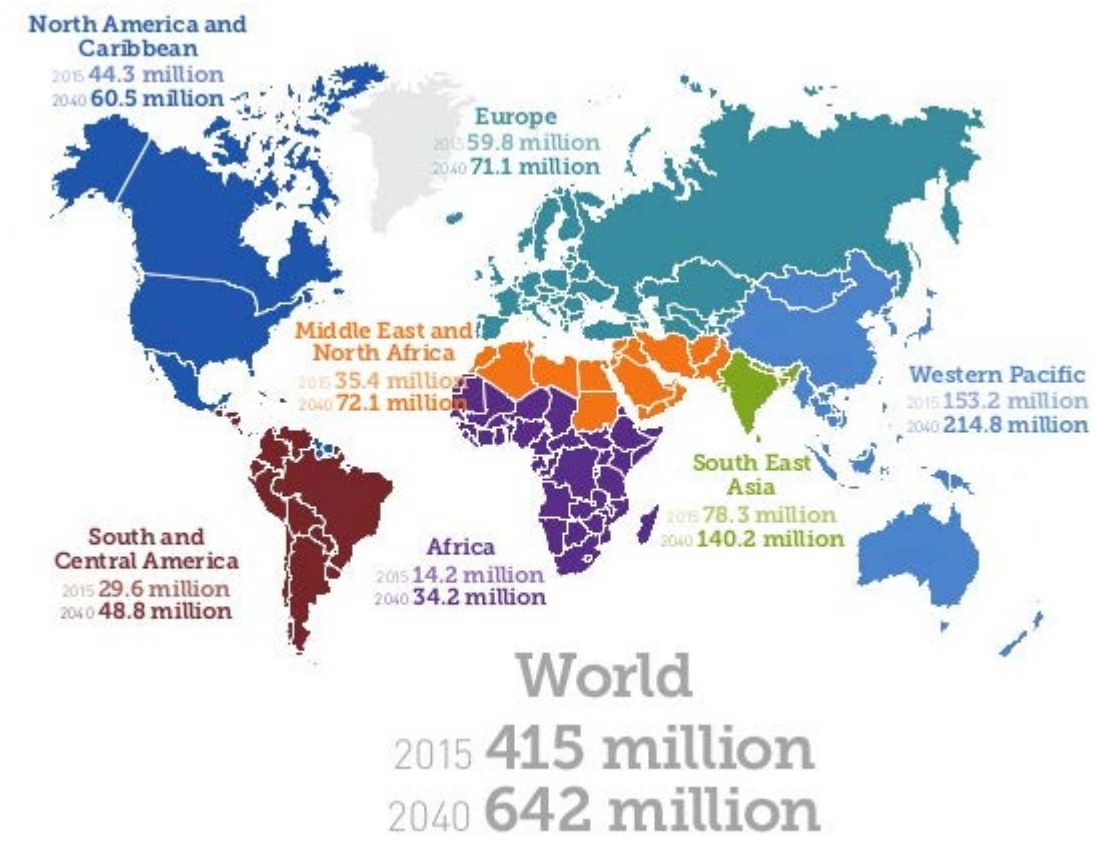

Figure 1.3: Map of the World, showing the number of people in the adult and youth populations diagnosed with diabetes in 2015.
http://onedrop.today/review-world-diabetes-congress-new-developments-december-1-5-2015/

Obesity as it Relates to Type 2 Diabetes

The specific influence of obesity on type 2 diabetes risk is determined by the degree of obesity and by where most of the fat accumulates. Obesity is described as a state of increased body weight of sufficient magnitude to produce adverse health consequences [13]. The increasing prevalence of obesity constitutes a major health problem in the United States, with more than two thirds of all adults currently overweight or obese. The percentage of overweight or obese adults in the United States increased from 45% in 1991 to 58% in 2001 [14]. According to the

ADA, more than 85% of all adult type 2 diabetic patients are classified as being either overweight or obese, with 55% of those patients obese. Fat accumulation in the upper body region, including visceral adiposity, as reflected in increased abdominal girth, is associated with metabolic syndrome, type 2 diabetes, and cardiovascular disease[16] , although the mechanisms remain uncertain. Beyond differences in body fat distribution, recent evidence suggests that different subtypes of adipose tissue may be functionally distinct and affect glucose homeostasis differentially. Adult humans tend to have fewer brown fat cells[17], which play a role in thermogenesis and potentially influence energy expenditure and obesity susceptibility[18]. As such, there is a pressing need to have a better understanding of the functions of the different types of fat cells and their roles in metabolic homeostasis. Projects outlined within this thesis are aimed at improving bioanalytical technology used to study adipose tissue function.

1.1.3 Adipose Tissue, Adipocytes, and Adiponectin

Adipose Tissue

Adipose tissue is a complex organ with major effects on physiology. In the late 1940s, adipose tissue was mainly considered as a form of connective. That view changed once scientist realized that adipose tissue played an active role in nutrient homeostasis, serving as the site of calorie storage (as triacylglycerol) after feeding and as the source of circulating free fatty acids during fasting. In the late 1980s to mid-1990s, researchers discovered adipose-derived serum factors like adiponectin, leptin, resistin, retinol-binding protein 4 (RBP4), TNF-α, and MCP1[19]. These adipocyte-derived factors are collectively referred to as "adipokines"[30]. Each of these adipokines help with whole-body energy homeostasis, yet the function of some is better defined than others. Adipose tissue has now been determined as an endocrine organ at the center of

energy homeostasis. The studies of adipose tissue have greatly increased in number, especially on the developmental, functional, and pathophysiological aspects and how it correlates with T2D[19].

There are two main types of adipose tissue, subcutaneous and visceral, each found in different locations of the body. Subcutaneous fat is located under the skin and makes up about 80% of all fat tissue, mostly located in the back and abdominal wall. Visceral fat covers the organs of the abdominal cavity and makes up 10–20% of fat in men and 5–8% in women. The tissue is made up mostly of cells known as adipocytes but also contains macrophages, fibroblasts, and endothelial cells, which is consistent with connective tissue[20–22].

Adipocytes and Targeted Adipokines

Adipocytes are highly specialized cells that play a crucial role in energy regulation and homeostasis [23]. There are two major types of adipocytes in humans. White adipocytes consist of one large lipid droplet that is involved in fat storage. Brown adipocytes have many smaller lipid droplets and a larger number of mitochondria that produce energy; these cells help maintain the body's temperature. Adipocytes consist of a nucleus, a storage area, and a cell membrane, and they typically range in size from 60 – 150 μm. In our laboratory, we focus on detection of adiponectin and leptin, as these two adipokine hormones have significant effects on glucose homeostasis, inflammation, and food intake. Leptin helps regulate body fat, in part by telling the brain what level of fat is in the body and how that level is changing. Adiponectin helps regulate glucose production as well as fatty acid oxidation in the muscles and in the liver. Both of these hormones are important indicators of metabolic dieses such as diabetes and obesity[24].

Adiponectin

Even though adipose tissue is widely known as the storage depot for excess energy, its role as an endocrine organ was not recognized until the discoveries of leptin and adiponectin in the mid-1990s. Since then, there have been hundreds of molecules that have been identified as being secreted from adipose tissue, and many of them play a major role in regulation of metabolism. Adiponectin is the most abundantly secreted protein from adipose tissue, accounting for up to 0.05% of total plasma proteins.[22] As a monomer, adiponectin is a ~30 kDa hormone secreted by the adipocyte. In the bloodstream, it takes on higher order structures including: 1) trimers of ~90 kDa 2) hexamers of ~180 kDa [low-molecular weight (LMW)] and 3) 12-18mers of greater than 300 kDa [high-molecular weight (HMW)][25]. **Figure 1.4** shows a depiction of the macromolecular structure of the hormone, which consists of an N-terminal collagen-like tail (shown in orange) and a C-terminal globular head (shown in blue) [26]. The higher order adiponectin complexes are linked together by disulfide bonds. The HMW multimers are considered the most biologically relevant because the adiponectin receptors are most sensitive to this form [20–22,25–30]. Females tend to have higher levels of circulating adiponectin than males; in fact, normal blood levels in women are nearly double at 13.5 ± 7.9 μg mL^{-1} than they are in men at 7.2 ± 4.6 μg mL^{-1}. Adiponectin levels can range from 0.55 – 30 μg mL^{129}, and studies have proven that levels are reduced in obese patients, a trend that has been linked to insulin resistance and hyperlipidemia[20,27,30]. In this thesis, adiponectin detection is our

primary focus due to the lack of tools to investigate the dynamics of adiponectin secretion in its multimeric forms.

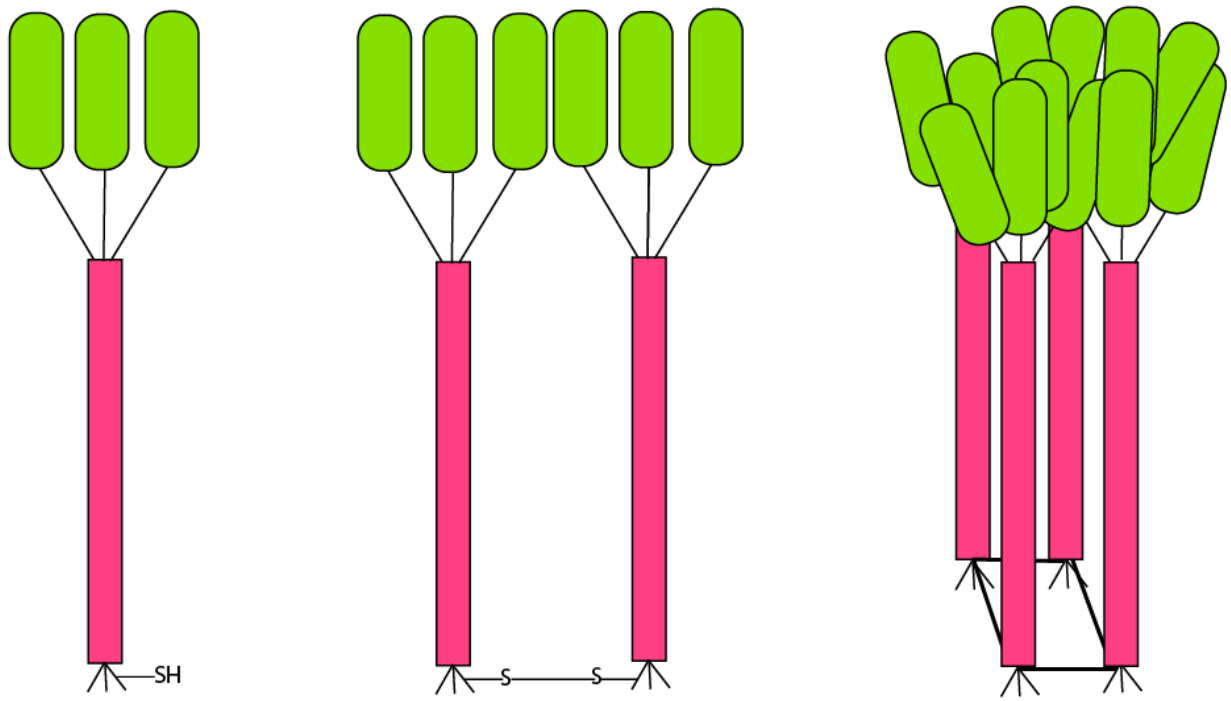

Figure 1.4: Different isoforms of adiponectin, which in the blood exists as trimers, hexamers, and higher molecular weight complexes. Linked by disulfide bridges, adiponectin consists of a globular C-terminal head (shown in green), and a collagen like N-terminal tail (shown in pink).

1.2 Immunoassays

1.2.1 Advances in Immunoassays

Methods used to detect proteins levels are of fundamental importance in biological fields. Technologies for protein separation, detection, and quantification have seen accelerated development with research into bioanalytical diagnostics. This vital step towards the development of chemical sensors includes identifying small concentrations of proteins that play

major roles in disease, as well as low-cost detection for researchers and clinicians, in turn benefitting patients. Needless to say, selection of an appropriate assay is crucial in determining the levels of protein in each sample and the overall success of one's research.

Enzyme-linked immunosorbent assay (ELISA)

The enzyme-linked immunosorbent assay developed by Engvall et al. remains the gold standard in protein quantification, and its inception established the widely quoted acronym, "ELISA." The assay typically uses IgG antibodies that are raised in animals[31,32]. The antibodies can either be monoclonal or polyclonal antibodies. In certain ELISAs, the researcher's primary antibody should be raised in an animal that is not the same from the sample of choice, followed by an anti-animal choice IgG secondary antibody, which is important for the primary and secondary antibody binding. The binding of the antigen and antibody is detected using an enzyme linked to a secondary antibody, which turns the antigen-antibody complex into a producer of colored product when the enzyme's substrate is added. ELISA is a highly useful method in detecting and quantifying proteins or antibodies, providing relatively fast, highly specific, and sensitive results. Essentially, ELISA has four concept steps made up of coating, blocking, reacting of antigen and antibody, and generating color. ELISA can be in either a competitive or non-competitive composition[33]. These two assays are used depending on the purpose of experiments and the types of antibodies and antigens.

Competitive ELISAs

The competitive ELISAs are also known as competitive inhibition ELISAs. The competitive assays implement two antigens, where one is coated on the microtiter plate and the

another is added in a sample solution containing a finite amount of primary antigen specific antibody which competes for binding to this antibody [33], as seen in **Figure 1.5A**. Technically, the primary antibody which is unlabeled, is incubated with the sample antigen, then the antibody-antigen complexes are added to a well plate, that has already been pre-coated. If there is any antibody that is not bound, it is removed by a series of washing steps. The more antigen that is in the sample, the less amount of antibody will bind to the antigen in the well, hence the term "competition". The next step is to add in a secondary antibody that is specific to the primary antibody and conjugated with an enzyme. The bound secondary antibody/enzyme will then react with the substrate that is added, and a specific color is generated. The intensity of the color is inversely proportional to the concentration of the antigens existing in the added sample. Competitive ELISAs are frequently used for antigen quantification and cross-reactivity testing of samples that are impure and crude, but samples can still give a significant signal. A downside to this assay is its fundamentally competitive nature. Typically, the sample being detected has only one epitope binding site, and the need for a competitive assay limits the ultimate sensitivity of the ELISA.

Non-competitive ELISAs

There are two types of non-competitive ELISAs: two-stage indirect ELISA and sandwich ELISA.

Two-stage indirect ELISA

This format is also called an antigen-coated ELISA. This is the simplest approach to ELISA, and is normally used for antibody quantification and not protein quantitation.

Essentially, a serial dilution of antigens is first coated on the solid phase of the microtiter plate by adsorption, followed by an incubation step with the primary antibodies, as shown in **Figure 1.5B**. The bound antigen-antibody (Ab-Ag) complexes are eventually detected by the addition of the secondary enzyme-conjugate antibodies that attach to the primary antibodies. Levels of enzyme-generated color are proportional to the concentration of the antigens in the sample, and the intensity can be measured by a microplate reader using visible absorbance at an appropriate wavelength[33]. The disadvantages of this assay include cross-reactivity that occurs with the secondary antibodies, which causes non-specific signaling, as well as the extra incubation steps that require more time to complete the assay.

Sandwich ELISA

The sandwich ELISA is the most commonly used analytical method for the detection and quantification of specific proteins [31–33]. There are two different types of sandwich ELISAs: 1) Indirect ELISA and 2) Direct ELISA. The sandwich ELISAs employ a pair of antibodies, one as the capture antibody and the other as the detector, directed against two or more distinct binding sites on antigens (epitopes), which makes the detection more specific against particular antigens. If we focus on the indirect ELISA, the capture antibodies are first coated on the microtiter plate. A series of dilutions of the antigens in the sample solution and antigen standards are added and captured by the antibodies on the surface. The bound antigens are then detected by adding a specific amount of detector antibodies, where the antigens get trapped, or sandwiched, in between the two antibodies. Multiple washing steps are performed in between each step in order to remove the extra unbound proteins and antibody probes. There is a direct relationship that exists between the concentration of the antigen-antibody and the intensity of the absorbance (or

fluorescence) signal (**Figure 1.5C**). One limitation of this type of ELISA come into view when we consider the proteins' epitopes, since finding two separate antibodies that can bind to both epitopes can be challenging. However, the major limitations of sandwich ELISAs are the high cost and assay times.

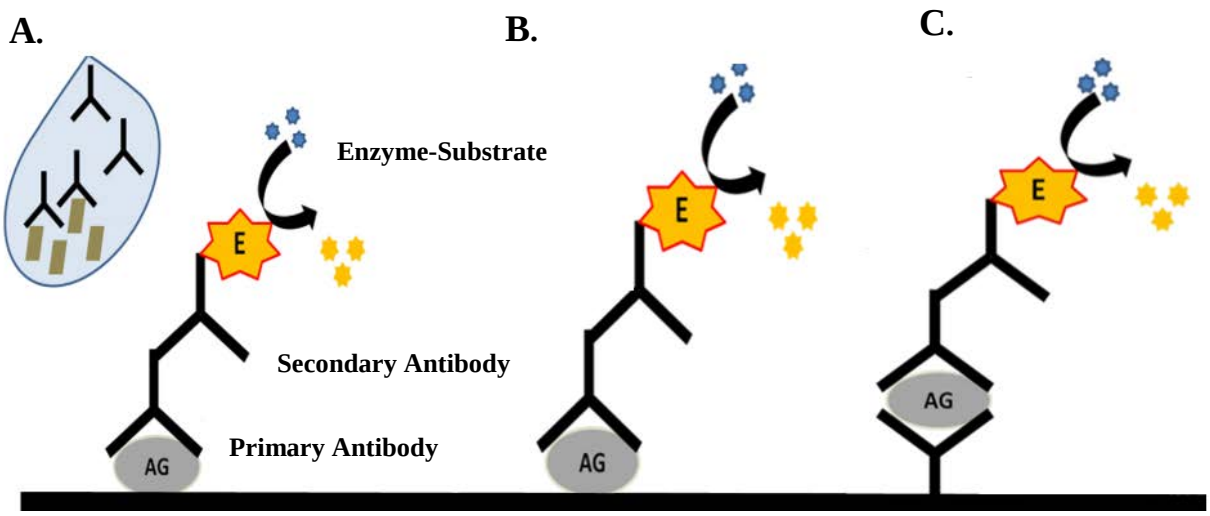

Figure 1.5: A) Competitive ELISA assay— Antigens in the solution compete for the antibodies binding with antigens coated on the plate. B) Two stage indirect ELISA assay—Multiple addition of antigen to plate and in mixed Ab-Ag solution C) Indirect Sandwich ELISA assay—1^{o} antibody used to anchor antigen followed by a series of 2^{o} antibodies (unlabeled and labeled)

1.2.2 Proximity Assays

When reporting major advances in immunoassays, one must consider the development of proximity assays. Even though ELISAs are well-developed methods for protein detection, the disadvantages often outweigh the advantages. Developed as an improved alternative to ELISA, proximity immunoassays have two major characteristics: 1) two probes bind to an antigen at different epitopes; and 2) the signal is based on the proximity connection between the two probes. Thus, the methods maintain the benefits of dual antibody target recognition, which was

used in both Western blotting and sandwich ELISAs. Three major proximity immunoassays have found success in today's immunoassay field: (1) Proximity Ligation Assay (PLA), (2) Molecular Pincers, and (3) Proximity Extension Assay (PEA).

The Proximity Effect

The proximity effect was nicely explained in a review article by Prof. X. Chris Le and his team from the University of Alberta [34]. Most proximity assays have three main distinguishable features: amplifiable DNA attached to antibodies can allow detection proteins; specificity is increased because the affinity binding helps the assembly of DNA that has two or more probes to one target; and the assays are homogeneous (no washing steps), which makes it simple for point-of-care applications. **Figure 1.6A** shows an illustration of the local concentration effect that is key to all proximity assays. If we consider binding of the two antibodies to the target molecule, this brings the two oligonucleotides to the same target with a typical intramolecular distance that is drastically decreased. These oligonucleotides now have local concentrations much greater than before[34]. The image shows a ~400,000-fold increase in local concentration which enhances the thermodynamic stability of the hybridization between the DNA strands. This local concentration increase only occurs for the DNA probes bound to the target, while the concentrations of the unbound DNA probes are not affected.[34] Importantly, this proximity effect allows DNA-conjugated antibodies to effectively serve as analyte-dependent switches that quantitatively report the presence of the analyte. One of the various methods used to quantify DNA hybridization can now be applied to protein detection.

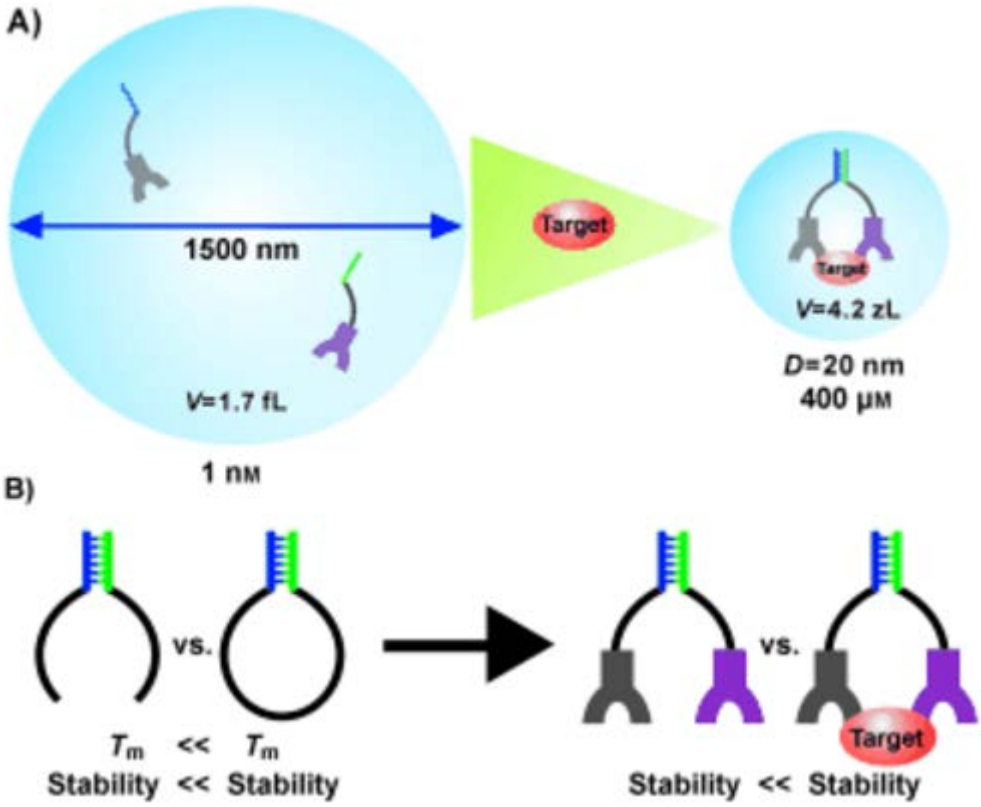

Figure 1.6: A) Proximity Effect: binding of a target molecule to oligonucleotides drastically increases the local concentrations of the oligonucleotides. B) shows the intermolecular versus intramolecular duplexes. The intramolecular complex has a higher melting temperature because it is more stable than the intermolecular complex.

Reprinted with permission from Copyright © (2016) John Wiley and sons[34]

Polymerase Chain Reaction (PCR)

To discuss proximity ligation assays (PLA), the fundamentals of the readout method, PCR, need to be understood. Traditional PCR uses gel electrophoresis for separation and detection of double-stranded DNA (dsDNA) products at the final phase, or end-point, of the PCR

reaction. The method, developed by Kary Mullis in the 1980s, employs DNA polymerase to make multiple new target strands of DNA that are complementary to the provided target strand. DNA polymerase selectively adds a nucleotide onto the 3'-OH group of the strand, and it needs a primer DNA that can hybridize with the first few nucleotides on the target. At the end of a typical PCR reaction, the target sequence will be accumulated in the billions of copies [35].

The components of PCR include a DNA template, which is the sample DNA that contains the target sequence. At the beginning of the reaction, high temperature (94-95 ^{o}C) is applied to the original dsDNA molecule to separate the strands from each other. DNA polymerase is an enzyme that synthesizes new strands of DNA complementary to the target sequence. The most commonly used of these enzymes is *Taq* DNA polymerase, derived from *Thermus aquaticus*, which is chosen because of its extreme temperature stability and high fidelity when copying DNA.[35] Forward and reverse primers, sparse pieces of single-stranded DNA that are complementary to the target sequence, are also needed to initiate target extension. The polymerase begins making new DNA from the end of each primer. Lastly, Deoxynucleotide triphosphates (dNTPs) are single units of the bases A, T, G, and C, which are essentially "building blocks" for new DNA strands. [36]

The reaction can be divided into 3 phases: denaturation, annealing, and extension. Phase 1: Denaturation separates the two strands of the DNA double helix by breaking the hydrogen bonds between the nucleotides to create single strands. This happens at very high temperature, around 94-95 ^{o}C. Phase 2: Annealing is when the temperature is lowered to allow the primers to bind the DNA. The optimal primer binding temperatures vary but are usually around 50-60 ^{o}C. Phase 3: Extension is when the temperature is ramped back up to about 72 ^{o}C to allow the DNA polymerase enzyme to make new strands of complementary DNA from random nucleotide

reagents in solution[37]. After multiple cycles of PCR, the number of target sequences exponentially increases to create approximately millions or billions of copies by the end of ~50 cycles[38]. Of course, PCR does have its limitations. The reaction generates an approximate doubling of copies of the target sequence in the exponential phase. Only in this phase is it possible to extrapolate back to determine the starting amount of the target sequence that was in the sample. After accumulation of pyrophosphate molecules and reagent limitations come into play, the PCR reaction eventually ceases to amplify target sequences at an exponential rate, and the reaction goes into the plateau phase. The plateau phase of the reaction means that most of the components are consumed, making the end point quantification of PCR products unreliable.

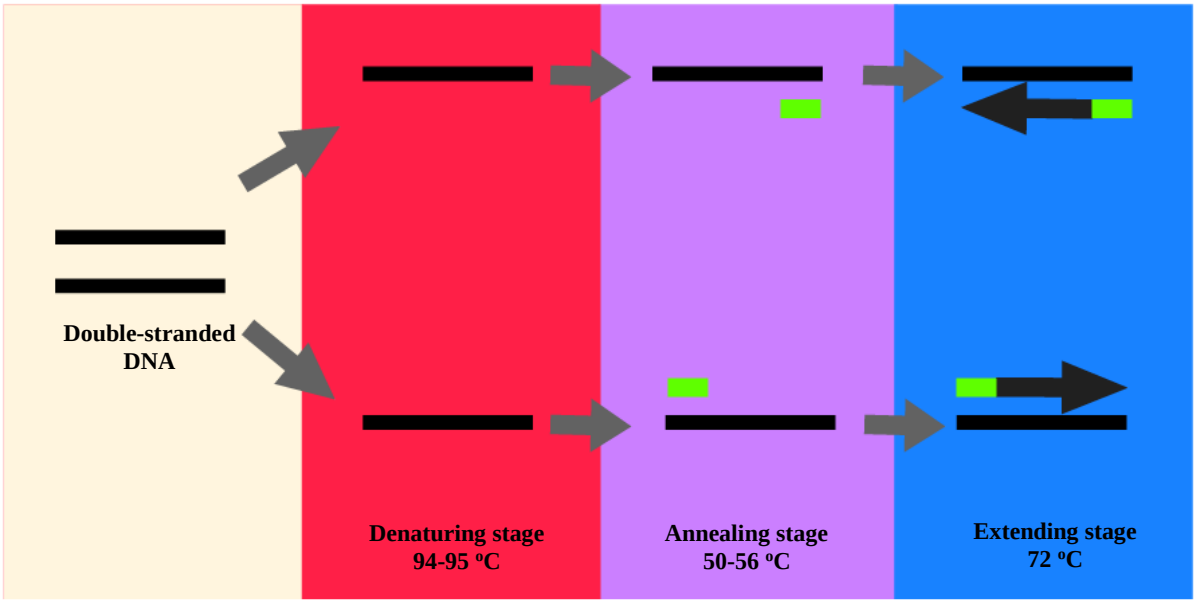

Figure 1.7: Polymerase Chain Reaction

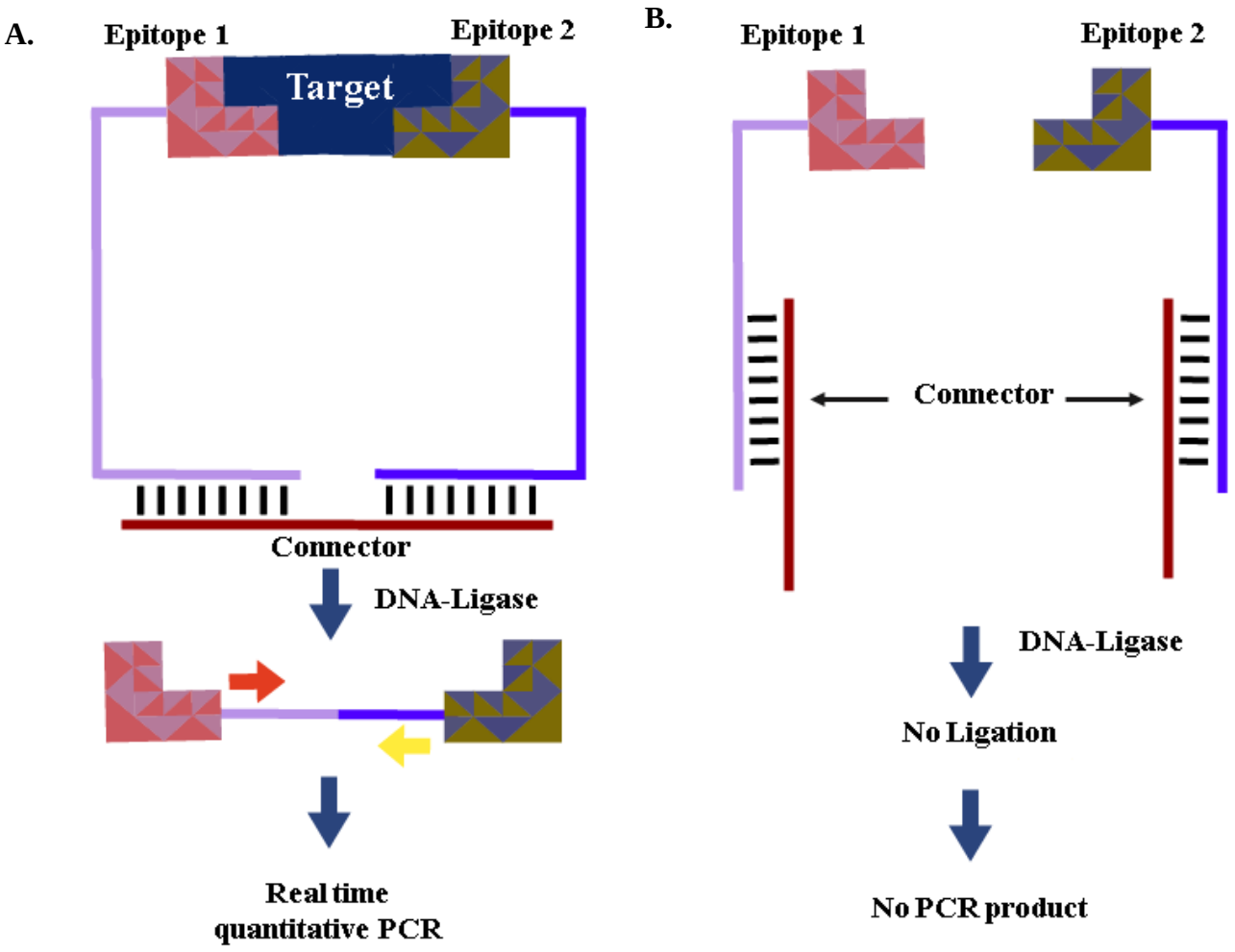

Figure 1.8: (A) Aptamers or antibodies will bind to distinct epitopes of the analyte. This brings the DNA sequence into close "proximity". The connector oligonucleotide is introduced to hybridize both ends. Eventually, ligated sequences will be PCR amplified using reverse and forward primer sequences (red and yellow arrows). Detection of the PCR product is achieved under conditions of real-time quantitative PCR. (B) Without the presence of the analyte, the connector oligonucleotide cannot act as a ligation template, which provides a background signal that can be subtracted from overall signal. [76]

Proximity Ligation Assay

The proximity assay concept was first adopted in a report by Landegren's group at Uppsala University, Sweden. In 2002, their lab designed and developed a method for in-vitro

analysis of proteins which coined the method proximity ligation assay (PLA)[39,40]. PLA products are detected via PCR. Comparing **Figure 1.5** and **Figure 1.8**, we can see that ELISA and PLA have several similarities. They both take advantage of the use of dual-antibody binding to the target molecule at different epitopes on the target protein. The major difference comes into play when we conjugate DNA to each the antibody or aptamer of choice in PLA. The tails can come close together or into proximity, once a short oligonucleotide called a connector is added in excess into solution. When the PCR reagents are added into the mixture, T4 DNA ligase is added as the last step. The ligase can fuse together the two DNA tails, and the generated sequence can be amplified during the subsequent PCR cycles. If there is no target protein available in solution, the two DNA tails cannot come together to bind (**Figure 1.8**). If we compare the sandwich ELISA method to Landegren's results, PLA has comparable sensitivity, detection limit, and a wider dynamic range. More importantly, this assay is homogeneous, which means washing steps are unnecessary, making it a single-tube immunoassay. Considering the sample preparation of binding the antibodies or aptamers to the target along with the connector, the timing for PLA is roughly one hour, and

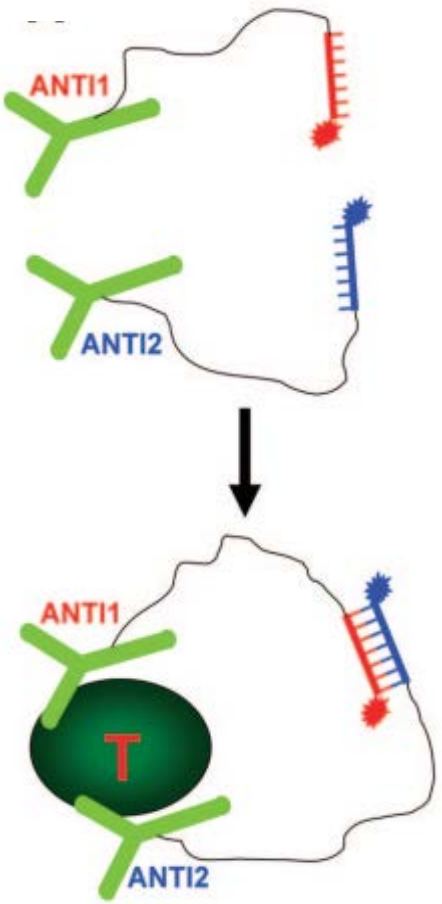

Figure 1.9: Molecular pincer assay. Molecular beacons for detecting proteins based on ANTI1 and ANTI2 depict antibodies labeled with signaling oligonucleotides. T corresponds to the target protein.

the downstream PCR assay can be completed in two hours using automated equipment. As a result, this technique is easier and much faster than

Molecular Pincers

In 2005, Heyduk et al. created an assay based on the proximity assay concept, coined "molecular pincers" [41]. In this method, they utilized two different aptamers or antibodies that can bind to different epitopes of a target protein, akin to ELISA and PLA. These antibodies are attached to short oligonucleotides via polyethylene glycol linkers. The oligos are fluorophore-labeled, one being a reporter molecule and the other a quencher or FRET acceptor molecule. In the absence of the analyte, the two aptamers or antibodies do not significantly interact, because the DNA tails cannot come into proximity to promote effective annealing. When the aptamers or antibodies bind to the target, it brings the two signaling oligonucleotides close to each other or into proximity, because the local concertation has been increased. In turn, the DNA can hybridize and the reporter and quencher molecules cause an analyte-dependent change in the fluorescence signal. These effects will be discussed further in in Chapter 2.

Proximity Extension Assay

Working from the general mechanism of PLA, Olink Bioscience developed an improved version and coined it as the proximity extension assay (PEA). Unlike PLA, PEA can be used for analysis in blood plasma samples. Common tissue sampling that doctors use to diagnosis patients can potentially be eliminated, due to the ease of collecting plasma samples. PEA, similar to PLA, brings the performance of highly sensitive methods for nucleic acid detection to the realm of protein detection, by converting the target-antibody binding event into a long chain of nucleotides, which can be measured by standard techniques. A schematic of PEA can be

found in **Figure 1.10**. A DNA polymerase uses the oligomer of one probe as a template to extend the oligomer of the other probe into a ~90 base pair strand. All of the formed strands are eventually detected and quantified by qPCR. A major added benefit of PEA is that it is capable

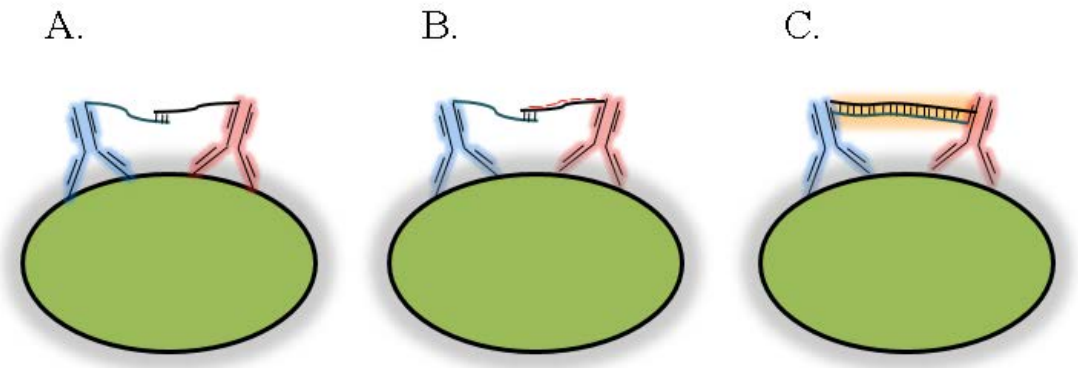

Figure 1.10: Schematic description of the Proximity extension reaction. (A) Two proximity probes bound to a target protein, linked together by hybridization of DNA oligomers. (B) Polymerase uses one oligomer as a template to (C) extend the other oligomer into a ~90 bp DNA strand (orange).

of performing parallel multiplexed assays, meaning that it can simultaneously detect multiple target proteins or macromolecules in the same sample.

1.2.3 Summary of Proximity Assays

The development of proximity assays successfully overcame major limitations of other protein based assays such as immuno-PCR, western blots, and ELISAs. Noteworthy are three key improvements: 1) The assays are homogeneous, such that no washing steps are needed and measurement time and complexity can be greatly reduced. 2) The binding probes can be aptamers or antibodies, which makes selection easier. 3) The reaction can be done in a single PCR tube at low volume, saving significant amounts of reagents and analytes. In this thesis work we chose the PLA assay format with which to develop an adiponectin assay. In

comparison to ELISA, PEA, and the molecular pincer assay, PLA retains all of the benefits for single-protein detection purposes (not multiplexed). The assay workflow is simple and requires very little sample volume (~1 μL or less), making it compatible with future applications to protein quantification in our group's microfluidic devices.

1.3 Electrochemistry Meets Immunoassays

A classic electrochemical (EC) protein sensor [42–45] is made up of: 1) recognition elements that specifically bind to the target protein; 2) a transducer which reports the change that is taking place on the interface with the recognition elements; 3) an electronic system communicates the result to the operator [42]. In order for an EC protein sensor to successfully qualify for a non-specialist market, it should meet a few requirements[42]. The biosensors should be based upon measurable parameters which can be distinguished by conductimetric, potentiometric, or amperometric techniques. Conductometric techniques are based on the flow of current that is established by migration of ions of opposite charge, when an electric field is applied between two electrodes immersed in the electrolyte solution[46]. Potentiometry is based on the potential difference that is created across a membrane which is placed between two solutions with charged species of different activity.[46] Potentiometric sensors are suited for measuring low concentrations in low volume samples because they do not chemically influence a sample.[47–50] The most popular technique is amperometry, because it measures current that is being generated from oxidation and reduction reactions[42 46] If the current is measured at a constant potential, it is referred to as amperometry, and if the current is measured in a controlled range of potential, it is referred to as voltammetry.[47] Modifications of the working electrode surface by immobilizing recognition elements, such as DNA, is a very efficient approach to reach maximum current

responses.[51] Bard and others introduced this concept of surface modification[52–54] about 35 years ago for the use of catalysis that can participate in EC reactions, and the concept has been highly employed and enhanced over the years for applications with a wide range of different EC sensors.[42,51]

1.3.1 Square Wave Voltammetry as Readout

There are a few types of pulse techniques used for electrochemical detection such as differential pulse voltammetry (DPV), normal pulse voltammetry (NPV), square wave voltammetry (SWV), and more. The main focal point of pulse techniques is the difference in the decay rates of the charging and faradaic currents. The charging current decreases much more rapidly than the faradaic current due to its decaying as an exponential function while the decreasing response of the faradaic current is inversely proportional to the square root of time (for diffusion-limited systems).[55,56] Therefore, at the completion of each well-timed pulse, the capacitive current is slim in comparison to that of the faradaic current.[57] This increased ratio of faradaic to non-faradaic current allows for a lower detection

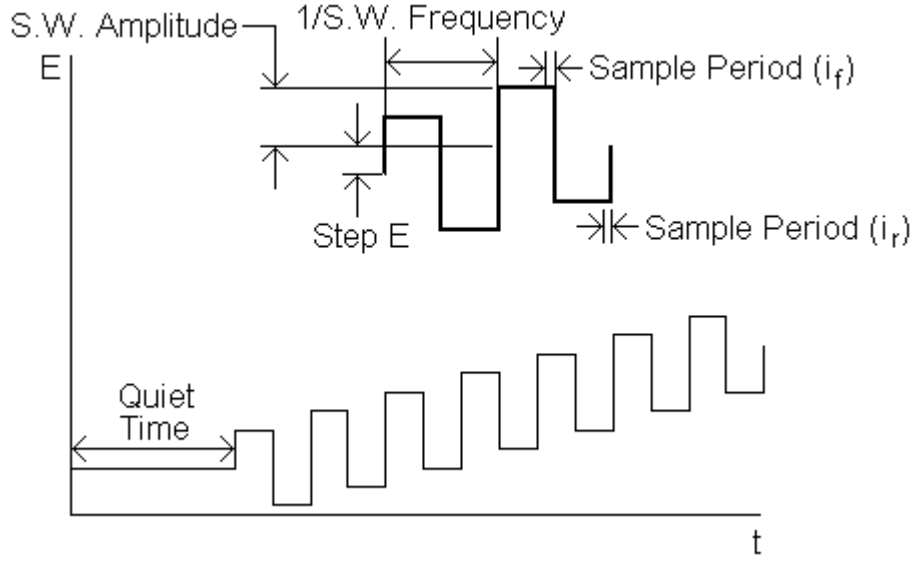

Figure 1.11: Potential wave form for square wave voltammetry.

https://www.basinc.com/manuals/EC_epsilon/Techniques/Pulse/pulse

limit as well as higher sensitivity and is ideal for analytical purposes.

SWV has been extensively used in the advancement of EC sensors and biosensors in recent years due to its high selectivity and sensitivity[58], and we have utilized SWV in our laboratory for protein sensing. SWV is similar to pulse polarography, which can offer high speed and sensitivity. In SWV, the current is measured twice during each cycle in the forward and reverse directions, which is often referred to as $i_{reverse}$ (i_r) and $i_{forward}$ (i_f). As shown in **Figure 1.11**, SWV output is given as the current difference, $\Delta i = i_f - i_r$.

In 1981, O'dea et al. calculated experimentally measurable parameters such as peak shifts, heights, and widths for different types of reactions and plotted them as a function of the appropriate rate constants.[59] This analysis exemplified why SWV is often operated at high frequency[55], where experiments can be accomplished quickly.[60] Each pulse results in a minute increment of potential, represented as “step E” in **Figure 1.11**.

1.3.2 DNA-driven Assay Formats

Within the chapters to follow, multiple DNA sequences are used and mentioned in all of our systems for assay development. For this reason, it is necessary to discuss the basic concepts of DNA and how it can be used as a reporter in various assay formats. To most people DNA is important only for its role in lineage. However, oligomer synthesis has advanced to the point that scientists can custom-design DNA-driven biosensors to detect proteins and other macromolecules. In fact, advances in DNA biotechnology are occurring at an exponential rate. In a rough equivalent of Moore's Law, the prices of DNA synthesis and sequencing are dropping at an exponential rate over time, a trend coined as "Carlson's law." (**Figure 1-12**). DNA is therefore a readily accessible material that can be inexpensively customized for research purposes. DNA interaction properties have been well studied, and we know that the strands can be made to form defined secondary and tertiary structures with well-characterized properties, facilitating their use in biosensor studies and clinical diagnostic research.

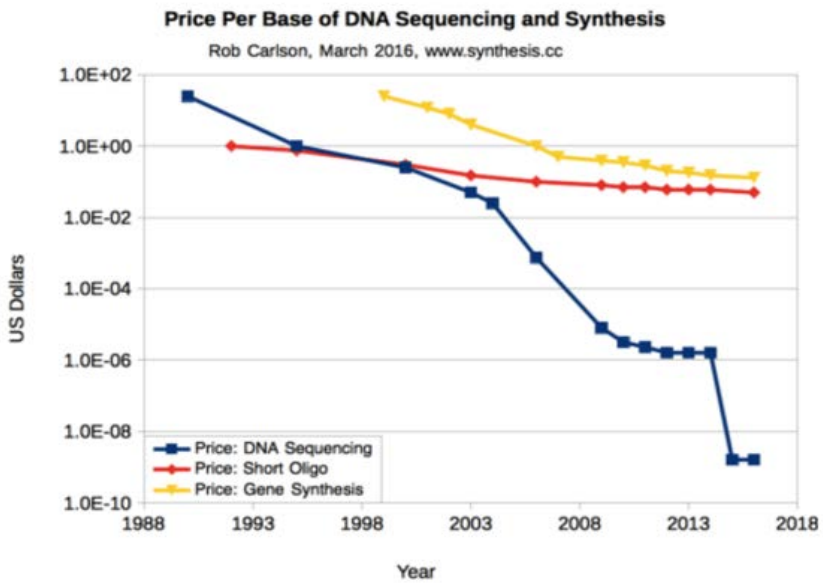

Figure 1.12: Carlson's Law. The price of DNA oligonucleotide and gene synthesis has been dropping exponentially over the past 20 years.

Image reprinted with courtesy of http://www.eusynbios.org/blog/2016/6/10/writing-our-genome

DNA is composed four nucleotide bases—adenine, cytosine, guanine, and thymine (A, C, G and T)—which can hybridize to form a double helix bound together by hydrogen bonds between complementary base pairs (A-T and C-G). The biophysical characteristic of DNA were nicely described in Dr. David Yu Zhang's thesis[61], where he cleverly compared DNA to velcro and magnets and determined the kinetics of DNA strand displacement reactions. **Table 1-1**, from Zhang's thesis [61] displays the terms and definitions of the frequently used concepts in DNA nanotechnology.

Preferred Term	Synonyms	Definition
Strand	Oligonucleotide Molecule Oligo	A continuous linear nucleic acid polymer covalently joined by phosphodiester bonds.
Complex	Molecule Tile	A non-covalently linked structure of multiple strands.
Domain	Subsequence Tract Section	Multiple continuous nucleotides in a strand that act as a unit in hybridization.
Toehold	Sticky end	A domain that serves too co-localize nucleic acid strands and complexes. Toeholds are typically short (4-10 nt).

Table 1.1: Common terms and their synonyms and definitions. [61]

DNA Strand Displacement

Within this thesis, we take advantage of DNA strand displacement reactions, where two strands with partial sequence complementarity hybridize to each other, displacing a pre-hybridized strand in the process. Strand displacement can be started by complementary single-stranded domains (referred to as toeholds) and typically progresses through branch migration steps (**Figure1.13**) [62–64]. Usually, in molecular biology, strand displacement describes a process

that is arbitrated by enzymes, like polymerases [65]. Although enzyme-free strand displacement and branch migration in DNA has been studied since the 1970s [66–76], they have only been applied to DNA nanotechnology within the past 10-15 years. A schematic of the DNA strand displacement process is given in **Figure 1-13**. In Chapter 4 of this thesis, a complementary DNA strand (toehold) was used to displace our redox-tagged molecule in order to create a bi-stable EC sensor that can enhance the SWV current.

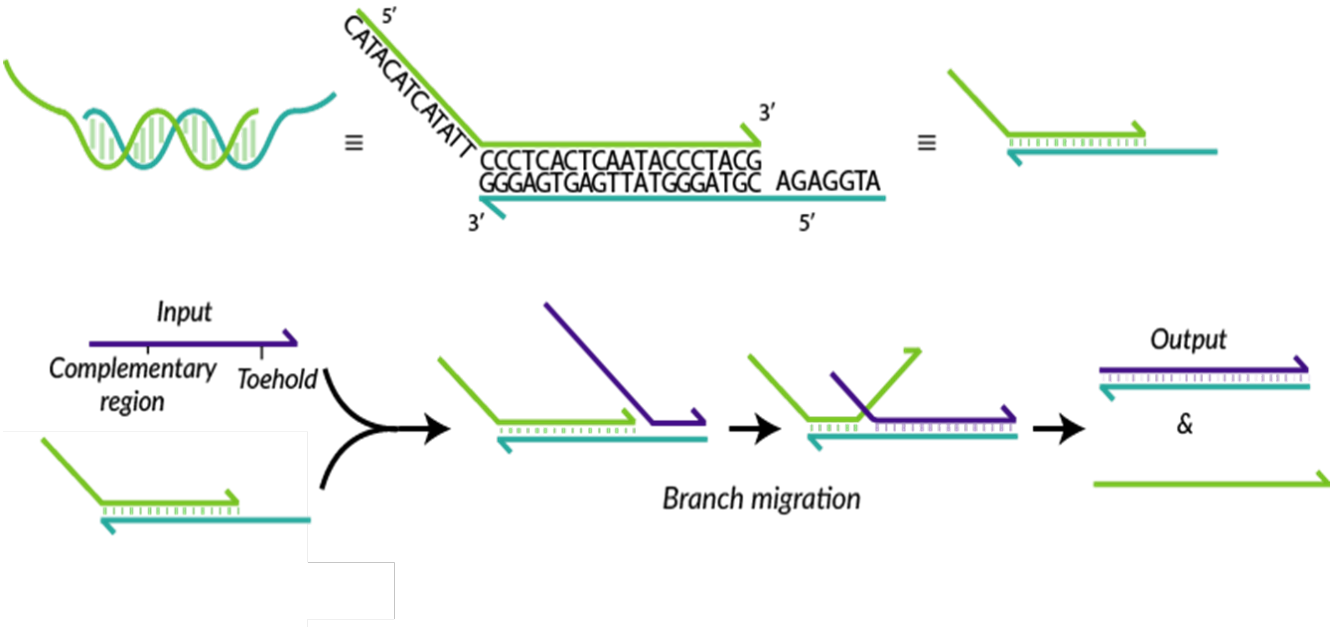

Figure 1.13: DNA strand displacement overview. Panel shows one example of this reaction. Single stranded DNA (purple) reacts with multi-stranded DNA (green/blue) to release green strand and form a purple/green complex. This reaction is facilitated by the "toehold" domains. The hybridization of these single-stranded toeholds colocalizes blue/purple, and allows the toehold domain to branch migrate. Branch migration is the random walk process in which one domain displaces another of identical sequence in binding to a complementary domain, via a series of single nucleotide dissociation and hybridization steps. At the completion of branch migration, complex blue/purple is formed and the green strand is released.[61]

Proximity Ligation Assay: Asymmetric

In the Easley laboratory, we have taken advantage of DNA-driven assays, chiefly for protein detection. For example, asymmetric PLA was developed, which improved the dynamic range of PLA by 2 orders of magnitude through reduction of the background complex formation in solution. Varying the DNA connector strand from the normal 20 bases to an asymmetrical 16 total bases allowed large background reductions with only modest signal reductions.

Electrochemical Proximity Assay

Our laboratory has also previously developed a unique immunoassay that combines the proximity effect with electrochemical sensing. Others have employed aptamer-based, structure switching protein detection methods on electrodes[77], where protein binding typically results in signal loss. These systems provided homogeneous, EC detection of interferon gamma at a 60 pM detection limit. However, the flexibility of this approach is severely limited due to the requirement of a structure-switching aptamer, which will not exist against many targets. In our system, termed the electrochemical proximity assay (ECPA), aptamer or antibody-oligo binding was decoupled from signal readout using DNA hybridization, creating a more flexible system amenable to detection of any protein with aptamer or antibody pairs. **Figure 1.14** shows a schematic of ECPA, where upon the binding of two antibody-oligo conjugates to protein targets, the EC-active methylene blue (MB) is positioned closer to the gold electrode for SWV readout. The combination of this proximity-dependent assay with EC current enhancement via SWV allowed for a homogeneous, highly selective and sensitive detection of target proteins with detection limits in the femtomolar range, which could feasibly be utilized in a point-of-care system in the future. [78,79]

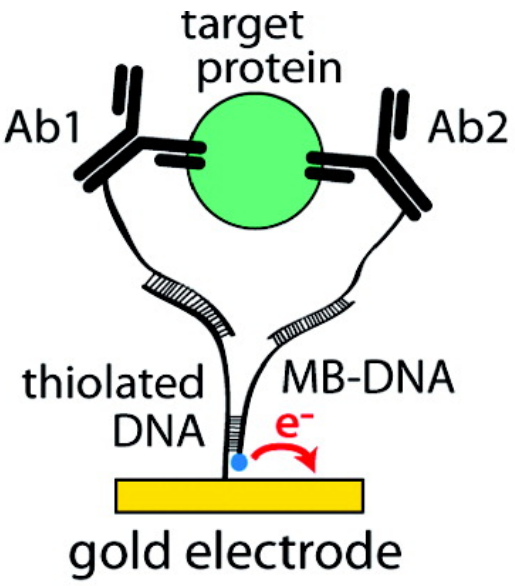

Figure 1.14: Electrochemical Proximity Assay (ECPA) combines the proximity effect and SWV detection of a redox-tagged molecule to bring it near the gold surface, which increases the current relative to the target protein[78].

1.4 Additional Comments

Within this chapter, we have outlined several important concepts relevant to this thesis work. In chapter 2, a proximity ligation assay (PLA) is introduced and optimized using a dual-antibody pair, which specifically binds to the globular domain region of the adipose-secreted protein, adiponectin; this protein is important in diabetes, obesity, and metabolic syndrome, as discussed above. In chapter 3, we conduct an important study to evaluate the distance dependence of the placement of our redox-tagged DNA strand with respect to the working electrode surface, for use in SWV readouts in DNA-driven assays. Finally, in chapter 4, we carefully engineer a DNA hybridization-driven system—incorporating strand displacement reactions—and we create a bistable switch that combines the proximity effect of DNA with electrochemical detection by SWV. This system sets the stage for future proximity-driven protein assays that could take advantage of our bistable switch-based strand displacement reactions.

1.5 References

(1) Endocrine Web. About the Endocrine System: Endocrine Glands and Hormones http://www.endocrineweb.com/endocrinology/about-endocrine-system (accessed Jun 11, 2016).

(2) Smitka, K.; Marešová, D. *Prague Med. Rep.* 2015, *116* (2), 87–111.

(3) D'Amour, K. A.; Bang, A. G.; Eliazer, S.; Kelly, O. G.; Agulnick, A. D.; Smart, N. G.; Moorman, M. A.; Kroon, E.; Carpenter, M. K.; Baetge, E. E. *Nat. Biotechnol.* 2006, *24* (11), 1392–1401.

(4) Chandran, M.; Phillips, S. A.; Ciaraldi, T.; Henry, R. R. *Diabetes Care*. 2003 26 (8), 2442-50.

(5) John E. Morley. Overview of the Endocrine System http://www.merckmanuals.com/professional/endocrine-and-metabolic-disorders/principles-of-endocrinology/overview-of-the-endocrine-system (accessed Mar 6, 2016).

(6) Lee, C.-H.; Olson, P.; Evans, R. M. *Endocrinology* 2003, *144* (6), 2201–2207.

(7) Reaven, G. M. *Annu. Rev. Med.* 1993, *44* (1), 121–131.

(8) Alberti, George; Zimmet, Paul; Shaw, J. *Int. Diabetes Fed.* 2006, 1–23.

(9) NIH - National Cancer Institute. Diabetes (Diabetes Mellitus) http://www.ncbi.nlm.nih.gov/pubmedhealth/PMHT0024704/ (accessed Mar 6, 2016).

(10) Lebovitz, H. E. *Clin. Chem.* 1999, *45* (8 Pt 2), 1339–1345.

(11) The Cost of Diabetes: American Diabetes Association® http://www.diabetes.org/advocacy/news-events/cost-of-diabetes.html?referrer=https://www.google.com/?referrer=http://www.diabetes.org/advocacy/news-events/cost-of-diabetes.html.

(12) WORLD DIABETES CONGRESS: NEW DEVELOPMENTS http://onedrop.today/blog/2015/12/16/review-world-diabetes-congress-new-developments-december-1-5-2015/ (accessed Jun 3, 2016).

(13) Spiegelman, B. M.; Flier, J. S. *Cell* 2001, *104* (4), 531–543.

(14) Isomaa, B.; Almgren, P.; Tuomi, T.; Forsén, B.; Lahti, K.; Nissén, M.; Taskinen, M. R.; Groop, L. *Diabetes Care* 2001, *24* (4), 683–689.

(15) Eckel, R. H.; Kahn, S. E.; Ferrannini, E.; Goldfine, A. B.; Nathan, D. M.; Schwartz, M. W.; Smith, R. J.; Smith, S. R. *Diabetes Care* 2011, *34* (6), 1424–1430.

(16) Björntorp, P. *Diabetes Care* 1991, *14* (12), 1132–1143.

(17) Cypess, A. M.; Lehman, S.; Williams, G.; Tal, I.; Rodman, D.; Goldfine, A. B.; Kuo, F. C.; Palmer, E. L.; Tseng, Y.-H.; Doria, A.; Kolodny, G. M.; Kahn, C. R. *N. Engl. J. Med.* 2009, *360* (15), 1509–1517.

(18) Frontini, A.; Cinti, S. *Cell Metab.* 2010, *11* (4), 253–256.

(19) Rosen, E. D.; Spiegelman, B. M. *Cell* 2014, *156* (1–2), 20–44.

(20) Ayorga, M. *Rev. Med* 2007, *15* (August), 225–242.

(21) National Library of Medicine. Obesity. http://www.ncbi.nlm.nih.gov/pubmedhealth/PMH0004552/ (accessed Mar 6, 2016).

(22) Oh, D. K.; Ciaraldi, T.; Henry, R. R. *Diabetes, Obes. Metab.* 2007, *9* (3), 282–289.

(23) Gil-Campos, M.; Cañete, R.; Gil, A. *Clin. Nutr.* 2004, *23* (5), 963–974.

(24) Yadav, A.; Kataria, M. A.; Saini, V.; Yadav, A. *Clin. Chim. Acta* 2013, *417*, 80–84.

(25) Desruisseaux, M. S.; Nagajyothi; Trujillo, M. E.; Tanowitz, H. B.; Scherer, P. E. *Infect. Immun.* 2007, *75* (3), 1066–1078.

(26) Schraw, T.; Wang, Z. V; Halberg, N.; Hawkins, M.; Scherer, P. E. *Endocrinology* 2008, *149* (5), 2270–2282.

(27) Davis, K. E.; Scherer, P. E. *Biochem. J.* 2008, *416* (2), e7-9.

(28) Xie, L.; O'Reilly, C. P.; Chapes, S. K.; Mora, S. *Biochim. Biophys. Acta* 2008, *1782* (2), 99–108.

(29) Shetty, S.; Kusminski, C. M.; Scherer, P. E. *Trends Pharmacol. Sci.* 2009, *30* (5), 234–239.

(30) Plaisance, E. P.; Lukasova, M.; Offermanns, S.; Zhang, Y.; Cao, G.; Judd, R. L. *Am. J. Physiol. Endocrinol. Metab.* 2009, *296* (3), E549-58.

(31) Goodwin, P. R. *J. AOAC Int.* 2004, *87* (6), 1383–1390.

(32) Besler, M. *TrAC - Trends Anal. Chem.* 2001, *20* (11), 662–672.

(33) Immer, U.; Lacorn, M. In *Handbook of Food Allergen Detection and Control*; 2015; pp 199–217.

(34) Zhang, H.; Li, F.; Dever, B.; Wang, C.; Li, X. F.; Le, X. C. *Angew. Chemie - Int. Ed.* 2013, *52* (41), 10698–10705.

(35) Sigma Life Science. *Science (80-81).* 2008, 1–40.

(36) Heid, C. A.; Stevens, J.; Livak, K. J.; Williams, P. M. *Genome Res.* 1996, *6* (10), 986–994.

(37) Some, P.; Barrier, L.; Gualberto, J. *Plant Sci.* 2004, *167* (1), 183.

(38) Adler, M.; Wacker, R.; Niemeyer, C. M. *Analyst* 2008, *133* (6), 702–718.

(39) Fredriksson, S.; Gullberg, M.; Jarvius, J.; Olsson, C.; Pietras, K.; Gústafsdóttir, S. M.; Ostman, A.; Landegren, U. *Nat. Biotechnol.* 2002, *20* (5), 473–477.

(40) Gullberg, M.; Gustafsdottir, S. M.; Schallmeiner, E.; Jarvius, J.; Bjarnegard, M.; Betsholtz, C.; Landegren, U.; Fredriksson, S. *Proc. Natl. Acad. Sci.* 2004, *101* (22), 8420–8424.

(41) Heyduk, E.; Heyduk, T. *Anal. Chem.* 2005, *77* (4), 1147–1156.

(42) Grieshaber, D.; MacKenzie, R.; Vörös, J.; Reimhult, E. *Sensors* 2008, *8* (3), 1400–1458.

(43) North, J. R.; Lowe, C. R.; Köhler, G.; Milstein, C.; Gronow, M.; Liedberg, B.; Nylander, C.; Lundström, I.; Matsuoka, H.; Karube, I.; Suzuki, I.; Aizawa, M.; Mattiasson, B.; Danielsson, B.; Mosbach, K.; Peterson, J. I.; Goldstein, S. R.; Fitzgerald, R. V.; Schultz, J.; Mansouri, S.; Goldstein, I. J.; Guilbault, G. G.; Ishimori, Y.; Karube, I.; Suzuki, S.; Roederer, J. E.; Bastiaans, G. J.; Aizawa, M.; Kato, S.; Suzuki, S.; Yamamoto, N.; al., et; Yamamoto, N.; al., et; Janata, J.; Huber, R. J.; Collins, S.; Janata, J.; Sibbald, A.; Whalley, P. D.; Covington, A. K.; Kuriyama, T.; Kimura, J.; Kawana, Y.; Janata, J.; Blackburn, G. F.; Pockrand, I.; al., et; Weber, W. H.; Eagen, C. F.; Nylander, C.; Liedberg, B.; Lind, T.; Burton, D. R.; Keating, M. Y.; Rechnitz, G. A.; Thompson, M.; Krull, U. J.; Worsfold, P. J. *Trends Biotechnol.* 1985, *3* (7), 180–186.

(44) Yuan, C. C.; Peterson, R. J.; Wang, C. D.; Goodsaid, F.; Waters, D. J. *Clin. Chem.* 2000, *46* (1), 24–30.

(45) Thévenot, D. R.; Toth, K.; Durst, R. A.; Wilson, G. S. *Biosens. Bioelectron.* 2001, *16* (1–2), 121–131.

(46) Blanco-López, M. C.; Lobo-Castañón, M. J.; Miranda-Ordieres, A. J.; Tuñón-Blanco, P. *TrAC Trends Anal. Chem.* 2004, *23* (1), 36–48.

(47) Chaubey, A.; Malhotra, B. D. *Biosens. Bioelectron.* 2002, *17* (6–7), 441–456.

(48) Bakker, E.; Pretsch, E. *Trends Analyt. Chem.* 2005, *24* (3), 199–207.

(49) D'Orazio, P. *Clin. Chim. Acta.* 2003, *334* (1–2), 41–69.

(50) Hutchins, R. S.; Bachas, L. G. *Anal. Chem.* 1995, *67* (10), 1654–1660.

(51) Goyal, R. N.; Bishnoi, S. *Indian J. Chem. 51*, 205–225.

(52) Itaya, K.; Bard, A. J. *Anal. Chem. Anal. Chem.* 1978, *50* (11), 1487–1489.

(53) Lennox, J. C.; Murray, R. W. *J. Electroanal. Chem. Interfacial Electrochem.* 1977, *78* (2), 395–401.

(54) Moses, P. R.; Wier, L.; Murray, R. W. *Anal. Chem.* 1975, *47* (12), 1882–1886.

(55) Gupta, V. K.; Jain, R.; Radhapyari, K.; Jadon, N.; Agarwal, S. *Anal. Biochem.* 2011, *408* (2), 179–196.

(56) Uslu, B.; Ozkan, S. A. *Anal. Lett.* 2011, *44* (16), 2644–2702.

(57) In *Solid State Electrochemistry I*; Wiley-VCH Verlag GmbH & Co. KGaA: Weinheim, Germany; pp I–XXI.

(58) Chen, A.; Shah, B. *Anal. Methods Anal. Methods This J. is [a] R. Soc. Chem.* 2013, *5* (5),

2158–2173.

(59) O'Dea, J. J.; Osteryoung, J.; Osteryoung, R. A. *Anal. Chem.* 1981, *53* (4), 695–701.

(60) Molina, A.; Gonzalez, J.; Laborda, E.; Li, Q.; Batchelor-McAuley, C.; Compton, R. G. *J. Phys. Chem. C* 2012, *116* (1), 1070–1079.

(61) Zhang, D. Y. Dynamic DNA Strand Displacement Circuits, California institute of Technology, 2010.

(62) Ellington, A. D.; Szostak, J. W. *Nature* 1992, *355* (6363), 850–852.

(63) Isaacs, F. J.; Dwyer, D. J.; Ding, C.; Pervouchine, D. D.; Cantor, C. R.; Collins, J. J. *Nat. Biotechnol.* 2004, *22* (7), 841–847.

(64) Isaacs, F. J.; Dwyer, D. J.; Collins, J. J. *Nat. Biotechnol.* 2006, *24* (5), 545–554.

(65) Penchovsky, R.; Breaker, R. R. *Nat. Biotechnol.* 2005, *23* (11), 1424–1433.

(66) Winkler, W.; Nahvi, A.; Breaker, R. R. *Nature* 2002, *419* (6910), 952–956.

(67) Amontov, S.; Jäschke, A. *Nucleic Acids Res.* 2006, *34* (18), 5032–5038.

(68) Stojanovic, M. N.; Mitchell, T. E.; Stefanovic, D. *J. Am. Chem. Soc.* 2002, *124* (14), 3555–3561.

(69) Tabor, J. J.; Levy, M.; Ellington, A. D. *Nucleic Acids Res.* 2006, *34* (8), 2166–2172.

(70) Dirks, R. M.; Lin, M.; Winfree, E.; Pierce, N. A. *Nucleic Acids Res.* 2004, *32* (4), 1392–1403.

(71) Zadeh, J. N.; Steenberg, C. D.; Bois, J. S.; Wolfe, B. R.; Pierce, M. B.; Khan, A. R.; Dirks, R. M.; Pierce, N. A. *J. Comput. Chem.* 2011, *32* (1), 170–173.

(72) Puglisi, J. D.; Tinoco, I. *Methods Enzymol.* 1989, *180*, 304–325.

(73) Liu, Y.; Tuleouva, N.; Ramanculov, E.; Revzin, A. *Anal. Chem.* 2010, *82* (19), 8131–8136.

(74) Hu, J.; Wang, T.; Kim, J.; Shannon, C.; Easley, C. J. *J. Am. Chem. Soc.* 2012, *134* (16), 7066–7072.

(76) Famulok, M. *Nat. Biotechnol.* 2002, *20*, 448–449.

(78) Zhang, D. (2010). Dynamic DNA strand displacement circuits. Ph.D. California Institute of Technology.

Chapter 2

Development of a Proximity Ligation Assay for Adiponectin Multimers

2.1 Introductory remarks

A homogeneous, binding-induced, hairpin-like assay was developed and shown capable of measuring trace amounts of proteins in homogeneous solutions [1]. The assay format, proximity ligation assay (PLA; see chapter 1), utilized DNA oligonucleotides attached to antibodies targeting adiponectin protein complexes. Interestingly, when designed for the large adiponectin multimers, it appeared that the assay mechanism was altered from its standard form. When two or more affinity probes bound to the same target protein complex, these DNA tails were further excluded from hybridizing together by an added connector oligonucleotide. Ligation products were amplified and detected by real-time, quantitative polymerase chain reaction (qPCR). In this chapter, we will show that fewer DNA strands were formed by enzymatic DNA ligation, but in a specific, target protein-dependent manner.

2.1.1 Affinity probes and assay formats

In a classic affinity assay, a signal is developed only if an affinity probe binds to its target molecule. To make that assay multiplexed, the affinity probes should be labeled with multiple

different reporter molecules, or the different target molecules should be captured in different locations to permit discrimination. Prior to analysis, probes are labeled (usually covalently) with specific reporter molecules, and the reporter molecules on the probes are then quantified. In mmunofluorescence, antibodies are labeled with different fluorophores, and multiple proteins can be measured in cells and tissues by using a fluorescence microscope. In flow cytometry, fluorescent labels have allowed simultaneous detection of ten or more different proteins at the same time [2]. However, a limitation to directly measuring fluorescence is that over-bleeding or cross talk between different dyes could occur as a result of spectral overlap. [3] In mass cytometry, antibodies are labeled with specific mass tags, known elements which can be recognized and quantified by mass spectrometry (MS). In MS, there is typically no overlap between the mass tagged antibodies, thus the level of multiplexing can be greater than with fluorophores [4,5]. DNA oligonucleotides provide another means for labeling, opening the methods to strand-displacement reactions, etc., as discussed in chapter 1. The affinity probes that bind can be recognized via techniques for sequencing of conjugated DNA strands, and the level of multiplexing is exponential to the number of bases that can be read. Also, the DNA oligonucleotides can be enzymatically amplified or copied, which can be used to greatly improve the sensitivity of an assay. The technique of choice that is widely used for assays based on DNA amplification is real-time, quantitative polymerase chain reaction (qPCR) [6–8]. Of particular interest in this chapter, PLAs use DNA as the reporter molecule and utilize qPCR for quantitative readout.

DNA aptamers were originally the preferred affinity probes in PLA, since addition of sections of signaling DNA to aptamers is usually simple and straightforward.[9] However, due to the lack of availability of two aptamers for most target protein molecules, including adiponectin,

we explored the use of both monoclonal and polyclonal antibodies to use in developing an adiponectin PLA, as discussed further below. Antibodies have been successfully used in PLA, through direct covalent attachment of signaling oligo's or by using non-covalent streptavidin-biotin coupling. [10] PLA has been carried out in the homogenous and the solid phase formats [1,11]. Tedious experimental procedures, such as washing, are not required for the homogenous format. Affinity identification, DNA ligation, and PCR amplification are completed in a single tube, easing the burden on the experimenter and simplifying high-throughput analyses. In our laboratory, we have developed global oligonucleotide signaling sequences to be used with target proteins that play roles in diabetes and obesity, such as insulin, adiponectin, and leptin. The global sequences include two separate DNA "tails" as readout probes that will be covalently attached to the antibody of interest. Global sequences of this type, while not useful for multiplexing, allow accurate performance comparisons between antibody-oligo based PLAs during assay development.

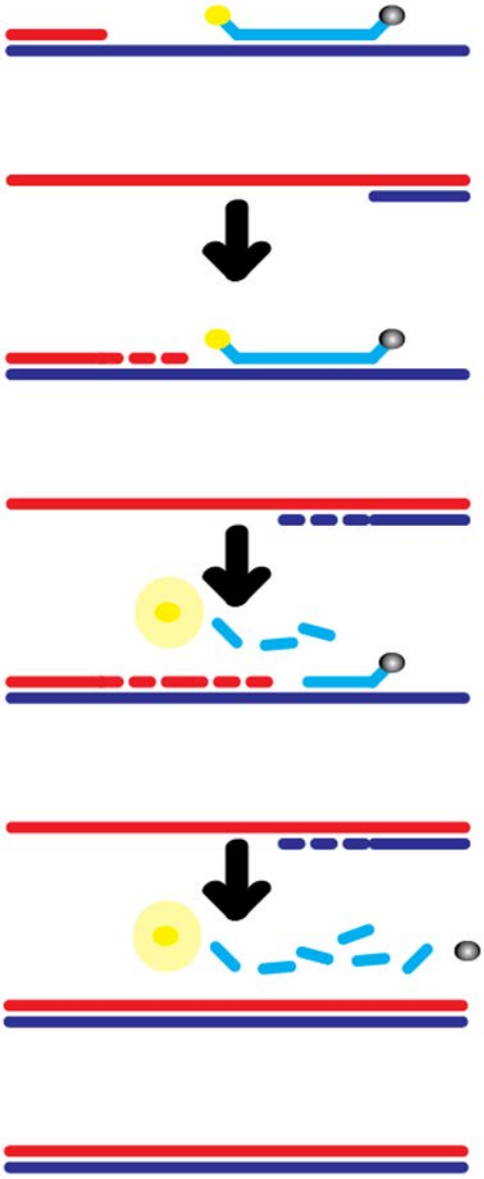

Figure 2.1: Schematic of qPCR. a) Annealing phase; b) extension phase I; c) extension phase II; d) end of PCR cycle.

2.1.2 Quantitative Polymerase Chain Reaction (qPCR)

In qPCR, the amplification product is measured as the **D.** ion is progressing, in real time. This real-time detection aspect is allowed by inclusion of a fluorescent reporter molecule in the reaction that produces an increased fluorescence signal with an increasing amount of product DNA. The fluorescence chemistries employed for this purpose include DNA binding dyes, such as N',N'-dimethyl-N-[4-[(E)-(3-methyl-1,3-benzothiazol-2-ylidene)methyl]-1-phenylquinolin-1-ium-2-yl]-N-propylpropane-1,3-diamine (SYBR Green), and/or fluorescently labeled sequence-specific primers or probes, such as TaqMan probes. With TaqMan probes, during the annealing phase in PCR, the fluorophore- and quencher-labeled probe anneals to the target of interest between the forward primer and reverse priming sites. In the extension phase, the primers bind the DNA template, and a new complementary DNA sequence is synthesized by Taq DNA polymerase. The labeled probe is cleaved by the enzyme during the extension phase, thus the reporter dye will be separated from the quencher dye, releasing highly fluorescent reporters (**Figure 2.1**). The quantified fluorescence is proportional to the total number of copies that have been generated, allowing determination of the starting amount.

A key benefit of qPCR over standard PCR is the ability to determine the initial number of copies of template DNA with high sensitivity and with high sequence accuracy. Furthermore, qPCR readout does not require physical separation of products, such as in gel electrophoresis, meaning that user bench time is reduced and throughput increased. Finally, downstream contamination is much less problematic in qPCR, since reactions are fully contained within PCR tubes and do not require removal for separation. Typically, reaction tubes are disposed of following analysis.[12] If we observe the raw data from qPCR from some of our adiponectin PLA runs at varying amplifiable template concentrations (**Figure 2.2**), as the reaction progresses to give a detectable amount of products, one can see the exponential phase of amplification as the linearly increasing region (note the log-scale y-axis). The threshold cycle number $C(_t)$ is defined within this region using software (horizontal line in figure). For the PLA assay readout data set shown in Figure 2.2, it is clear that the threshold cycle number was inversely dependent on the concentration of ligated DNA template. For the sample with the most amplifiable amount of target, the $C(_t)$ averaged around 26, and successive decreases in amplifiable target caused a shift in $C(_t)$ to larger numbers (to the right in the figure). Interestingly, the amount of amplifiable template appeared to be inversely proportional to the

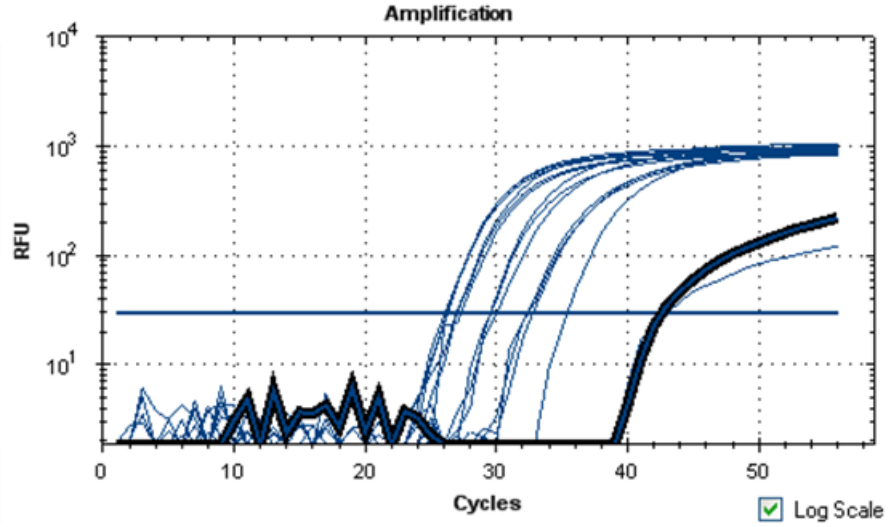

Figure 2.2: Quantitative Polymerase Chain Reaction raw data.

amount of targeted adiponectin protein complexes in our developed PLA, results which will be discussed further below.

2.1.3 Proximity Ligation Assay (PLA)

As discussed in chapter 1, one of the most robust yet simple protein assays that has been developed is the proximity ligation assay (PLA) [9] . In analytical terms, PLA surpasses immuno-PCR methods[13]—methodology to detect antigens using specific antibodies labeled with dsDNA—since the label in PLA is used for signal generation by qPCR without the need for assay washing steps. Herein, a PLA was developed toward detection of adiponectin multimers.

2.2 Experimental Methods

2.2.1 Reagents and materials

All solutions were prepared with deionized, ultra-filtered water (Fisher Scientific). T4 DNA ligase was purchased from New England BioLabs. Mouse Adiponectin standards were obtained from Millipore as a part of the mouse adiponectin ELISA Kit. Human thrombin and ATP were obtained from Sigma-Aldrich. All oligonucleotides except the Taqman probe were obtained from Integrated DNA Technologies (IDT; Coralville, Iowa), with purity and yield confirmed by mass spectrometry and HPLC. Nucleotide sequences of DNA are given in **Table 2-1**. Buffer reagents were purchased from VWR. The binding buffer used for mouse standards and Adipo-Arm1 or Adipo-Arm2 incubations consisted of 50 mM Tris-HCl, 100 mM NaCl, and 1 mM $MgCl_2$ with 1% BSA at pH 7.4. Two aliquots of the same antibody were purchased as

proximity probes, both from the adiponectin 1G12 clone from Fitzgerald Industries (Acton, MA). All antibodies were received lyophilized then were reconstituted with binding buffer. Antibody All-in-One Conjugation Kits were purchased from Solulink (San Diego, CA).

Adipo-Arm1	**/5AmMC6//iSp18/CCC AAC CCA ACC AAC CCA ACC CTC AAC CCA AAT CAA CAT TTA ATC G**
Adipo-Arm2	**/5Phos/GCG CCG GCG CAC CCA ACT CAA CCC TCC CTC CCT CCC ACC TCC CAC CTA /iSp18//3AmMO/**
Global Connector	**5' AAAGCGCCGGCGCCGATTAAATGAAT3'**
Global Forward Primer	**5' AACCCAACCAACCCAACCC 3'**
Global Reverse Primer	**5' TAGGTGGGAGGTGGGAGG 3'**
Global Taqman Probe	**5' CAACCCAAATCAACATTTAATCGGCGCCG 3'**

Table 2.1: Oligonucleotide Sequences Used in the Experimental Model of PLA

2.2.2 Preparation of Antibody-oligonucleotide Probes

The antibody-oligonucleotide conjugates used in the adiponectin PLA were prepared by conjugating Adipo-Arm1 to adiponectin antibody 1G12 and Adipo-Arm2 to a second aliquot of adiponectin antibody 1G12, respectively. Conjugation reactions and purification steps were accomplished using an Antibody-Oligonucleotide All-In-One Conjugation Kit (Solulink), according to the manufacturer's instructions. Briefly, the oligonucleotides were first activated with the heterobifunctional Sulfo-S-4FB (N-succinimidyl-4-formylbenzamide) crosslinker, and their quantities were confirmed using absorbance; specifically, $A_{260\ nm}$ of unmodified activated oligonucleotides and the $A_{260\ nm}$ to $A_{360\ nm}$ ratio after the modification of activated oligonucleotides. Similarly, antibodies were activated with a separate heterobifunctional crosslinker, S-HyNic (succinimidyl-6-hydrazino-nicotinamide). Activated oligonucleotides and

antibodies were then mixed and incubated at room temperature for 2 h. Once the conjugation reaction was stopped, conjugates were further purified using the supplied magnetic affinity matrix. The final concentrations of the conjugates were determined by the Bradford protein assay. Adipo-Arm1-1G12 and Adipo-Arm2−1G12 were synthesized with 75% and 86% recovery from the initial number of antibodies (100 µg).

2.2.3 Proximity Ligation Assay

Temperature control was achieved using a Mastercycler-EP gradient thermal cycler (Eppendorf). Adiponectin and oligonucleotide solutions were made as described.[9] An amount of 4 µL of a reaction mixture containing 2 µL of binding buffer, 1 µL Adipo-Arm1-1G12, and 1 µL Adipo-Arm2-1G12 was incubated at 37 °C for 30 min before adding 1 µL of connector which is 400-fold higher in concentration of the probe (C_{20}). An additional 30 min of incubation at 22 °C was performed to stabilize complexes. These 5 µL samples were then brought to a total volume of 50 µL for the ligation and amplification mixture, which contained 100 mM NaCl, 50 mM Tris-HCl at pH 7.5, 1.9 mM $MgCl_2$, 0.1% BSA, 26.8 unit T4 DNA ligase, 73 µM ATP, 0.18 mM dNTPs, 0.45 µM forward and reverse PCR primers, 45 nM Taqman probe for the 5′ nuclease assay, and 1.5 units of AmpliTaq Gold polymerase (ABI). The reactions were transferred to a qPCR instrument (CFX96, Bio-Rad) for temperature cycling under the following time program: 5 min at 22 °C for ligation, 10 min at 95 °C, and then 45 cycles of 15 s at 95 °C and 60 s at 60 °C.

2.3 Results and Discussion

2.3.1 Signal and Background in Proximity Ligation Assay

When dealing with PLA, it should be understood that target-independent ligation (background) can possibly occur and is caused by two sources which have been outlined by Kuhn et al. [14]and Leslie et al.[15] : 1) based on the binding equilibrium, a fraction of antibody-oligos can always bind with the 20-base connector sequences in the assay ($C_{20,PLA}$) even in the absence of the target protein, and 2) T4 DNA ligase is capable of ligating a small fraction of ssDNA sequences, even in the absence of a connector sequence.[15,14] Both of these result in target-independent ligations that increase the background levels in the assay. Basically, without the presence of target, this background formation limits the total amount of antibody probes that will be used, which can largely affect the sensitivity, in turn affecting the dynamic range. As stated earlier, we now know that by modifying the DNA connector, one can modify the overall binding affinity and tune the signal to background ratio. If we decrease the connector length from 20 nt to 16 nt, we have shown that the overall background will be reduced [16].

2.3.2 Proximity Ligation Assay for Adiponectin

As discussed in chapter 1, adiponectin is a primary endocrine hormone secreted from adipocytes, and its level in blood is an important indicator of diabetes, obesity, and other metabolic diseases. Recent observations have shown acute adiponectin secretion in response too nutrient and hormone signals, implying the existence of a readily-releasable pool of vesicles. Unfortunately, the tools to investigate the dynamics of adiponectin secretion are lacking. We decided to take on the challenge to develop a proximity ligation assay (PLA) to quantify adiponectin in smaller volume samples. In the beginning, we recognized that there may be complications in detecting adiponectin. First, adiponectin takes on many formations (trimers,

Low Molecular Weight (LMW), High Molecular Weight (HMW)), making it difficult to design antibody-oligo conjugates that will bind to all forms. Secondly, there is only one binding epitope that is known on the adiponectin monomer's globular region, so finding antibody pairs for the assay could also cause an issue. We decided to use the same antibody (1G12) with two different oligo sequences, since the protein is typically in a multimeric form.

Background Formation

To evaluate levels of measurements of adiponectin PLA background, we focused on optimizing the conditions of the assay, such as the probe and connector concentrations. We tested the following Ab-oligo probe concentrations: 0.25 nM, 0.50 nM, 1.0 nM, 1.5 nM of both Adipo-Arm1-1G12 and Adipo-Arm2-1G12 (maintaining a $C_{20,PLA}$ excess of 400-fold). As seen in **Figure 2.3**, as the probe concentration increased, the threshold cycle ($C_{(t)}$) value decreased, indicating a higher amount of background ligations. We also tested the $C_{20,PLA}$ connector concentrations that are added in excess to the probe concentration: 4- 40- 400 fold. The connector concentration exhibiting the lowest background out of those tested was the 400-fold level, as seen in **Figure 2.4**.

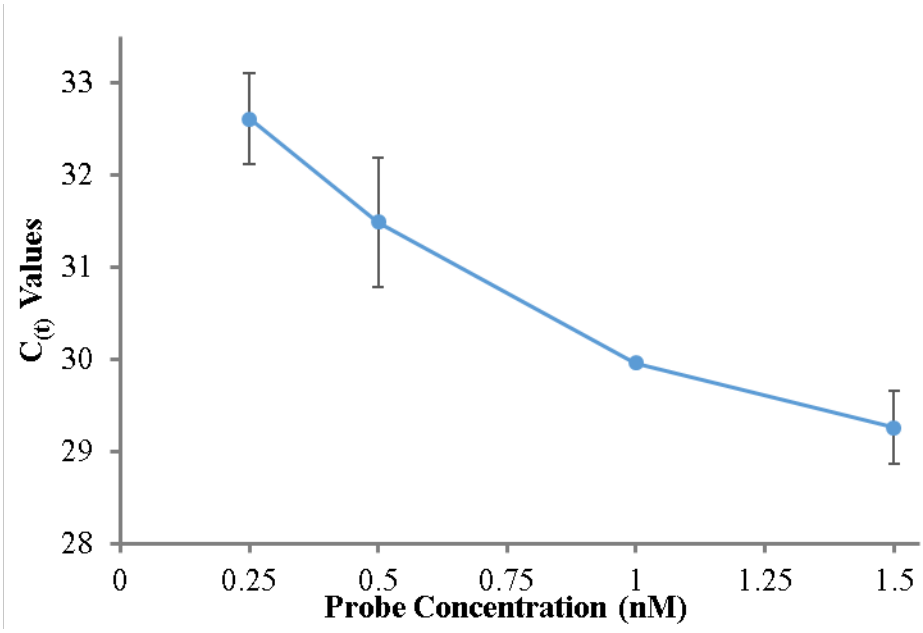

Figure 2.3: Complex Formation without the target gives the assay background of the Ab-Oligo conjugate. As the probe concentration increases, the $C_{(t)}$ value decreases, giving a high background signal.

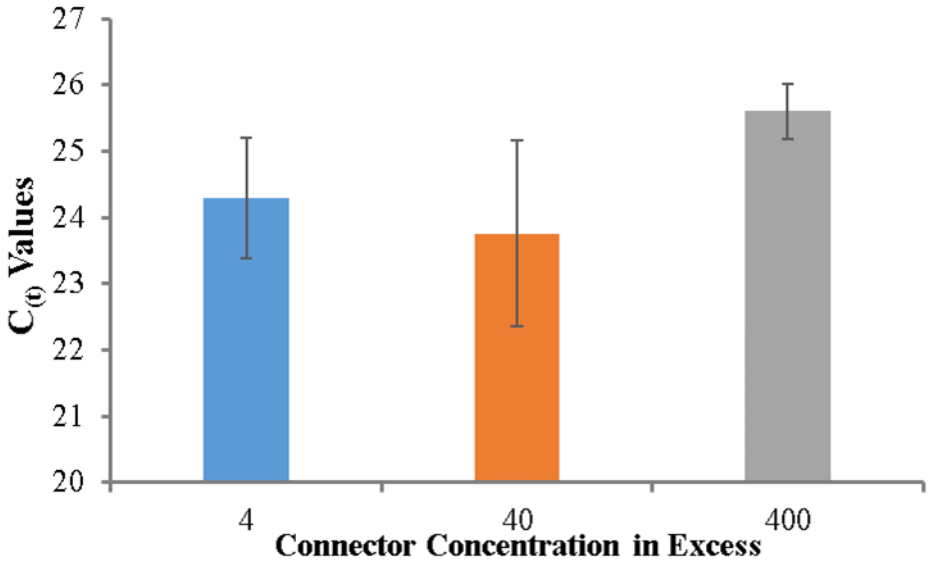

Figure 2.4: Connector concentration in excess to 500 pM probe s. 4: excess concentration 2 nM C_{20}, 40: excess concentration 20 nM C_{20}, 400: excess concentration 200 nM C_{20} provides the lowest background signal.

Signal

The signal of PLA results from a four-part complex composed of the target protein (T), two proximity probes (DNA-conjugated antibodies; Adipo-Arm1-1G12 and Adipo-Arm2-1G12), and the connector oligonucleotide ($C_{20,PLA}$). The three separate DNA molecules are made to bind into a structure that will promote the T4 DNA ligase enzyme to covalently join the two proximity probes. Ideally, when the target is present, more complex is formed over background due to the proximity effect that increases the local concentrations of the oligonucleotide tails.[17–20] The amount of ligated product is thus proportional to the amount of target protein in solution, and qPCR is used to identify these products. qPCR exponential amplifies the products, making the method highly sensitive. Due to its simplicity and sensitivity, PLA has been widely used and gained much success in a variety of applications.

In order to test for the presence of this four-part complex with our adiponectin PLA probes, we purchased mouse adiponectin standards, which came in lyophilized form, and we reconstituted them with binding buffer and measured the concentration to be 584 ug/L using the Nano-Drop 1000 small-volume spectrophotometer (Thermo Scientific). This concentration is equivalent to 20 nM of adiponectin monomer. As described above, the experiment was conducted in a similar manner. The only difference is the addition of 2 µL of buffer that was added for background is replaced with 2 µL of adiponectin standards. First, selectivity tests with both adiponectin and human thrombin were conducted under these conditions to test whether the dual Ab-oligonucleotide sequence selectively binds to the target (**Figure 2.5**). As expected, there was no change in $C_{(t)}$ value with added levels of human thrombin, indicating that our probes did not significantly bind this protein. Interestingly, with increasing levels of adiponectin standard, the $C_{(t)}$ values increased, suggesting that the presence of the target protein

was actually *inhibiting* the formation of PLA ligation products. Although this response was in the reverse direction compared to our expectations, it nonetheless appeared to be selective toward adiponectin.

To help understand this inverse assay response, we further varied adiponectin standard concentrations over the range of 1.0 to 8.0 nM and used higher probe concentrations probes (10 nM). As shown in **Figure 2.6**, the $C_{(t)}$ values again increased in response to adiponectin standards. This response, selective to adiponectin, was linear over the tested range, with an R^2 value of 0.9937. The limit of detection (LOD) was calculated to be 303 pM from 2 µL samples, meaning that 600 attomoles of adiponectin could be detected using our assay format.

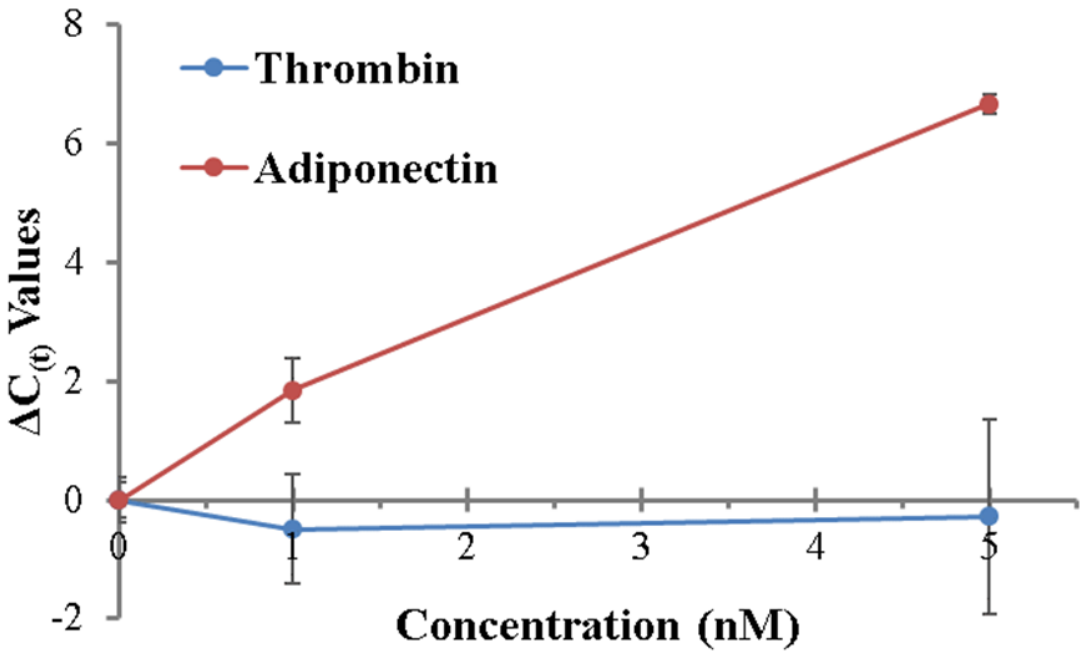

Figure 2.5: Verified with various concentrations of thrombin and adiponectin samples. Only adiponectin shows a shift in $C_{(t)}$ values. Proving that the dual antibody selection is functional.

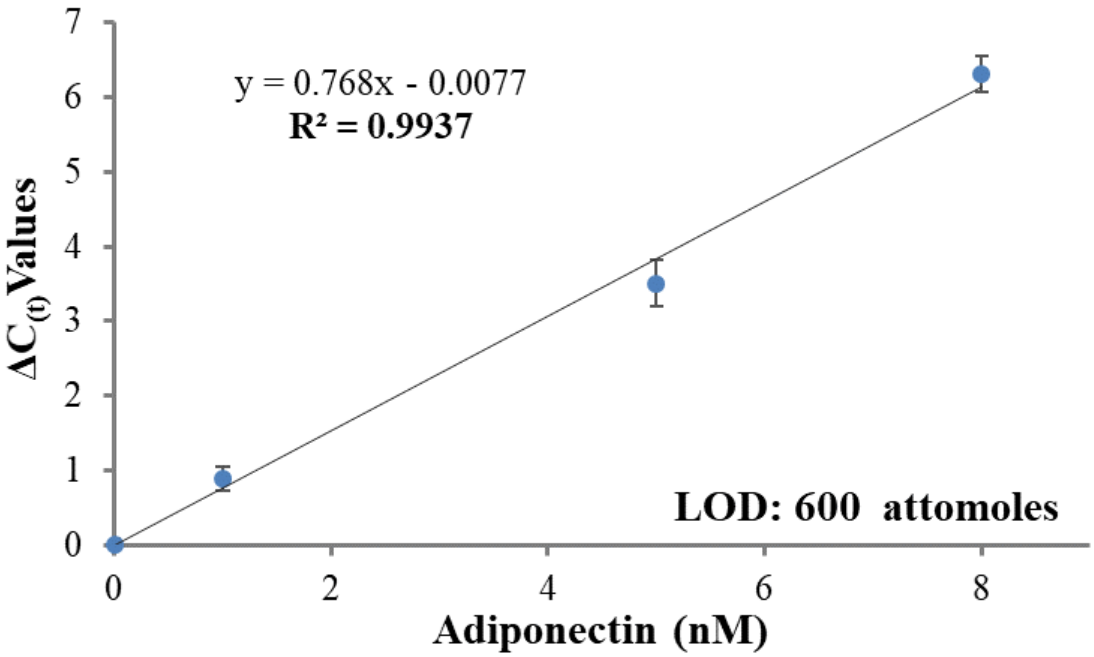

Figure 2.6: Complex formation with 10nM probes and various adiponectin standards.

2.4 Conclusion and Future Directions

Using our approach toward development of a PLA for adiponectin multimers, we observed an adiponectin selective response from the probes when the target protein was added. qPCR showed a significant shift in $C_{(t)}$ values that was linear with adiponectin concentration, yet the values changed in the reverse direction compared to our expectations. In other words, fewer ligation products were produced in the presence of the target protein. Since the adiponectin hormone forms various multimer complexes in serum (approximate MW of 30 kDa per monomer), we hypothesize that the DNA tails were insufficiently long to allow hybridization with the connectors (**Figure 2.7**). It is feasible that the single binding sites on each monomer were far enough apart to *exclude* connector formation and subsequent ligation. In future work, the DNA tail sequences should be elongated to test this hypothesis. On the contrary, it is also possible to exploit this ligation exclusion effect to develop other assays specific for protein multimers of interest.

Regardless of the direction of the assay response, since we achieved a specific response to adiponectin, this assay should still be useful for secretion quantification from adipose tissue extracted from mice. With the ultimate goal of creating an electrochemical biosensor that can detect adiponectin, the current form of the assay could be used, and a DNA hybridization assay could be developed for detection of ligated product, such as the hairpin switch assays outlined in chapter 4. This way, one could maintain the assay's favorable characteristics, such as its homogeneous nature, but remove the need for many cycles of PCR for quantification.

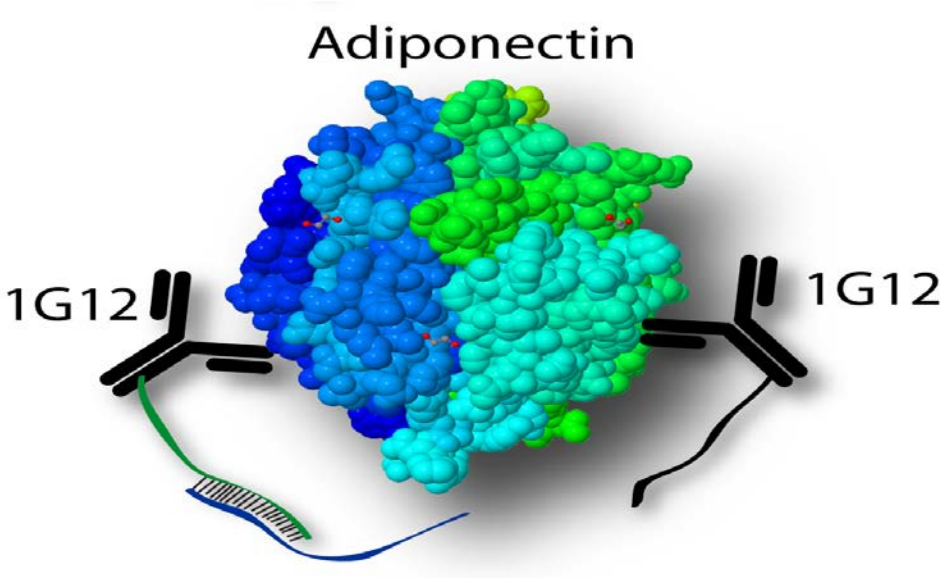

Figure 2.7: Theoretical schematic of the target protein molecule in a larger dimer formation in solution therefore DNA elongation may be required.

2.5 References

(1) Gustafsdottir, S. M.; Schallmeiner, E.; Fredriksson, S.; Gullberg, M.; Söderberg, O.; Jarvius, M.; Jarvius, J.; Howell, M.; Landegren, U. In *Analytical Biochemistry*; 2005; Vol. 345, pp 2–9.

(2) Autissier, P.; Soulas, C.; Burdo, T. H.; Williams, K. C. *Cytometry. A* 2010, *77* (5), 410–419.

(3) Perfetto, S. P.; Chattopadhyay, P. K.; Roederer, M. *Nat. Rev. Immunol.* 2004, *4* (8), 648–655.

(4) Bandura, D. R.; Baranov, V. I.; Ornatsky, O. I.; Antonov, A.; Kinach, R.; Lou, X.; Pavlov, S.; Vorobiev, S.; Dick, J. E.; Tanner, S. D. *Anal. Chem.* 2009, *81* (16), 6813–6822.

(5) Bendall, S. C.; Simonds, E. F.; Qiu, P.; Amir, E. D.; Krutzik, P. O.; Finck, R.; Bruggner, R. V; Melamed, R.; Trejo, A.; Ornatsky, O. I.; Balderas, R. S.; Plevritis, S. K.; Sachs, K.; Pe'er, D.; Tanner, S. D.; Nolan, G. P. *Science* 2011, *332* (6030), 687–696.

(6) Ullal, A. V; Peterson, V.; Agasti, S. S.; Tuang, S.; Juric, D.; Castro, C. M.; Weissleder, R. *Sci. Transl. Med.* 2014, *6* (219), 219ra9.

(7) Fan, R.; Vermesh, O.; Srivastava, A.; Yen, B. K. H.; Qin, L.; Ahmad, H.; Kwong, G. A.; Liu, C.-C.; Gould, J.; Hood, L.; Heath, J. R. *Nat. Biotechnol.* 2008, *26* (12), 1373–1378.

(8) Nong, R. Y.; Wu, D.; Yan, J.; Hammond, M.; Gu, G. J.; Kamali-Moghaddam, M.; Landegren, U.; Darmanis, S. *Nat. Protoc.* 2013, *8* (6), 1234–1248.

(9) Fredriksson, S.; Gullberg, M.; Jarvius, J.; Olsson, C.; Pietras, K.; Gústafsdóttir, S. M.;

Ostman, A.; Landegren, U. *Nat. Biotechnol.* 2002, *20* (5), 473–477.

(10) Gullberg, M.; Gustafsdottir, S. M.; Schallmeiner, E.; Jarvius, J.; Bjarnegard, M.; Betsholtz, C.; Landegren, U.; Fredriksson, S. *Proc. Natl. Acad. Sci.* 2004, *101* (22), 8420–8424.

(11) Fredriksson, S.; Gullberg, M.; Jarvius, J.; Olsson, C.; Pietras, K.; Gústafsdóttir, S. M.; Ostman, A.; Landegren, U. *Nat. Biotechnol.* 2002, *20* (5), 473–477.

(12) Freeman, W. M.; Walker, S. J.; Vrana, K. E. *BioTechniques*. 1999, pp 112–125.

(13) Adler, M.; Wacker, R.; Niemeyer, C. M. *Analyst* 2008, *133* (6), 702–718.

(14) Kuhn, H.; Frank-Kamenetskii, M. D. *FEBS J.* 2005, *272* (23), 5991–6000.

(15) Leslie, D. C.; Sohrabi, A.; Ikonomi, P.; McKee, M. L.; Landers, J. P. *Electrophoresis* 2010, *31* (10), 1615–1622.

(16) Kim, J.; Hu, J.; Sollie, R. S.; Easley, C. J. *Anal. Chem.* 2010, *82* (16), 6976–6982.

(17) Zhou, H.-X. *Biochemistry* 2001, *40* (50), 15069–15073.

(18) Tian, L.; Heyduk, T. *Biochemistry* 2009, 48, 264–275.

(19) Zhang, H.; Li, F.; Dever, B.; Wang, C.; Li, X. F.; Le, X. C. *Angew. Chemie - Int. Ed.* 2013, *52* (41), 10698–10705.

(20) Li, F.; Tang, Y.; Traynor, S. M.; Li, X.-F.; Le, X. C. *Anal. Chem*. 2016, 88, 8152-8157

Chapter 3

Distance Dependence of Square Wave Voltammetry Current in DNA-Driven Assays

3.1 Introductory Remarks

Single-stranded DNA probes (ssDNA) immobilized on gold (Au) electrode surfaces are a common element in many recent chemistry, biotechnology and nanotechnology applications.[1] Here, using square-wave voltammetry (SWV), we examine the length dependence of signal from a redox-tagged molecule, methylene blue-DNA (MB-DNA), when bound via ten base pairs to a self-assembled monolayer of thiolated-DNA (SH-DNA).[2] SWV is a robust pulse voltammetry technique, which can effectively increase the signal-to-noise ratio. We conducted a SWV pulse frequency study based on thirteen different lengths of SH-DNA to examine the changes in signal when MB-DNA is moved away from the electrode surface. Originally, we hypothesized that at higher frequencies the redox molecule would give a heightened signal when closer to the surface. Although this hypothesis was confirmed, the study revealed several important nuances of SWV-based, DNA-driven sensors. The results of this study are important for any of the various DNA-driven assay on electrodes, particularly for conceptualizing and designing new electrochemical biosensors.

3.2 Prior work

Much of the important work in developing DNA-driven, bioanalytical sensors via electrochemistry has been carried out by the Plaxco, White, and Revzin laboratories. Their combined work has paved the way for reagent-less, structure-switching, and electrochemical (EC) aptamer-based DNA sensors. Recent papers include their works on probe flexibility on Au surfaces via SWV [3], aptamer-based EC sensors[4], and diffusion models for surface-tethered redox molecules [5]. These papers are very improtant to the EC community, due to the profound effects that biosensors have made on clinical diagnostics and research applications. When developing an EC-sensor it is important to examine the self assemble monolayer (SAM)[6] as well as the redox-tagged molecule that will be reacting with the SAM by testing the paramaters of your EC measuring teqnique of choice, including response time and percent signal change.

The Plaxco group presented a simple means of finding the best conditions for optimal signal gain of a sensor. This analysis method accounts for often complex binding changes that affect the overall efficiency of a redox-tagged molecule as it comes near and exchanges electrons with the gold working electrode. In their case, they used SWV readout, which is highly sensitive to the reaction rates at the working electrode. These systems contain thiolated ssDNA with MB attached to the opposite end of the molecule, which is highly flexible. When varying SWV frequency (f_{SWV}), they noticed frequency-dependent changes in current corresponding with either the unbound or bound target complex of the DNA probe. The "signal gain" was defined as the difference in target-bound and unbound SWV currents divided by the unbound current, representing the target-dependent signal enhancement. As seen by analysis of one example sensor in **Figure 3.1C-D**, at lower frequencies the bound signal was higher than the unbound signal, yet

in higher frequencies the bound signal was significantly lower in comparison to the unbound signal[3]. This analysis showed that their sensor could be used over a range of frequencies, in either "signal-on" or "signal-off" modes, but it also highlighted the importance of characterizing the f_{SWV} dependence of any newly developed sensor.

Huang and White presented a computational model of current from a DNA-tethered MB molecule on a gold electrode, a model that helps to explain the behavior of our sensors presented within this chapter[5]. This work modeled surface confined MB-DNA systems that locked the redox molecule into an imaginary hemisphere at the electrode coupled with a tethered linker that varied in length (5-20 nm), which allowed them to observe the random-walk diffusion of the redox molecule within this hemisphere and to estimate the electrochemical current at different potential scanning rates. Cyclic voltammetry (CV) was used as the modeled and experimentally confirmed technique. They varied the parameters of CV by tuning the scan rate (mV/s) over a range including the standard reduction potential of MB. This model revealed that the electrochemical diffusion layer thickness and the length of the tethered linker play vital roles in determining the collision rate (i.e. electron transfer rate) of the redox molecule and the surface of the electrode[5]. The authors suggested that a sensor's EC response should be qualified by comparing the diffusion layer thickness, the time scale of the experiment, and the length of the tethered linker. As they lowered the scan rate (<500 mV/s), the EC reaction behaved as if the redox molecule was adsorbed to the surface, making the current proportional to the scan rate, which gave a linear response. At higher scan rates (>500 mV/s), the redox collision rate was diffusion limited, since the diffusion layer was thinner compared to the tether length. As such, EC current showed a linear response to the square root of the scan rate[5]. The authors suggest a general rule that these sensors will behave as either adsorbed redox molecules or as freely diffusing redox molecules, depending on the EC scan

rate, and that the switch between the two phenomena occurs when the diffusion layer thickness, $L_{DL} = (2Dt)^{1/2}$, is approximately 10 times the length of the tether linker (L_{MB}). This analysis suggested f_{SWV} to be very important parameter in our studies to follow. In essence, since we utilize SWV, the f_{SWV} could be used to vary the diffusion layer thickness (L_{DL}) at the electrode and to modify the behavior of our sensor to allow optimal conditions to be met.

3.2.1 Square Wave Voltammetry: Tunable Frequency Study

Square-wave voltammetry (SWV) is well established for observing surface-confined reactions, mainly because it can largely negate non-faradaic background charging currents, also known as capacitance current. In SWV, the experimental timescale is controlled by either the overall scan rate or the pulse frequency (f_{SWV}) used, which can have noticeable effects on the signal output. In early studies from the Murray group[7], they showed that target binding resulted in a change in the rigidity of immobilized DNA probes, and there was also a measurable increase in molecular weight. Ikeda and co-workers detected mismatched duplexes on gold surfaces using SWV [8], and their work showed that it is possible to differentiate between rigid dsDNA duplexes and their more flexible mismatched dsDNA duplexes, with the SWV system tuned to the right paramaters.[8] Their conclusion gave many electrochemical assay developers the mindset to further explore parameters such as f_{SWV} and varying scan rate more closely, since this parameter can help distinguish molecular weight or flexibility changes of the complexes on the surface. This issue will be discussed later in the chapter.

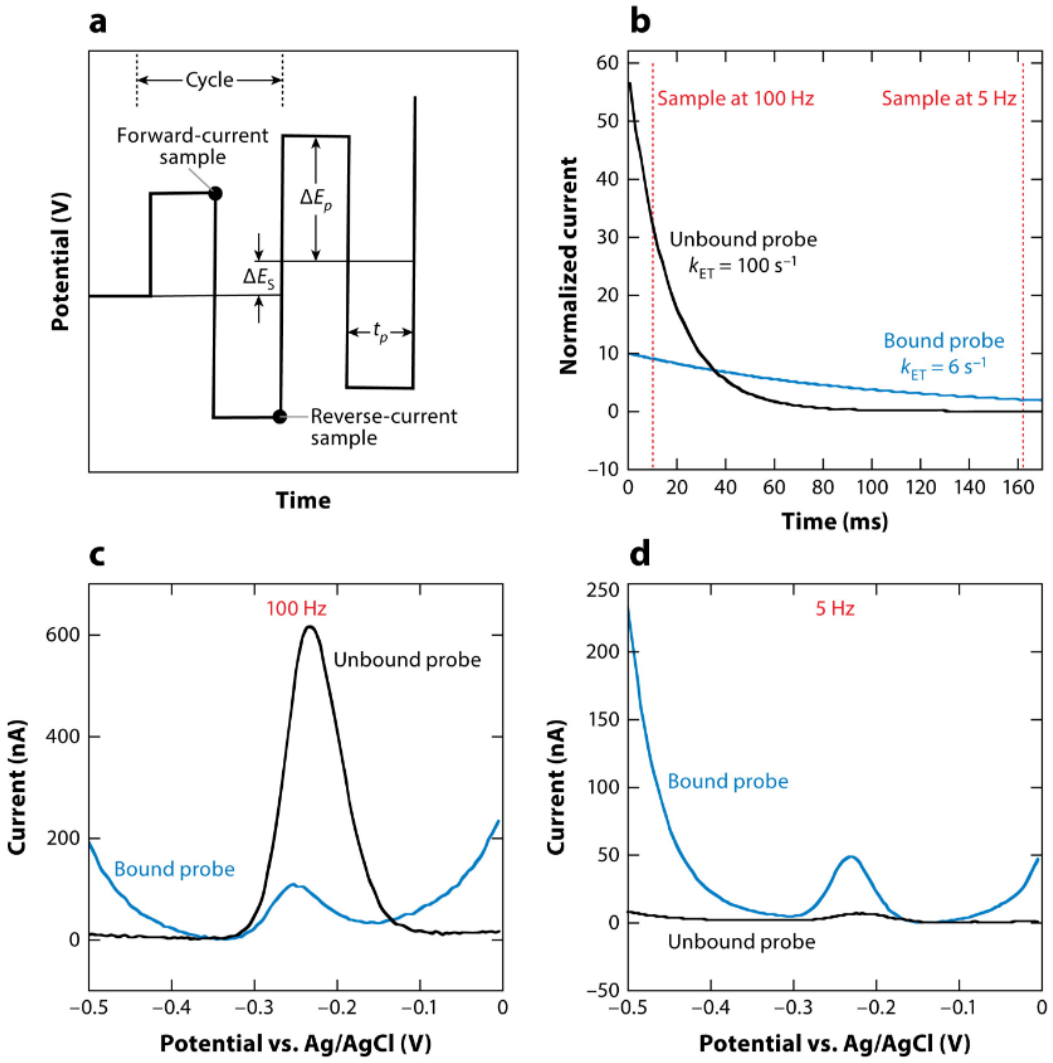

Figure 3.1: a) is an example of the SWV waveform that shows the measurement being taken from the forward and the reverse direction, respectively b) represents the electron transfer rates at 100 Hz and 5 Hz. At high frequencies, the charge transfer process is more rapid and provides more current. Versus, the charge transfer at low frequencies gives more current because the rate is slower. This result shows a shift in signaling polarity—from signal off to signal on—in sensor performance c) at 100 Hz, more current is the result of unbound probe and minimal current from the bound probe. (d) at 5 Hz, the charge transfer reaction of the unbound probe has decreased because the sample has already been measure by time the transfer has been taken place, and the bound probe has increased [3,12].

3.3 Experimental Methods

3.3.1 Reagents and Materials

All solutions were prepared with deionized, ultrafiltered water (Fisher Scientific). The following reagents were used as received: 4-(2-hydroxyethyl)-1-piperazineethanesulfonic acid (HEPES) (99.5%), sodium perchlorate ($NaClO_4$) (98.0-102.0%), tris-(2-carboxyethyl) phosphine hydrochloride (TCEP), and 6-Mercapto-1-hexanol (97.0%) from Sigma-Aldrich (St. Louis, MO). Methylene blue-conjugated DNA (MB-DNA) was purchased from Biosearch Technologies (Novato, CA), purified by reverse phase HPLC. Oligonucleotides were obtained from Integrated DNA Technologies (IDT; Coralville, Iowa), with purity and yield confirmed by mass spectrometry and HPLC, respectively. Sequences (listed 5′ to 3′) for polyadenine SH-DNA are listed in **Table 3.1**.

Table 3.1	Single-Stranded Thiolated-Poly(n) Adenine DNA Used in Length Dependence Study
0A_Bistable_Thio_G10	/5ThioMC6-D/GCATGGTGACATTTTTCGTTCGTTAGGGTTCAAATCCGCG
1A_Bistable_Thio_G10	/5ThioMC6-D/AGCATGGTGACATTTTTCGTTCGTTAGGGTTCAAATCCGC
2A_Bistable_Thio_G10	/5ThioMC6-D/AAGCATGGTGACATTTTTCGTTCGTTAGGGTTCAAATCCG
3A_Bistable_Thio_G10	/5ThioMC6-D/AAAGCATGGTGACATTTTTCGTTCGTTAGGGTTCAAATCC
4A_Bistable_Thio_G10	/5ThioMC6-D/AAAAGCATGGTGACATTTTTCGTTCGTTAGGGTTCAAATC
5A_Bistable_Thio_G10	/5ThioMC6-D/AAAAAGCATGGTGACATTTTTCGTTCGTTAGGGTTCAAAT
6A_Bistable_Thio_G10	/5ThioMC6-D/AAAAAAGCATGGTGACATTTTTCGTTCGTTAGGGTTCAAA
7A_Bistable_Thio_G10	/5ThioMC6-D/AAAAAAAGCATGGTGACATTTTTCGTTCGTTAGGGTTCAA
8A_Bistable_Thio_G10	/5ThioMC6-D/AAAAAAAAGCATGGTGACATTTTTCGTTCGTTAGGGTTCA
9A_Bistable_Thio_G10	/5ThioMC6-D/AAAAAAAAAGCATGGTGACATTTTTCGTTCGTTAGGGTTC
11A_Bistable_Thio_G10	/5ThioMC6-D/AAAAAAAAAAAGCATGGTGACATTTTTCGTTCGTTAGGGT
14A_Bistable_Thio_G10	/5ThioMC6-D/AAAAAAAAAAAAAAGCATGGTGACATTTTTCGTTCGTTAG
19A_Bistable_Thio_G10	/5ThioMC6-D/AAAAAAAAAAAAAAAAAAAGCATGGTGACATTTTTCGTTC

Abbreviations: G10=Gold 10, /5ThioMC6-D/= disulfide bond flanked by two six-carbon spacers (IDT)

3.3.2 Preparation of the Gold Electrodes

The electrodes used to measure the length dependence of MB-DNA were fabricated using a gold working electrode (CH Instruments, d = 2.0 mm). The gold electrode was first immersed into fresh piranha solution (H_2SO_4/H_2O_2, 3:1) for 5 min, rinsed with D. I. water, and dried under a stream of nitrogen gas. (*Caution: piranha solution is dangerous to human health and should be used with extreme caution and handled only in small quantities*.) Then, electrodes were polished carefully to a mirror surface with an aqueous slurry of 0.05 μm diameter alumina particles, followed by successive washing in an ultrasonic cleaner with water and ethanol at a 1:1 ratio. Electrodes were then rinsed with D.I. water and dried under flowing nitrogen gas. The gold electrodes were further cleaned by a series of oxidative and reductive scans in 0.5 M H_2SO_4 by scanning the potential from −0.35 to +1.5 V at a scan rate of 4.0 V s^{-1} for 20 cycles using CV, again with a scan rate of 0.1 V s^{-1} for 4 cycles, then finally washed with D. I. water dried under flowing nitrogen gas.

3.3.3 DNA Monolayer Assembly

The volume for the preparation of electrode-immobilized probe is dependent upon the number of electrodes to be prepared and is intended to conserve reagents. Prior to modification of the electrode, a mixture of 200 μM SH-DNA and 10 mM TCEP was made at a 1:3 ratio, respectively in a 200 μL PCR tube. The tube was incubated for 60 minutes at room temperature (25°C) for reduction of disulfide bonds in the S-DNA. The solution was then diluted to a total volume of 300 μL in HEPES buffer (10 mM HEPES and 0.5 M $NaClO_4$, pH 7.0) to a final concentration of 1.25 μM. Unless otherwise noted, all solutions used in the experiments to

follow were made with this HEPES buffer. For immobilization, the previously cleaned gold electrode was transferred directly to the diluted and reduced S-DNA solution and incubated for 60 min at room temperature in the dark. Following the formation of a self-assembled monolayer (SAM), excess S-DNA physically adsorbed on the electrode surface was removed with deionized water rinse (~ 20 s). The stream of deionized water should flow gently over the modified electrode, not directly normal to the surface at high flow rate. Modified electrodes were immediately transferred to 3 mM 6-mercaptohexanol (MCH) solution for 60 min at room temperature in the dark (**Figure 3-2**). It is important to note that 6-Mercaptohexanol solution should be prepared immediately before use, and it is better to do so in the fume hood due to the strong odor. MCH is used in the final step as both a spacer molecule that removes and replaces loosely bound nucleic acids and as a passivating molecule to prevent nonspecific adsorption of solution components[9].

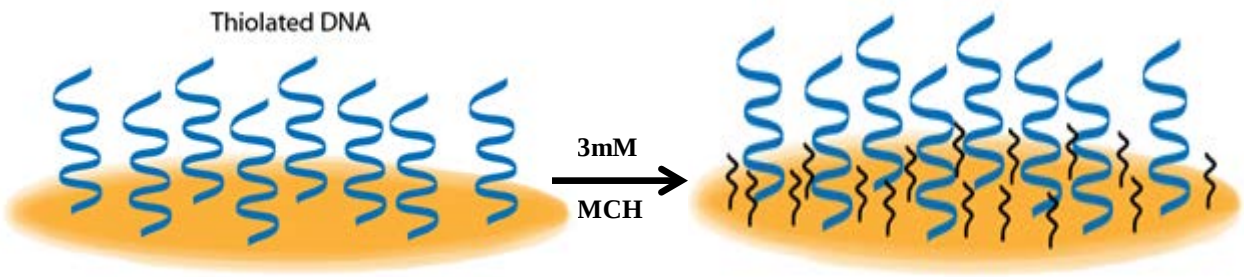

Figure 3.2: Thiolated-DNA modified gold working electrode before and after transferred to 3 mM 6-mercaptohexanol solution.

3.3.4 Electrochemical Measurements

Electrochemical Interrogation

All measurements were performed using a Reference 600 Potentiostat (Gamry Instruments Inc, Warminster, PA). Square wave voltammetry was performed using a step

potential of 1 mV and 50mV amplitude at various frequencies. Net peak currents were recorded for the data presented herein. All sensors were tested before and after incubation for overnight saturation of target concentration. Data was analyzed using Microsoft Excel. A linear fit baseline correction was used to correct all baselines.

3.4 Results and Discussion

3.4.1 Our Hypothesis

With current literature based on electrochemical biosensors thriving in the analytical field, our group decided to investigate not only DNA-driven assay responses to targets, but to gain clarity about the distance dependence of the redox molecule attached to the DNA probes. Our SH-DNA from which the monolayer was formed consisted of 40 nucleotides, and the strands were modified near the electrode (and near the target binding region) by adding a series of polyadenines to the 5' end. To ensure consistency in overall molecular weight, an equal number of strands were removed from the 3' ends of the DNA, so that the MB-DNA (100 nM) could bind to the first 10 nucleotides of the DNA monolayer. By enhancing our understanding of the distance dependence of SWV current at the electrode, we will be better equipped to design the surface-based hairpin switch assays discussed in Chapter 4. We hypothesized that by moving the MB-DNA further away from the electrode surface, the SWV current would decrease in proportion to the number of nucleotides included in the spacer region, over the range of all frequencies. (**Figure 3.3**).

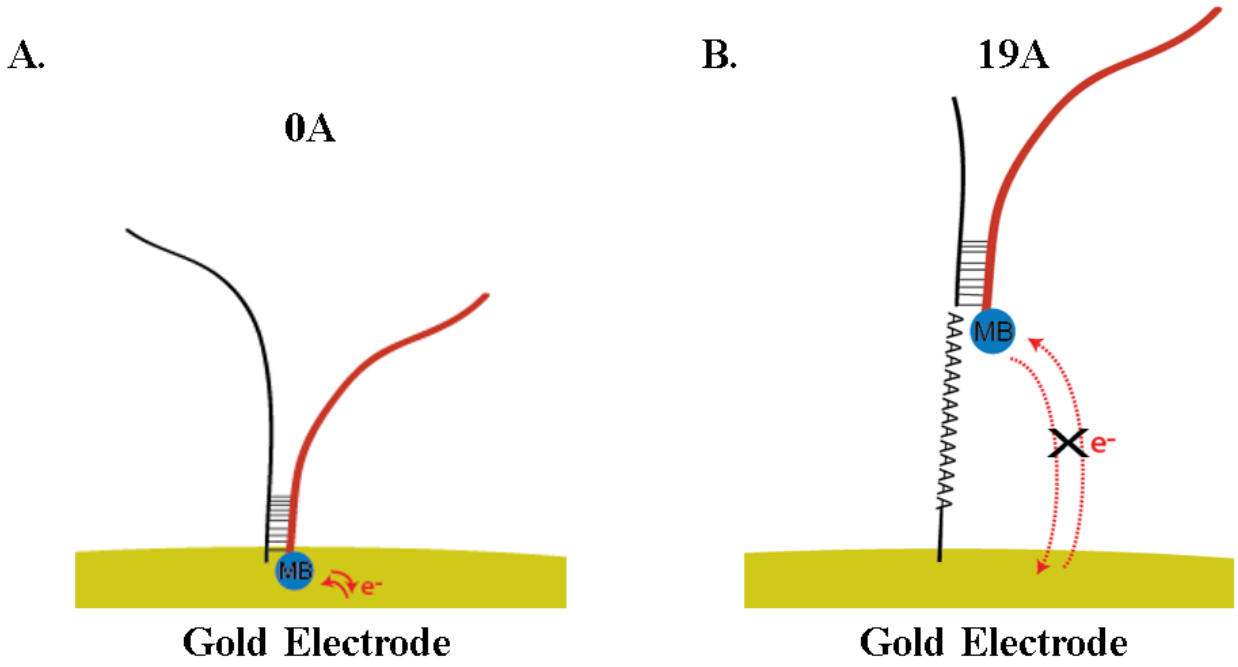

Figure 3.3: Hypothesis A) MB-DNA at its shortest distance from the surface (No adenine spacers, 0A) B) 19-adenine spacer added to increase the distance of the MB-DNA from the surface (19A). Electron transfer is not as proficient

Figures are not drawn to scale

3.4.2 SWV measurements by varying the pulse potential frequency

We used the batch processing feature of the potentiostat's software, the "sequence wizard," to serially vary the f_{SWV} over the range from 1 to 1000 Hz, while scanning from -0.45 V to 0 V. During this study of the distance dependence of MB-DNA current, we found that each different polyadenine-S-DNA length exhibited curious behavior as a function of f_{SWV}. At low frequencies, we observed that the MB-DNA farthest from the electrode surface such as 19A_Bistable_Thio_G10 (19-adenine spacer), had a higher net peak current than the MB-DNA

closer to the surface, such as 0A_Bistable_Thio_G10 (no adenine spacer), which can be observed in the SWV data shown in **Figure 3.5A**. Conversely, the application of a high frequency reversed this phenomenon (**Figure 3.4B**). Frequency is inversely related to time, so one might speculate that the behavior could be related to the different kinetics of hybridization of the different polyadenine-S-MB-DNA complexes. However, to avoid kinetic differences, we allowed the electrodes to incubate overnight (16 h) in 100 nM of each MB-DNA so that the complex would reach equilibrium prior to measurement. Since hybridization kinetics were ruled out, the most likely explanation for this effect is that at low f_{SWV}, the electron transfer (oxidation and reduction) from the MB-DNA closest to the surface (no spacer, 0A) is essentially complete before the current is sampled in each SWV pulse, which leads to a much smaller signal at 1 Hz. In contrast, as the f_{SWV} parameter is increased (to 6 Hz or higher), the MB-DNA that is closest to the working electrode surface (0A) is strongly increased in comparison to the MB-DNA farthest away (19A) due to the delayed electron transfer reactions of the MB-DNA attached to the 19A probe, as a result of the extended tethered diffusion range.

Electrochemical Reaction Rates

The current and the frequency relationship in SWV is dependent on the rate at which the electrons are transferred to and from (oxidation and reduction) the electrode and MB, which is mainly governed by the distance range at which the MB label can exhibit tethered diffusion [5]. Moreover, in comparing spacer lengths, for example 0A and 19A, there will be a frequency at which the two current-versus-frequency curves cross. Above this crossover frequency, more rapid electrode-MB collisions (shorter spacer) produce greater current; below it, the situation is reversed (**Figure 3.4A-B**). SWV is particularly suitable as a readout method because it can

distinguish between these different cases. Although our hypothesis was confirmed at high frequencies, where a larger spacer resulted in less overall current, it was rejected at low frequencies, thus our results disproved our original hypothesis.

Since our system is primarily surface bound, SWV is essentially being used to measure the apparent electron transfer rates at the surface. As described previously, this can be observed by finding the "characteristic electrochemical reaction time" which appears as a maxima in the relationship of i_p/f_{SWV} vs $1/f_{SWV}$ (where i_p is peak current in amps and f_{SWV} is the SWV frequency in Hz) [10,11]. Performing such an evaluation on the various lengths of our sensors demonstrates that all 13 lengths exhibit significant, distance-dependent changes in characteristic reaction times. The fixed position of MB-DNA defined the apparent electron transfer rate and its characteristic reaction time, as seen in **Figure 3.5** Thus, as shown by this analysis, the characteristic electrochemical reaction time exhibits predictable behavior with respect to the distance of the redox moiety from the electrode surface.

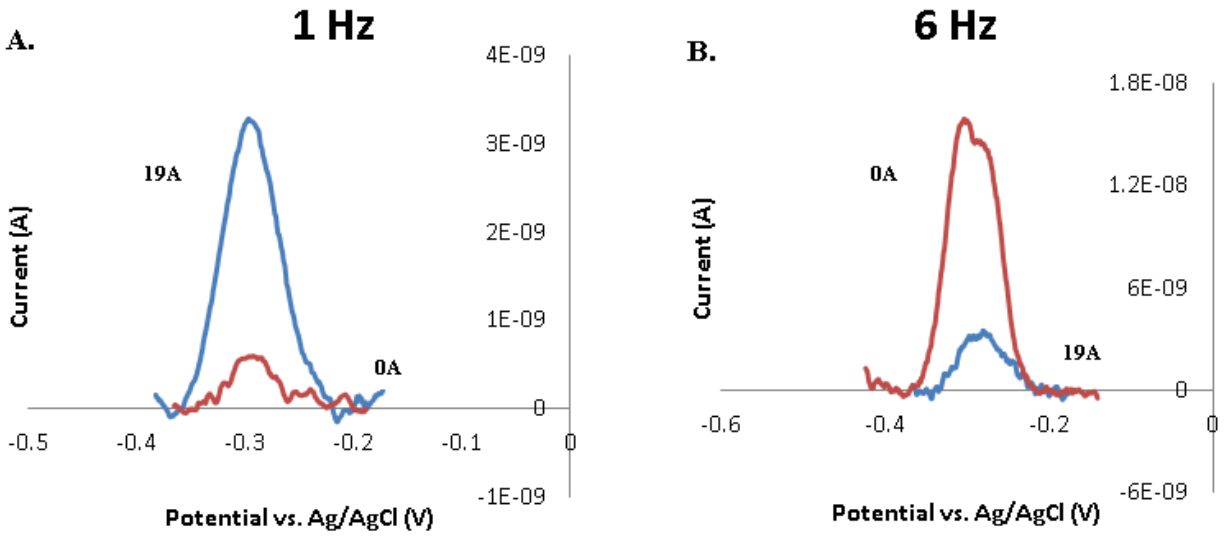

Figure 3.4: A) The rapid transfer reaction of the 0A probe will have largely decayed before the current is sampled, thus leading to a much smaller signal at 1 Hz, than that obtained from 19A. B) In contrast, if f_{SWV} is set to 6 Hz or higher, the 0A current is higher than 19A due to the delayed electron transfer reaction of the 19A probe because of the extended tethered diffusion range.

It is interesting to note that, although the fastest electron transfer reaction occurred with the 0A spacer, the poly-adenine length of 4A showed the highest overall peak current (**Figure 3.6**). This effect is likely a result of repulsion of DNA hybridization by the electric double layer on the electrode surface, since it does not occur with more stable DNA hybridization reactions with more than the 10 base pairs shown here (data not shown). Studies of this effect are part of another student's dissertation work and will not be discussed further in this thesis. However, this effect explains why the bi-stable hairpin switch sensor developed in Chapter 4 was designed with a 4A spacer.

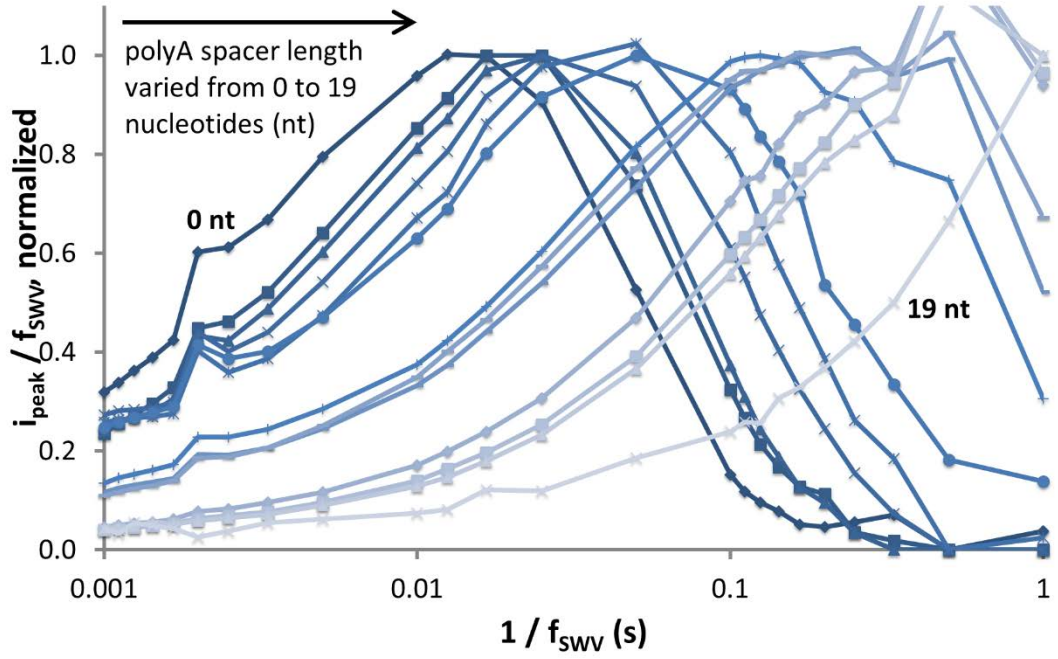

Figure 3.5: The relationship between peak current/f and 1/f exhibits a maxima at a critical frequency related to the apparent electron transfer rate. As the polyA length increases; there is a shift in this critical frequency from left to right which is due to a decrease in electrochemical reaction rate.

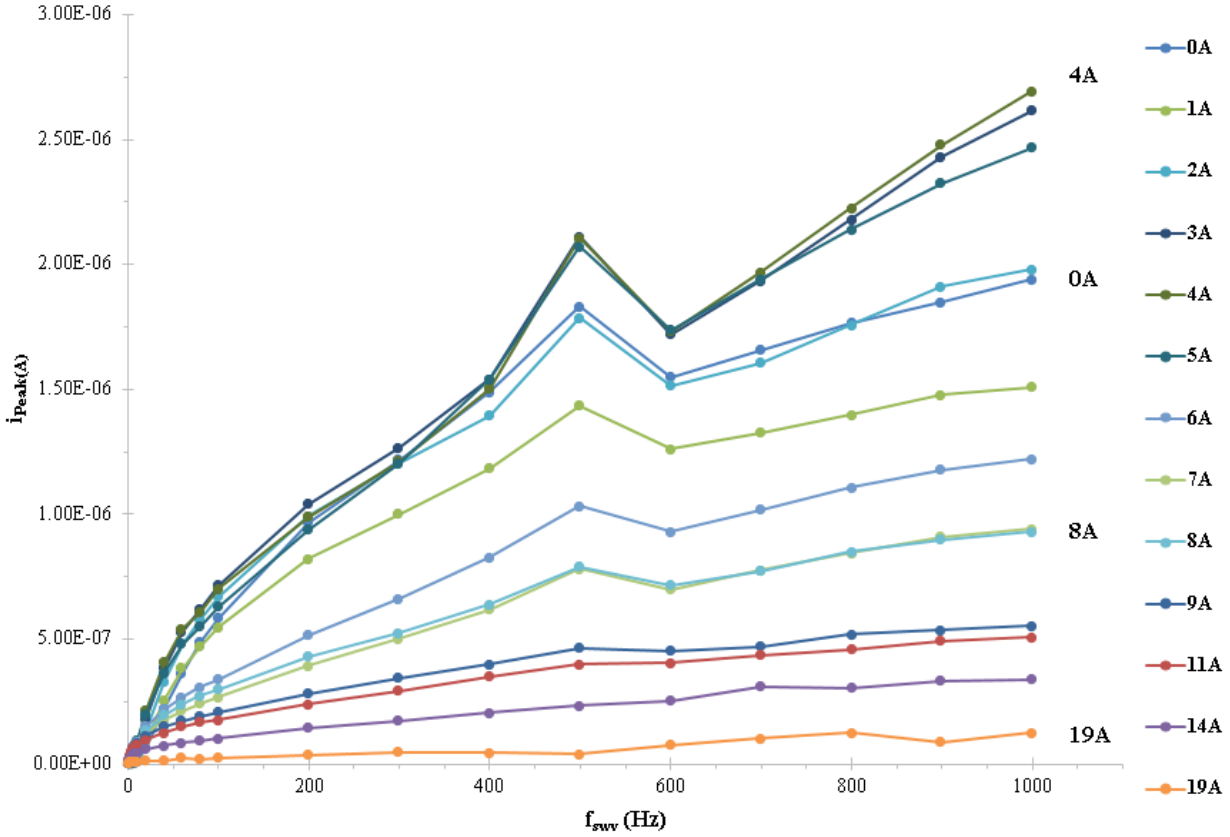

Figure 3.6: Peak height versus SWV frequency relationship. The highest current output is the distance of MB-DNA that is moved from the electrode by a 4a spacer.

DNA-Tethered Methylene Blue as it relates to Diffusion

Here, we have observed the MB-DNA displaying behavior similar to the model of a tethered diffusion system described by Huang and White [5]. In our case, since the amplitude of the square wave in SWV is relatively large (50 mV), we can compare our f_{SWV} to the cyclic voltammetric scan rate in their model system. In this way, we can say that as we move our MB-DNA farther from the surface, the hemispherical radius of diffusion is increased, which allows the MB to move more freely and reduce the collision rate with the electrode, thereby reducing the electron transfer rate. If this model accurately describes our system, the SWV current should

be linearly proportional to the square root of f_{SWV}[5]. This can be understood by the depictions and data shown in **Figure 3.7**. At one extreme, at high f_{SWV} or with long spacers (or both), the system will behave similarly to a diffusion-limited reaction (**Figure 3.7A**). Indeed, our data shows a clear dependence on the square root of f_{SWV} (**Figure 3.7B**), as expected. At the other extreme, at low f_{SWV} or with short spacers (or both), the system will behave as if it is an adsorbed redox molecule (**Figure 3.7C**). Again, our results agree with this model at low frequency (**Figure 3.7D**). Ovearall, the tethered MB in our system behaves similarly to either an adsorbed or a diffusion limited system, depending on the distance of the MB moiety relative to the diffusion layer thickness [5]. When we have the MB tethered by a 0A spacer, it reacts as an adsorbed molecule, which should occur when the diffusion layer thickness (L_{DL}) is at least ~10 times larger than the spacer length (**Figure 3.7C**). If the MB is tethered by a 19A spacer, the diffusion layer thickness should be at least ~10 times smaller than the tether, i.e. the MB hemisphere length (L_{MB}), and the system will behave as if it is diffusion limited (**Figure 3.7A**).

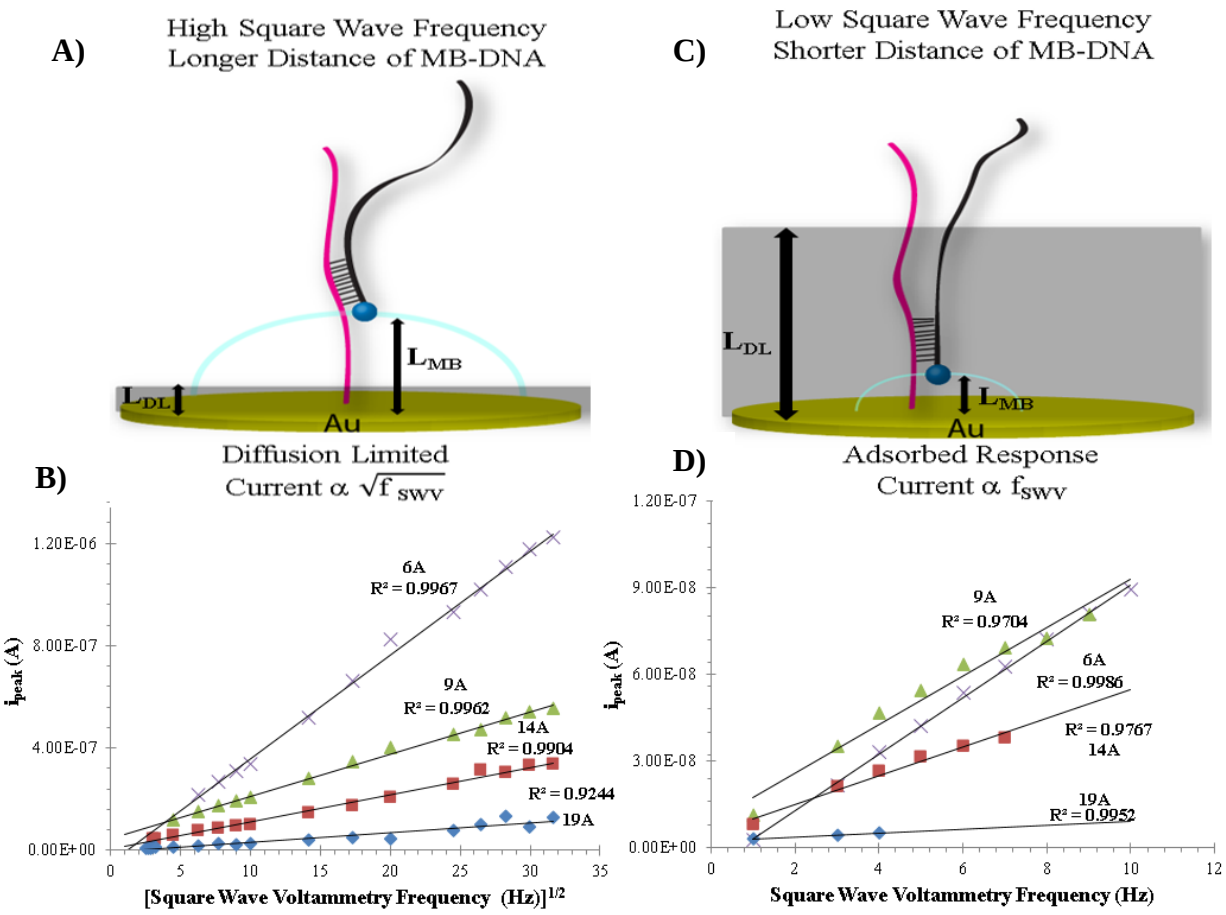

Figure 3.7: Methylene Blue DNA tethered to an electrode surface bound to a ssDNA linker with various lengths to measure the length dependence of MB. A) Longer linker increases the L_{MB} from the surface, which decreases the L_{DL} by 10 fold. B) Experimental data obtained with various lengths (6A, 9A, 14A, 19A) When using high SWV frequencies, the voltammetric peak height current is proportional to the square root of the frequency. C) Shorter linker decreases the L_{MB} from the surface, gives rise to $L_{DL.}$ D) At low frequencies, the peak height current is proportional to the SWV frequency which increase current.

A, C are not drawn to scale, R^2 value based of the average of three independent electrodes. Error bars not shown for clarity

3.5 Conclusions

In this chapter, we have evaluated the distance dependence of MB-DNA signal in square wave voltammetry by varying the length of a spacer region in the DNA sequence. Although we hypothesized that moving the MB-DNA further from the electrode would decrease current at all square wave frequencies (f_{SWV}), our observations showed that this was only true at higher frequencies. This behavior was explained by comparing our system to the tethered diffusion model of Huang and White [5]. Ultimately, this work has resulted in the characterization of our system as a function of spacer length (0A through 19A), which is exemplified in **Figure 3.8**. In our system, the characteristic electrochemical reaction time (t_{ec}) exhibited a predictable increase (slower reaction) as the polyadenine spacer length was increased from 0A to 19A. As discussed in chapter 4, this information was essential in designing our novel, surface-bound, bistable hairpin switch sensor. Broadly, we believe this information gathered on the distance dependence of MB-DNA signal in SWV should be beneficial for the development and/or optimization of any DNA-driven electrochemical biosensors.

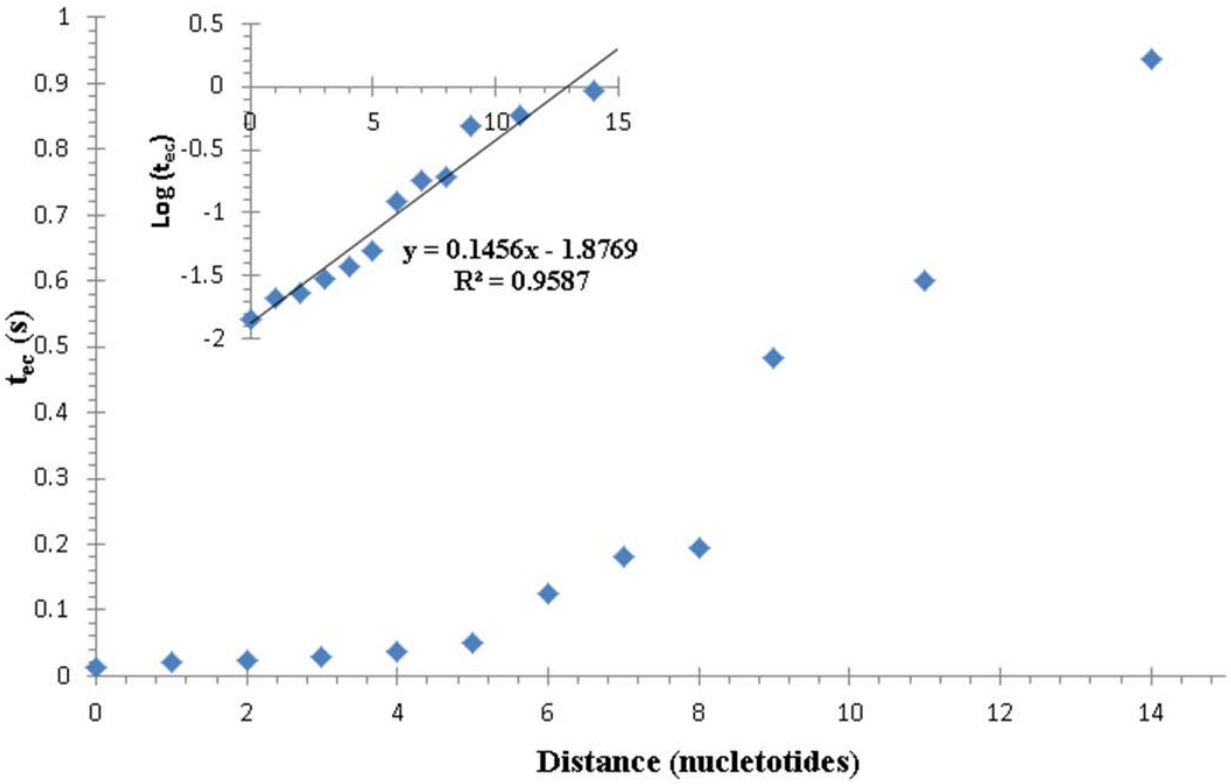

Figure 3.8: The distance dependence of the electrochemical reaction time of MB-DNA is shown above. As the MB-DNA increases in distance from the electrode, the electrochemical reaction time (t_{ec}) also increases. The insert shows the log scale of the linear relationship between the nucleotide length and $t_{ec.}$

3.6 References

(1) Kimura-Suda, H.; Petrovykh, D. Y.; Tarlov, M. J.; Whitman, L. J. *J. Am. Chem. Soc*. 125, 30, 9014-9015.

(2) Xiao, Y.; Lai, R. Y.; Plaxco, K. W. *Nat. Protoc.* 2007, *2* (11), 2875–2880.

(3) White, R. J.; Plaxco, K. W. *Anal. Chem.* 2010, *82* (1), 73–76.

(4) Liu, Y.; Tuleouva, N.; Ramanculov, E.; Revzin, A. *Anal. Chem.* 2010, *82* (19), 8131–8136.

(5) Huang, K.-C.; White, R. J. *J. Am. Chem. Soc.* 2013, *135* (34), 12808–12817.

(6) Ricci, F.; Zari, N.; Caprio, F.; Recine, S.; Amine, A.; Moscone, D.; Palleschi, G.; Plaxco, K. W. *Bioelectrochemistry* 2009, *76* (1), 208–213.

(7) Murray, R. W. *Acc. Chem. Res.* 1980, *13* (5), 135–141.

(8) Ikeda, R.; Kobayashi, S.; Chiba, J.; Inouye, M. *Chemistry* 2009, *15* (19), 4822–4828.

(9) Arinaga, K.; Rant, U.; Kneževi, J.; Pringsheim, E.; Tornow, M.; Fujita, S.; Abstreiter, G.; Yokoyama, N. *Biosens. Bioelectron.* 2007, *23*, 326–331.

(10) Jeuken, L. J. C.; Mcevoy, J. P.; Armstrong, F. A. *J. Phys. Chem. B* 106, 9, 2304-2313.

(11) Komorsky-Lovrić, Š.; Lovrić, M. *J. Electroanal. Chem.* 1995, *384* (1–2), 115–122.

(12) Schoukroun-Barnes, L. R.; Macazo, F. C.; Gutierrez, B.; Lottermoser, J.; Liu, J.; White, R. J. *Annu. Rev. Anal. Chem* 2016, *9*, 163–181.

Chapter 4

Amplification-free Bistable Nucleic Acid Switch using Square Wave Voltammetry

4.1 Introductory remarks

Based on the high demand for inexpensive, sensitive, and robust nucleic acid sequence technologies, we have designed and developed a novel electrochemical biosensor based on a bi-stable hairpin switch. The electrochemical bi-stable switch sensor (E-BSS) targets the quantification of nucleic acids, such as DNA, RNA, microRNA (miRNAs) in a sequence-specific manner by exploiting parameters of square-wave voltammetry (SWV) without the need of washing steps or external reagents. The system was designed by exploiting our understanding of the distance dependence of SWV current as a function of f_{SWV} (see chapter 3). By modifying the cleverly designed bistable allosteric DNA catalyst from Zhang and Winfree [1], we hypothesized that a surface-confined MB-DNA signaling strand could be moved closer to the electrode in a target-dependent manner. The results herein have supported our hypothesis. This assay design should provide a generalizable sensing strategy for rapid, highly selective, and cost-effective detection of any DNA or RNA targets, and the instrumentation is ideal for point-of-care applications.

4.2 Prior work

Electrochemical DNA Sensors

There has been increased interest in the development of fast, sensitive, and cost-effective nucleic acid sensing devices for sequence-specific detection of clinically, environmentally, and government security-relevant nucleic acid targets. [2–4] These sensors have gained much attention for their appealing features such as high sensitivity and fast response as well as low power usage, cost, and reagent requirements.[5,6] Since the creation of electrochemical DNA sensors, numerous techniques have been developed, most of them applied to the improvement of sensitivity and selectivity for better electrochemical DNA detection.[7–11] There are various types, such as the "sandwich-type" which is popularly used.[9,12] A typical "sandwich" DNA sensor utilizes a pair of DNA probes that are designed to bind to the target sequence. The capture probe is immobilized on the surface of electrodes, and then the target DNA and the redox tagged molecule are added in solution and are brought into the proximity of the electrode surface. After the formation of the complex "sandwich" (capture probe, target, and redox-molecule), the redox moiety is localized to the surface and produces the measurable electrochemical current signal using a voltammetric technique. Clearly, DNA immobilization at the surface plays an important role in the performance of these DNA sensors. To better control this process, Tarlov and co-workers proposed an innovative mixed self-assembled monolayer (SAM), which consisted of thiolated oligonucleotides and a dilution molecule, 6-Mercapto-1-hexanol (MCH) [13]. MCH is beneficial because it not only helps sensing DNA oligos stand up at the surface, but it can also repel non-specific adsorption of DNA or matrix proteins that are not useful in the reaction[14]. SH-DNA and MCH mixed monolayers are ideal for electrochemical (EC) DNA sensors because they are able

to bind and create signal from DNA targets at low concentrations with high DNA specificity. In all work presented in this dissertation, MCH-stabilized mixed monolayers have been used.

DNA Engineering

A sizeable fraction of the pioneering work in the computational aspects of DNA engineering and sensing has been conducted by the Winfree group at the California Institute of Technology. Their work consists of molecular engineering that uses only nucleic acids molecules as a framework for constructing mechanical and catalytic components that can create artificial "DNA circuits." These customizable circuits could feasibly control processes of cells and organisms in the future.[1,15–24] In their paper entitled, "Dynamic Allosteric Control of Noncovalent DNA Catalysis Reactions," they designed and demonstrated an allosteric molecule of DNA that, in its active configuration, can catalyze a noncovalent cyclic reaction composed of only DNA strands participating in hybridization and strand-displacement interactions.

One of the major advantages of using only DNA sequences is that the arrangement of strand interactions is determined by domain complementarities, leveraging the reverse complementary of DNA sequences (base pairing) and allowing these reactions to be designed in a more-or-less computational manner. Winfree et al. successfully created a catalytic cycle that can be controlled by adding in a switchable allosteric catalyst strand (AC) to either speed up or slow down the reaction. The inhibitor (Inh) and an activator (Act) strands, which in this case were two single-stranded pieces of DNA, controlled the catalytic activity of the allosteric catalyst (AC). The terms AC-ON and AC-OFF were used to describe the DNA's transition states in the cycle, which can be interchanged due to thermodynamics. The AC-ON state consisted of a 10 base-pair hairpin structure, and the AC-OFF state was an 8 base-pair hairpin; the AC-ON state is

more thermodynamically favored. As depicted in **Figure 4.1**, where each number represents a domain (**Table 1.1**), the AC-ON is converted to the AC-OFF state by reaction with an inhibitor strand (Inh), which binds to AC at the domain $\overline{9}$ and removes domain 10. Similarly, with the addition of the activator strand (Act), the catalytic activity can be restored as AC-OFF rearranges to the thermodynamically favored AC-ON state.

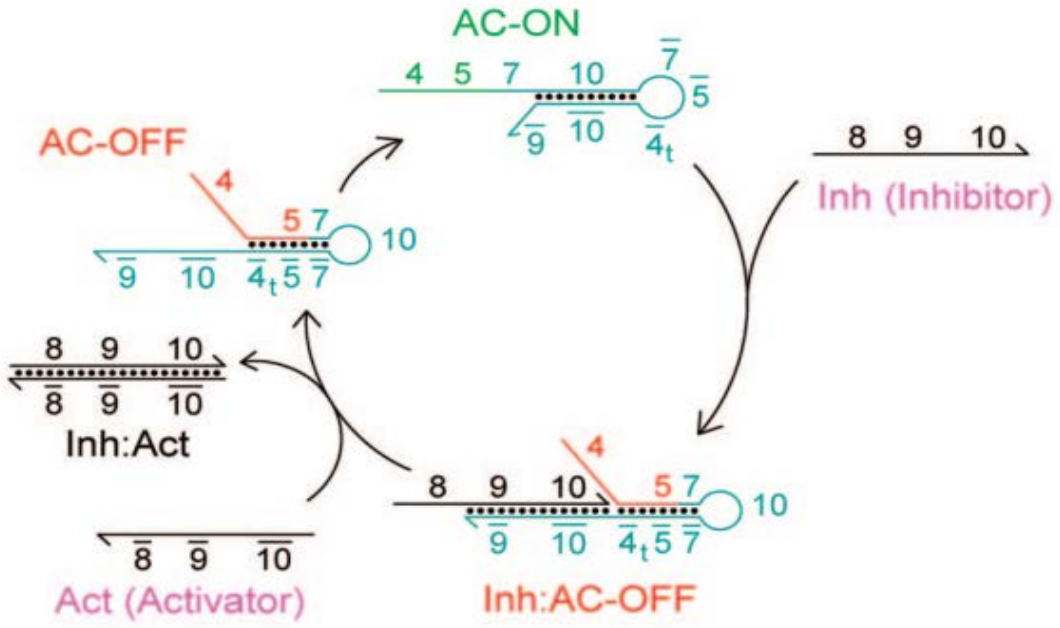

Figure 4.1: Zhang and Winfree design of an allosteric catalyst state that changed via the addition of inhibitor (Inh) and activator (Act). Inh binds to AC-ON to form the Inh:AC-OFF complex. Act binds to Inh:AC-OFF to remove the AC-OFF duplex and the waste product of Inh:Act. AC-OFF then spontaneously converts to AC-ON.

Reprinted with permission Copyright © (2008) American Chemical Society [1]

Based on this approach, we created a DNA switch sensor for electrochemical readout. Using the system in **Figure 4.1** as a model of our EC sensor design, we simply removed the Activator step. Our sensing approach (see **Figure 4.6** below) consists of an equivalent to AC-ON as our surface-confined DNA sequence, where the signaling molecule (MB) is held away from the electrode. Our target DNA strand is represented by the Inh strand in **Figure 4.1**, such

that the MB label is moved closer to the electrode surface in the presence of target DNA. It should be noted that, in this analogy, our sensor's "Signal-ON" and "Signal-OFF" states are mimics of the "AC-OFF" and "AC-ON" state in **Figure 4.1**.

MicroRNA detection

The widespread adaption of polymerase chain reaction (PCR) to detect small DNA/RNA such as microRNA (miRNA), although valuable, exhibits various disadvantages such as the use of multiple reagents, expense, and significant time consumption. miRNAs are short (~22 nucleotides) noncoding RNA molecules that regulate gene expression post-transcriptionally, mainly by binding with messenger RNAs (mRNA) to inhibit the production of proteins. [25,26] These small RNAs used to be considered "junk DNA" for many years until accumulating evidence linked miRNA to diseases including cancer, various developmental defects, and now even diabetes[27], which is a major focus of our laboratory's research. Poy et al. uncovered the correlation of various miRNAs in pancreatic endocrine cell lines. Among those, miR-375 was shown to be overexpressed. miR-375 participates in the glucose-stimulated insulin secretion process, and its inhibition enhances insulin secretion. [28,29] It is interesting to note that miRNAs only make-up a minute fraction of total RNA mass (0.01%). [30] Since there is minimal content available in biological samples of miRNA, there has been a strong push to improve sensitivity by using various nucleic acid (NA) amplification strategies. Although there are a variety of electrochemical methods developed for NA detection, these are mostly concentrated on using nanostructured materials to improve sensitivity. [31,32]

4.3 Experimental methods

4.3.1 Reagents and materials

All solutions were prepared with Ultra-Pure distilled Water (Invitrogen). The following reagents were used as received: sodium chloride purchased from British Drug House, and dimethyl sulfoxide (DMSO) purchased from Anachemica. BioPerformance certified 4-(2-hydroxyethyl)-1-piperazineethanesulfonic acid (HEPES) tris (2-carboxyethyl) phosphine hydrochloride (TCEP), mercaptohexanol, gold etchant, and chromium etchant from Sigma-Aldrich. Gold-sputtered glass slides (100 nm Au with 5 nm Cr adhesion layer) were purchased from Deposition Research Lab (St. Charles, MO), with dimensions of 1.0 in. × 3.0 in. × 0.44 in. (width, length, thickness). AZ 40XT (positive photoresist) and AZ 300 MIF developer was obtained from MicroChemicals. Polydimethylsiloxane (PDMS) was purchased from Dow Corning. Human serum purchases from BioIVT. Methylene blue-conjugated DNA (MB-DNA) and miR-MB-DNA was purchased from Biosearch Technologies (Novato, CA), purified by RP-HPLC. Oligonucleotides were obtained from Integrated DNA Technologies (IDT; Coralville, Iowa), with purity and yield confirmed by mass spectrometry and HPLC, respectively. Loop-DNA and miR_Loop-DNA sequence was PAGE purified due to the length of the oligonucleotide. Sequences (listed 5′ to 3′) for the EC bistable sensor are listed in **Table 4.2**. LabVIEW system design software was used to operate our in-house built temperature controller.

4.3.2 Fabrication of bistable switch

There are various software packages can be used to design oligonucleotide sequences, and the design proposed here should function similarly for many different sequences.[33] Our laboratory typically uses the design software referred to as the Nucleic Acid Package (NUPACK), with design structures optimized at room temperature. The sequences listed in **Table 4.2** below were designed in such as manner, thus these sequences represent just one possible set of optimal sequences for such a sensor. The gold-bound SH-DNA sequence (4A_Thiol) is the same as described in **Table 3.1**; only domains e through j (**Table 4.1**) were designed for this work. First, random sequences composed of only A, C, and G were generated for domains e-i. Sequences for the complementary barred domains were constructed accordingly. Next, DNA structures that were expected to be problematic, such as poly-G regions and poly-A regions, were altered by hand. The remaining sequences were then designed by NUPACK as appropriate to form the desired DNA/RNA strand complexes. Finally, the strands were checked in the NUPACK analysis package to minimize hybridization crosstalk.

Domain	Sequence	Length (nt)
a	5’-AAAA-3’	4
b	5’-GCATGGT-3’	7
c	5’-GAC-3’	3
d	5’-ATTTTTCGTTCGTTAGGGTTCAAATC-3’	26
e	5’-AGACG-3’	5
f	5’-AAG-3’	3
g	5’-AAAGAAAAGA-3’	10
h	5’-AGA-3’	3
i	5’-AGAAAGAAGAAAGAGA-3’	16
j	5’- TT TCC TCT TTT TCT-3’	14

Table 4.1 Domain Sequences for DNA E-BSS

Strand	Domains	Sequence
4A_Thiol	a b c d	/5ThioMC6-D/AAAAGCATGGTGACATTTTTCGTTCGTTAGGGTTCAAATC
Loop	i h g b f e $\overline{d}$	AGAAAGAAGAAAGAGAAGAAAAGAAAAGAGCATGGTAAGAGACGGATTTGAACCCTAACGAACGAAAAAT
MB-DNA	$\overline{i}$ j $\overline{f}$ $\overline{b}$	TCTCTTTCTTCTTTCTTTTCCTCTTTTTCTCTTACCATGC
Target	$\overline{f}$ $\overline{b}$ $\overline{g}$	TCTCTTACCATGCTCTTTTCTTT
miR_4A_Thiol		/5ThioMC6 D/AAAACGAACGAGCGGACAGGTGTTCGTTAGGGTTCAAATC
miR-MB-DNA		TCTCTTTCTTCTTTCTTTTCCGTCTTTTTTTGTTCGTTCG/MB/
miR_Loop-DNA		AGAAAGAAGAAAGAGAAGACGGTAATCTCACGCGAGCCGAACGAACAAATGGATTTGAACCCTAACGAAC
miRNA-375		UUUGUUCGUUCGGCUCGCGUGA
Scrambled RNA		GUUCUGCUGUCUGCCGAGUGUU

Table 4.2 Oligonucleotide Sequences used in DNA/RNA E-BSS

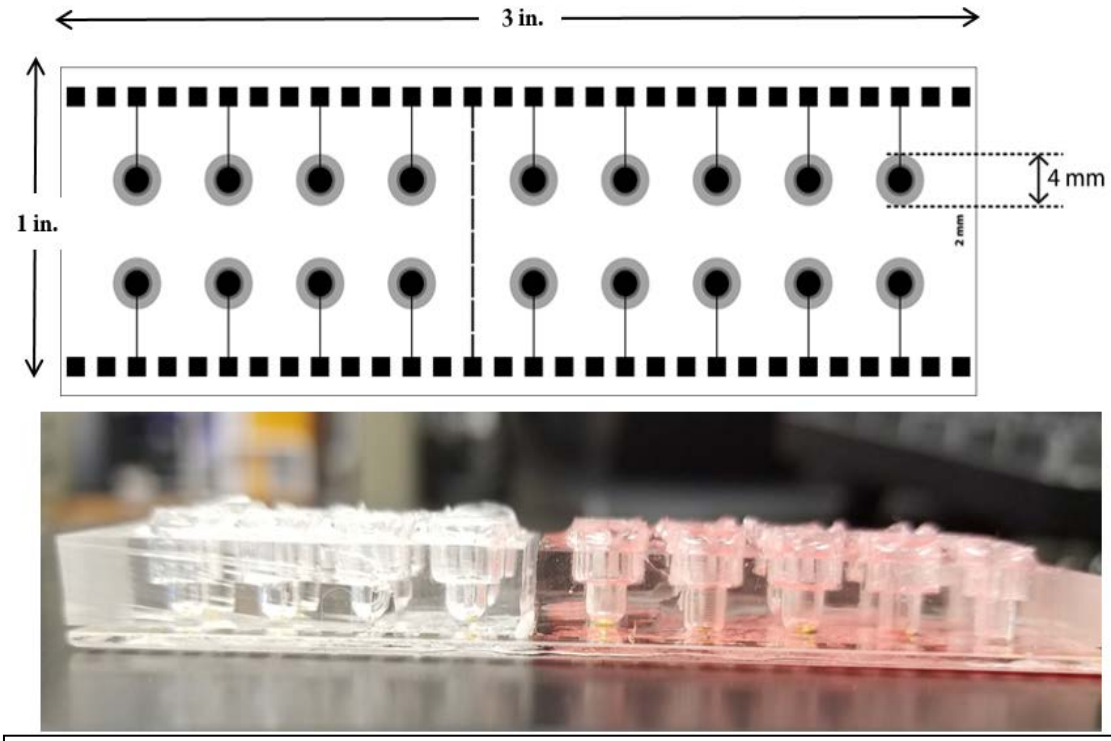

Figure 4.2: Photomask design used for gold-on-glass slide (GoG) preparation. At the top, the microscopic slide mask design is shown, where 18 individual electrodes can be made from a single microscope slide sized GoG. The light grey depicts the, fluidic portion of one chip (4 mm). At the bottom, this is a side view of the GoG chip that has been plasma oxidized to PDMS. The bottom reservoir hold minute amounts of solution to reduce overall volume. The top reservoir houses the reference and counter electrode.

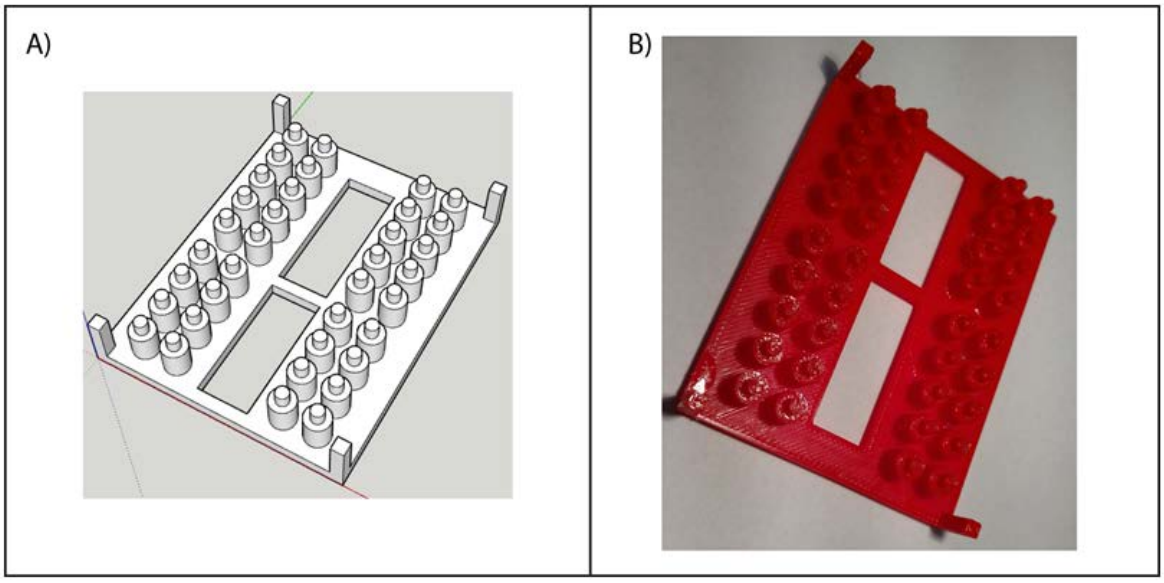

Figure 4.3: 3D-CAD (left) and printed PLA template (right) used for PDMS electrochemical cell fabrication.

4.3.3 Preparation of Gold on Glass electrodes and EC Cells

The preparation of SAMs in early experiments used a commercially available electrode, but for most of the later experiments we used a customized gold-on-glass electrode (GoG). The electrode patterns were designed digitally in Adobe Illustrator, and Fineline Imaging (Colorado Springs, Colorado) printed the corresponding positive photomasks. The mask shown in **Figure 4.2** houses eighteen individual electrodes that can be fabricated on a single microscope slide. Using AZ 40XT photoresist, standard photolithographic procedures were followed to make the photoresist pattern on a gold-coated slide. Then the slide was introduced into gold enchant followed by chromium etchant for 30 s and 15 s, respectively. DMSO was heated to 110 ℃, and the electrode was immersed for 30 min, removing any leftover positive photoresist and exposing the patterned gold for the completed GoG slide. In order to create the EC cell, we customized PDMS reservoirs that were irreversibly plasma oxidized to the GoG slide after cleaning. Using a 3D printer (Makerbot Replicator 2), we created parts from 3D computer animated design (3D CAD) files that were designed in Sketchup (Trimble Navigation Limited). In **Figure 4.3** a 3D CAD scheme and printed mold are shown. With one mold, 36 individual electrochemical cells could be fabricated, and a single mold could be used multiple times.

4.3.4 Preparation of E-BSS Monolayer

Dithiol was reduced to a monothiol with TCEP at a 1:3, V: V ratio. Using 200 μM of thiolated DNA and10 mM TCEP which was placed in the dark for 1 hour. The solution was then diluted with HEPES buffer (pH 7.4) to form 1.25 μM for each individual thiolated DNA strand. Before plasma oxidation of the PDMS, the electrodes were cleaned with piranha solution (H_2SO_4:H_2O_2, 3:1, V: V), which is freshly prepared and placed on the surface of the electrode for

1 minute, then rinsed with deionized water. Once the PDMS is plasma oxidized and bonded to the GoG slide, 100 µL of the reduced solution (1.25 µM Thiol) was introduced into the electrochemical cell and placed in the dark for 1 hour. Following this step, the electrodes were introduced to 3 mM mercaptohexanol solution that incubated for 40 minutes, to assist with any non-specific binding. After rinsing, the buffer was added to these modified electrodes, and they were ready to use within 30 min. These electrodes were found to be stable for up to one week in 4 ℃.

4.3.5 Background measurements

With the total assay volume being 100 µL, MB-DNA was used at 150 nM, and Loop-DNA was set to 125 nM for DNA quantification. For RNA quantification, 250 nM miR_MB-DNA and 225 nM miR_Loop-DNA were used. Both MB-DNA and Loop were mixed and incubated for 30 min so that the complex could form (MB-DNA-Loop) prior to introducing it to the 4A_Thiol or miR_4AThiol strand for 30 min. Depending on the number of electrodes used for replicate measurements, in most cases triplicates or more ($n \geq 3$), the volume of mixed product MB-DNA-Loop complex was kept at a minimum. Once MB-DNA-Loop was added into the EC cell, it was incubated for 1 hour. To evaluate the background of the assay, i.e. the Signal-OFF state (**Figure 4.4**), measurements were taken via SWV at frequencies (f_{SWV}) of 40 Hz, 60 Hz, 80 Hz, 100 Hz, and 200 Hz. The temperature was held constant at 25 °C by the in-house built temperature controller.

4.3.6 Signal Measurements

After measuring the Signal-OFF complex, we added target strands at varying concentrations. The DNA concentrations used in this experiment were 0, 25, 50, 75, and 100 nM. miRNA-375 standards were tested at concentrations of 0, 25, 50, 100, 150, and 200 nM. Minute volumes could be used to add target strand, as low as 2 µL. Once the target was added into the complex, the solution was mixed and incubated for 1 hour at 25 °C in the dark. SWV pulse frequencies remained the same as listed above, and during experimental setup, the temperature was held at 25 °C using the temperature controller.

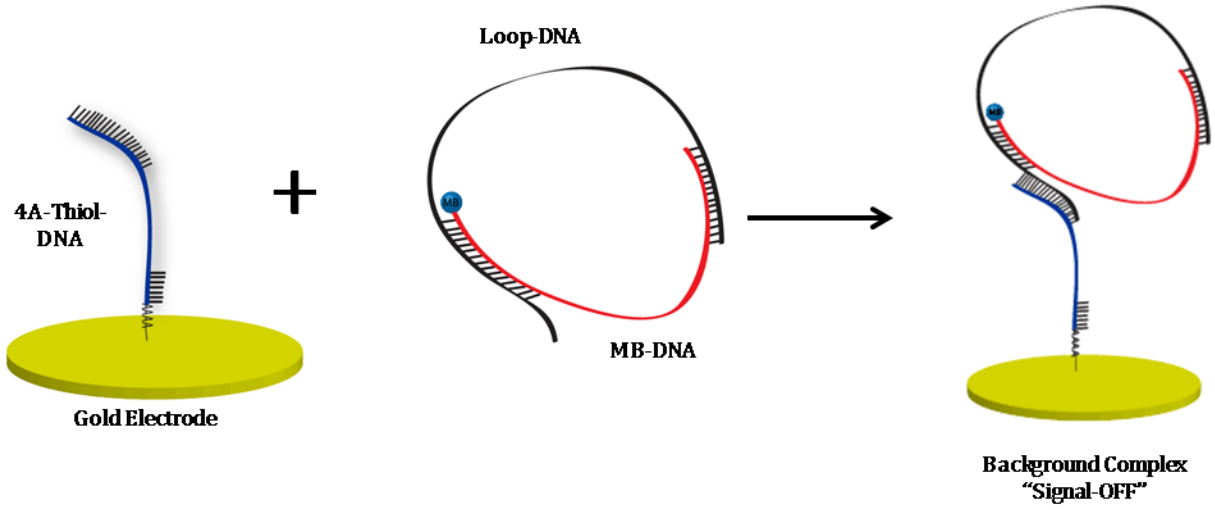

Figure 4.4: Schematic of the background complex or "Signal-OFF" with the bistable DNA switch based EC sensor.

4.4 Data Analysis

Peak Height Analysis

Raw data from SWV was exported to Microsoft Excel, using only the V_{step} and I_{diff}. The environmental noise was reduced using a 7-point moving average, followed by a linear fit

baseline correction (**Figure 4.5**). Five maximum current points were averaged from each SWV plot to give the overall peak height (I_P).

Signal Gain

The percent signal change was calculated according to the equation below, where i_{ON} is the peak height of the Signal-ON complex and i_{OFF} is the peak height of the Signal-OFF complex,

$$\text{Percentage Signal Change (\%)} = ((i_{ON} - i_{OFF})/i_{OFF}) \times 100 \quad \textbf{(1)}$$

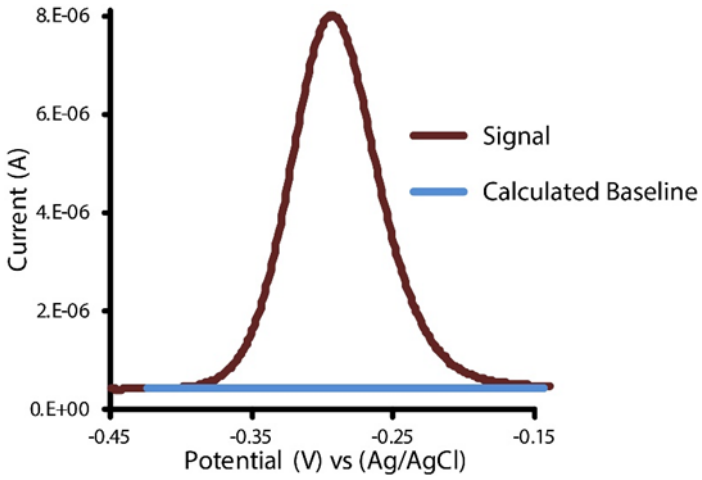

Figure 4.5: Linear baseline corrections versus raw data

4.5 Results and Discussion

Signal and Background in the bistable DNA switch

The principle of the bistable DNA switch sensor is depicted in **Figure 4.6**. In our system, we have created a bistable sensor, thus we have two available binding sites for the EC signaling strand, MB-DNA. In the absence of Target DNA, the MB-DNA portion will preferentially bind to the Loop strand, forming 13 base-pairs of hybridization (**Figure 4.6**, left), which represents background or the Signal-OFF state. In the presence of the Target DNA strand, the MB-DNA portion will be pushed away from the Loop strand by toehold-mediated strand displacement, and

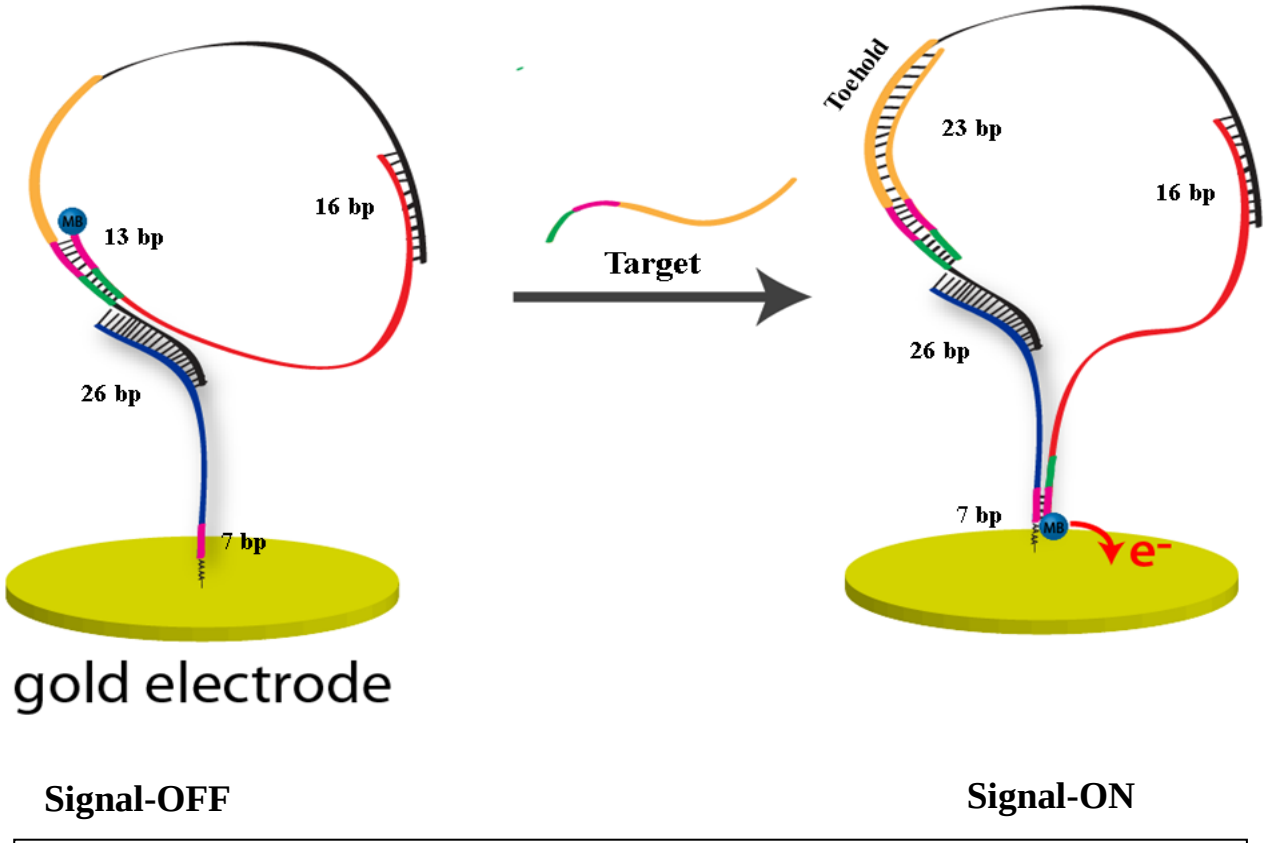

Figure 4.6: Schematic of Electrochemical Bi-Stable Switch (DNA). The multi-colored highlighted areas of the schematic represent the target binding sites. In Signal-OFF, the MB-DNA(red), which strongly (13bp) binds to the loop strand (black). The green and pink portions represent the partial complementarity binding between the target sequence and the MB-DNA sequence. In Signal-ON, the MB-DNA is forced to bind with the thiol-DNA strand (7bp) in pink. The location switch of the MB-DNA should then enhance electron transfer.

it will shift to bind to the 4A_Thiol strand, which is significantly closer to the electrode, representing the Signal-ON state of the sensor. Both locations for MB-DNA hybridization are stable in this hairpin format, but the 13-base complementarity to the Loop is stronger than the 7-base complementarity to the 4A_Thiol strand, which means that MB-DNA should prefer to bind in the loop—further from the electrode—in the absence of Target. The Target DNA, which is 23 nucleotides in length, contains a 10-nucleotide toehold that is complementary to the loop toehold section and partially complementarity to the portion hybridized with MB-DNA. Similar to allosteric catalyst design by Winfree (see **Figure 4.1**), once the Target is added, the competition between MB-DNA and Target for binding to the Loop strand allows MB-DNA to find the alternative conformation, i.e. bound to the 4A_Thiol near the gold electrode. If our DNA strand displacement and the bistable switch design concept is accurate, the system should function according to **Figure 4.6**.

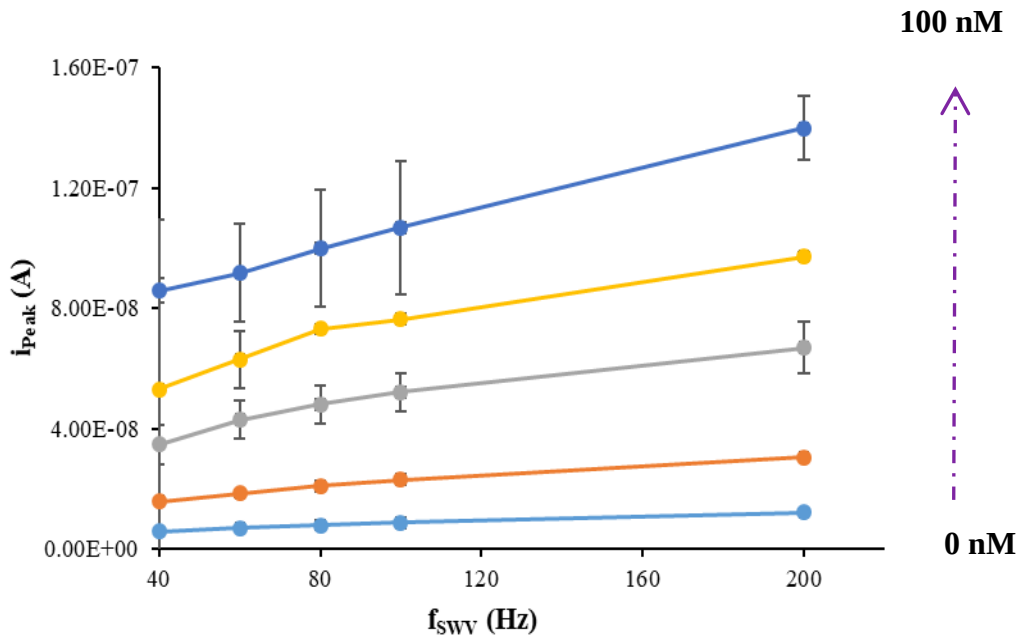

Figure 4.7: Sensors' response to various DNA target-bound concentrations (0 nM, 25 nM, 50 nM, 75 nM, 100 nM). Error bars represent the standard deviations of measurements taken from 3 independent electrodes.

Bistable Switch Assay Performance

As stated in chapter 3, SWV is one of the most commonly used electrochemical techniques for this class of biosensor, and the technique provides unique information related to the distance of the MB-DNA from the electrode. Our bistable switch sensor is therefore well suited for SWV readout. In the absence and presence of Target, we observed a well-defined MB redox peak around -0.24 V (vs Ag/AgCl) for our bistable switch sensor, consistent with the reduction potential of MB in this buffer (HEPES, pH 7.4). As

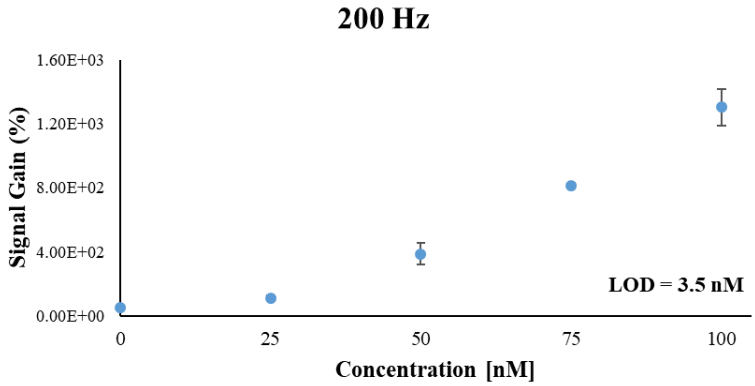

Figure 4.8: Percent Signal Gain of 200 Hz versus various concentration of DNA with a limit of detection of 3.5 nM.

predicted, by varying f_{SWV}, we found that our sensor exhibited the desired "signal on"-like behavior (increased current in proportion to target) particularly at higher frequencies (**Figure 4.7**). A large increase in MB current was observed in the presence of all Target concentrations tested, suggesting the formation of the presumed bi-stable Signal-ON complex. The Signal-ON (100 nM) state showed a ~14-fold increase in comparison to the target-free, Signal-OFF state. We have plotted the calibration curve at 200 Hz in **Figure 4.8**, showing signal gains of our sensor surpassing 10-fold (1000%). Interestingly, it appears that the sensor response changed from a square-root dependence on f_{SWV} at low [Target] to a more linear dependence on f_{SWV} at high [Target], which would be predicted from a shift in a position closer to the electrode in the Signal-ON state (**Figure 4.9**). This evidence strongly supports the intended mechanism underlying this new sensor architecture, which is based upon target-induced strand displacement of the bistable hairpin from one configuration to the other.

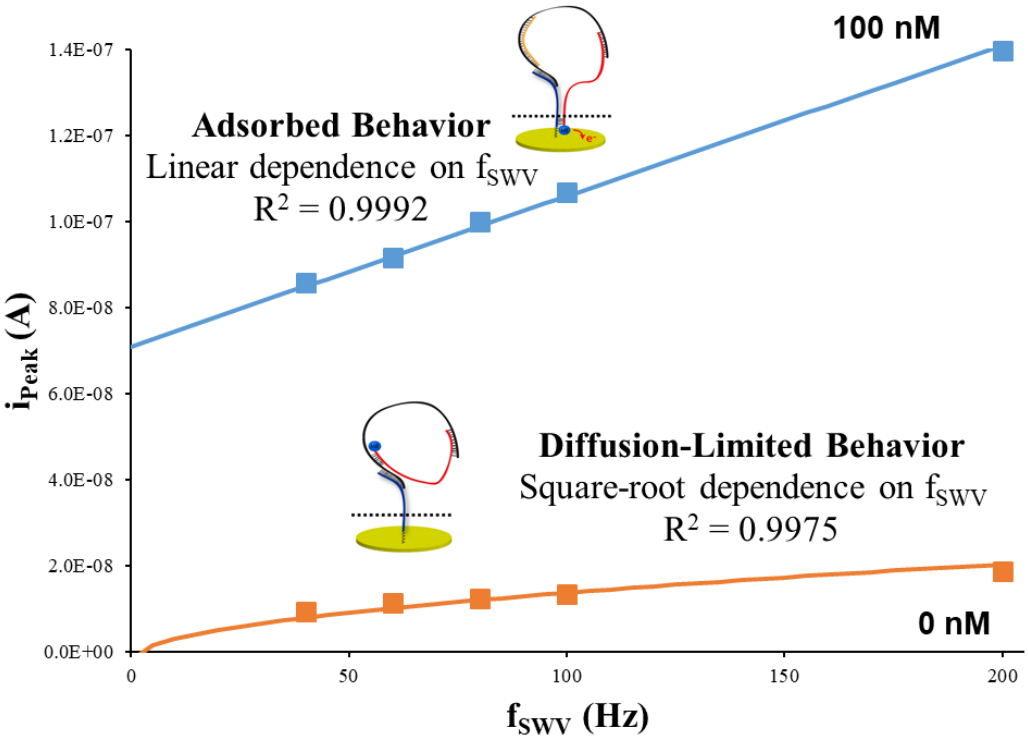

Figure 4.9: The sensor response changes from a square-root dependence on f_{SWV} at low concentrations of target to a more linear dependence on f_{SWV} at high concentrations of target

Signal and Background in the miRNA E-BSS

By applying this hairpin switch to bind and sense miRNA, we can create an amplification-free method, which is highly desired and more suitable for point-of-care measurements. Again, the target displaces the miR_MB-DNA to increase the faradaic current, by hybridizing to the complementary location inside the loop. The miRNA target of choice in this work was miR-375, considering it was highly expressed in pancreatic islets. MicroRNA-375 targets were tested from 0 nM to 200 nM using three different electrodes for each concentration. The percent signal gain of the miR-375 sensor displayed a LOD of 7.5 nM at 200 Hz (**Figure 4.10A**). We observed similar results in comparison to the DNA when looking at the adsorbed and diffusion limited behaviors (**Figure 4.11**). To evaluate the selectivity of the hybridization of

the toehold, we used a scrambled RNA sequence, which exhibited no signal gain. Since body fluids contain many species that could possibly interfere with sensitive miRNA detection, we also validated the assay in human serum. SWV scans at 200 Hz were obtained for 0 and 200 nM of miR-375 in 10-fold diluted serum, and whole human serum (H5 Obese BRH1315-216); the resultant data is shown in **Figure 4.10B**. The signal change increased with increasing miR-375 concentration, which suggests that the detection method is highly capable and promising toward detecting miRNAs in body fluids without target labels or prior amplification.

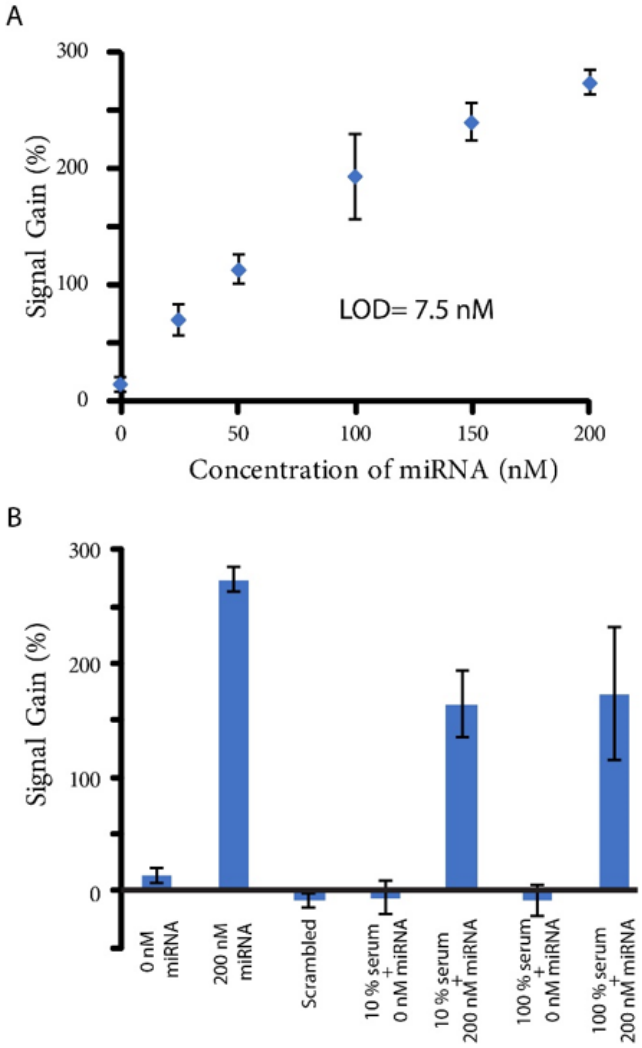

Figure 4.10. RNA-Based Bi-stable Switch. A) Percent signal gain of target bound concentrations (0-200 nM). B) Selectivity of E-BSS using human serum and scrambled RNA in comparison to 0 and 200 nM miRNA 375.

4.6 Conclusions

In this chapter, we have demonstrated a highly specific, amplification free electrochemical bistable switch sensor that can quantify small nucleic acids. The clear current difference of Signal-OFF versus Signal-ON was proven to be dependent on the distance of the MB placement from the electrode surface, which was investigated by our SWV studies with various modified thiolated DNA strands.

The target-responsive toehold mechanism utilized in the sensor was proven to follow a typical strand displacement mechanism in order to shift the MB-DNA to the electrode, and it was proven to be highly specific. This approach achieved a limit of detection of 3.5 nM for DNA and 7.5 nM for miRNA by SWV. The proposed assay obviates the need for amplification and labels for miRNA, ss-DNA, and removes any requirement for expensive enzymatic reagents, simplifying the overall process to a drop-and-read assay. Our results indicate that this electrochemical system has various advantages such as cost-effective preparation and fabrication, relatively fast operation, high selectivity, and good sensitivity. Overall, these results confirm that our new methodology should represent a useful candidate for detection and quantification of nucleic acids in biological and point-of-care applications.

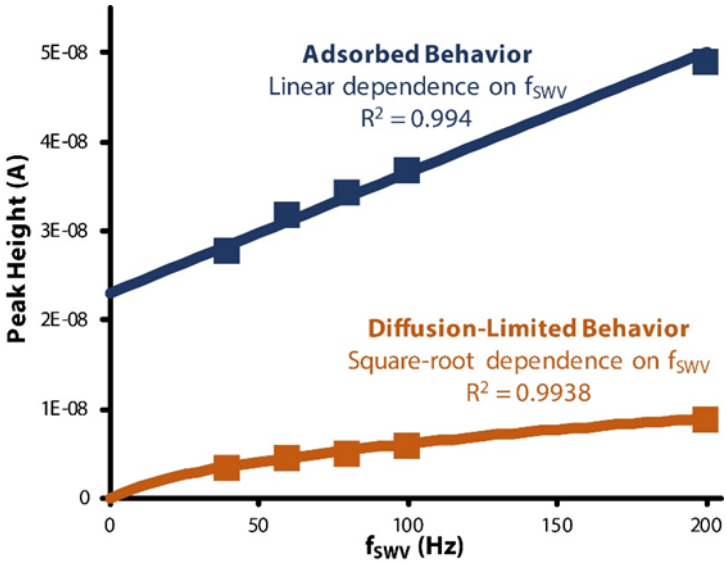

Figure 4.11. miRNA-375 sensor response: 0 nM shows a square-root dependence on f_{SWV} with the presences of no target, which exhibits diffusion limited behavior (R2=0.9938) 200 nM exhibits a linear dependence on f_{SWV} at high target concentrations, which have a more adsorbed-like

4.7 References

(1) Zhang, D. Y.; Winfree, E. *J. Am. Chem. Soc.* 2008, 130, 42, 13921-13926.

(2) Heller, M. J. *Annu. Rev. Biomed. Eng.* 2002, *4*, 129–153.

(3) McGlennen, R. C. *Clin. Chem.* 2001, *47* (3), 393–402.

(4) Broude, N. E. S. *Trends Biotechnol.* 2002, *20* (6), 249–256.

(5) Drummond, T. G.; Hill, M. G.; Barton, J. K. *Nat. Biotechnol.* 2003, *21* (10), 1192–1199.

(6) Lubin, A. A.; Plaxco, K. W. *Acc. Chem. Res.* 2010, *43* (4), 496–505.

(7) Xiao, Y.; Lai, R. Y.; Plaxco, K. W. *Nat. Protoc.* 2007, *2* (11), 2875–2880.

(8) Boon, E. M.; Ceres, D. M.; Drummond, T. G.; Hill, M. G.; Barton, J. K. Mutation D. *Nat. Biotechnol.* 2000, *18* (10), 1096–1100.

(9) Patolsky, F.; Lichtenstein, A.; Willner, I. *Nat. Biotechnol.* 2001, *19* (3), 253–257.

(10) Fan, C.; Plaxco, K. W.; Heeger, A. J. *Proc. Natl. Acad. Sci. U. S. A.* 2003, *100* (16), 9134–9137.

(11) Xiao, Y.; Lubin, A. A.; Baker, B. R.; Plaxco, K. W.; Heeger, A. *J. Proc Natl Acad Sci U S A.* 2006, 103(45): 16677–16680.

(12) Schoukroun-Barnes, L. R.; Macazo, F. C.; Gutierrez, B.; Lottermoser, J.; Liu, J.; White, R. J. *Annu. Rev. Anal. Chem* 2016, *9*, 163–181.

(13) Phares, N.; White, R. J.; Plaxco, K. W. *Anal. Chem.* 2009, *81* (3), 1095–1100.

(14) Steel, A. B.; Herne, T. M.; Tarlov, M. J.; H-j, A.; Biomol Struct, A. J. E. *Proc. Natl. Acad. Sci. U.S.A* 1997, *69* (3), 4670.

(15) Zhang, D. Y.; Turberfield, A. J.; Yurke, B.; Winfree, E. *Science* 2007, *318* (5853), 1121–1125.

(16) Ding, B.; Seeman, N. C. *Science (80-.).* 2006, *314* (5805).

(17) Seelig, G.; Yurke, B.; Winfree, E. J. Am. Chem. Soc. 2006, 128 (37), 12211–12220.

(18) Seelig, G.; Soloveichik, D.; Zhang, D. Y.; Winfree, E. *Science* 2006, *314* (5805), 1585–1588.

(19) Yurke, B.; Turberfield, A. J.; Mills, A. P.; Simmel, F. C.; Neumann, J. L. *Nature* 2000, *406* (6796), 605–608.

(20) Turberfield, A. J.; Mitchell, J. C.; Yurke, B.; Mills, A. P.; Blakey, M. I.; Simmel, F. C. D. *Phys. Rev. Lett.* 2003, *90* (11), 118102.

(21) Winfree, E.; Liu, F.; Wenzler, L. A.; Seeman, N. C. *Nature* 1998, *394* (6693), 539–544.

(22) Yin, P.; Choi, H. M. T.; Calvert, C. R.; Pierce, N. A. *Nature* 2008, *451* (7176), 318–322.

(23) Yan, H.; Zhang, X.; Shen, Z.; Seeman, N. C. *Nature* 2002, *415* (6867), 62–65.

(24) Rothemund, P. W. K. *Nature* 2006, *440* (7082), 297–302.

(25) Kilic, T.; Erdem, A.; Ozsoz, M.; Carrara, S. *Biosens. Bioelectron.* 2018, *99*, 525–546.

(26) Varkonyi-Gasic, E.; Wu, R.; Wood, M.; Walton, E. F.; Hellens, R. P. *Plant Methods* 2007, *3*, 12.

(27) Walker, M. D. R. *Diabetes*. *American Diabetes Association*, 2008, pp 2567–2568.

(28) Poy, M. N.; Hausser, J.; Trajkovski, M.; Braun, M.; Collins, S.; Rorsman, P.; Zavolan, M.; Stoffel, M. *Proc. Natl. Acad. Sci.* 2009, *106* (14), 5813–5818.

(29) Poy, M. N.; Eliasson, L.; Krutzfeldt, J.; Kuwajima, S.; Ma, X.; MacDonald, P. E.; Pfeffer,

S.; Tuschl, T.; Rajewsky, N.; Rorsman, P.; et al. *Nature* 2004, *432* (7014), 226–230.

(30) Cai, Z.; Song, Y.; Wu, Y.; Zhu, Z.; James Yang, C.; Chen, X. A. *Biosens. Bioelectron.* 2013, *41*, 783–788.

(31) Ge, S.; Liu, F.; Liu, W.; Yan, M.; Song, X.; Yu, J. *Chem. Commun.* 2014, *50* (4), 475–477.

(32) Zhang, K.; Dong, H.; Dai, W.; Meng, X.; Lu, H.; Wu, T.; Zhang, X. *Anal. Chem.* 2017, *89* (1), 648–655.

(33) Zadeh, J. N.; Steenberg, C. D.; Bois, J. S.; Wolfe, B. R.; Pierce, M. B.; Khan, A. R.; Dirks, R. M.; Pierce, N. A. *J. Comput. Chem.* 2011, *32* (1), 170–173.

Chapter 5

Modifications to the Electrochemical Proximity Assay

5.1 Introduction

In Chapter 1, I introduced various quantitative methods used to analyze proteins. Even with these developments, there remains a need for further improvements in cost, sensitivity, and improved workflow for point-of-care detection. One promising method is the use of electrochemistry-based sensors that utilize nucleic acids (NA) as recognition elements to enable the detection of a wide range of biologically relevant target analytes.[1] These sensors typically contain nucleic acids that are modified with one or more redox-active reporter molecules. Using this strategy, several reports demonstrate the detection of complementary DNA targets, single- and double-stranded DNA, proteins, and triplex-forming oligonucleotides. The use of specific, target-binding structures like aptamers enables an even broader range of target detection including proteins and small molecules.[1] In this chapter, the work will be focused on the development of electrochemical assays toward direct protein detection, although we will use DNA complementarity to study the assembly process. In this work, we have again taken advantage of important concepts such as the proximity effect to develop and modify electrochemical proximity assays (ECPA)[2] aimed at insulin and asprosin, protein hormones that are important indicators for diabetes, obesity, and metabolic syndrome.

Traditional ECPA is flexible in the sense that it can be extended to protein targets with two antibodies or aptamer pairs available. Figure: 5.1 shows a scheme of ECPA, where the target has two antibodies that bind different epitopes on the protein. The hybridization between MB-DNA and thiol-DNA, which was tested using 5, 7, and 10 base-pair connections, is stronger in the presence of the target, a result of the proximity effect.[2] In doing so, the EC signal is proportional to the concentration of the target protein. In our prior work, thrombin and insulin were successfully quantified with aptamer and antibody-oligo pairs respectively, with LODs of 50 pM for thrombin and 130 fM for insulin. This assay has taken a vital step toward developing point-of-care analysis systems with high sensitivity and selectivity. Even though ECPA has shown great promise, there a number of questions that remain concerning the fundamental signaling mechanism, in respect to frequency-dependence and distance-dependence while using square-wave voltammetry (SWV). In addition, the ideal generalizable protein assay, where no reagents must be added to the system, has yet to be developed.

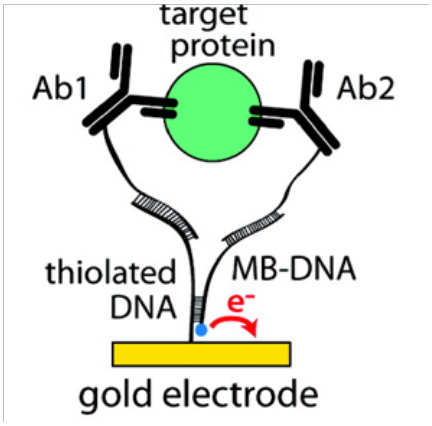

Figure 5.1: Scheme of ECPA in the presence of target, which has a 6-part structure.
Reprinted with permission from Copyright © (2012) American Chemical Society

Several improvements to ECPA have been made, such as the reusable version of ECPA developed by our group. [3] In recent reports by others, a ratiometric electrochemical proximity assay (REPA) was also developed using ferrocene-labeled DNA probe (Fc-P) and MB-labeled antibody-DNA (MB-DNA1-Ab1) on the same electrode. When they introduced another antibody-DNA conjugate, the proximity effect triggered protein binding so

that the MB was released from the electrode, and the Fc approached the surface due to the formation of a hairpin structure. This gave them a signal-OFF assay for MB and signal-ON type assay for Fc-P, in turn creating a dual-signal EC ratiometric readout (**Figure 5.2**).[4] This assay produced detection limits of 48 pg/mL for the PSA protein using alternative current voltammetry ACV, which is lower than other immunoassays using amplification techniques. [5,6]

While improvements have been made, it is important to test various configurations of a generalizable protein assay such as ECPA. In moving toward addition of fewer reagents, one option is to reduce the need for *labeled* reagents. In this chapter, we have developed a modified ECPA (mECPA) that senses the presence of the target-driven proximity complex without requiring separate addition of an MB-labeled DNA. By keeping the MB-labeled DNA anchored to the electrode surface, we hypothesized that the molecular weight of the proximity complex would significantly alter the SWV signal and provide a simpler protein assay workflow. Using our improved understanding of the distance and frequency dependences of SWV signal gained in prior chapters, this new assay format was explored in various ways.

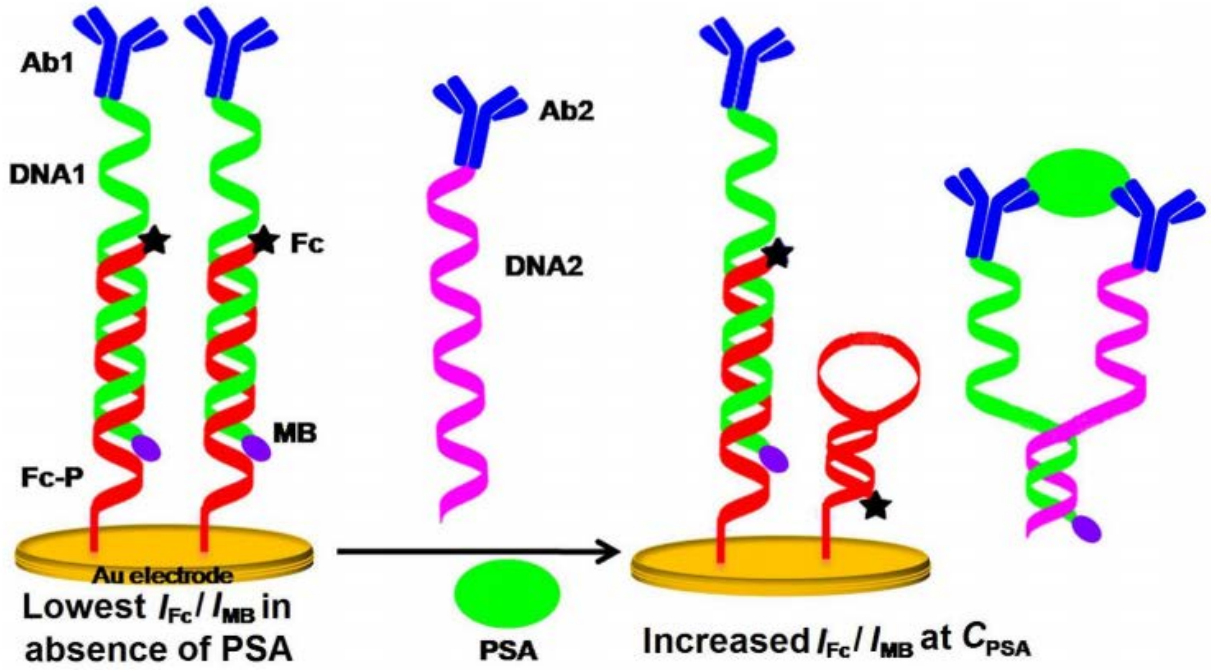

Figure 5.2 The RECPA assay used a Fc-P (red strand) modified gold electrode to hybridize MB-DNA1-Ab1 (green strand) for preparation of sensing interface. The PSA protein triggered the proximity effect of Ab1-PSA-Ab2, which led to the removal of MB-DNA1-Ab1 from the surface and the new formation of the hairpin structure with Fc-P. The assay was signal-OFF for MB and signal-ON for Fc for dual-signal electrochemical ratiometric readout.

5.2 Experimental Methods

5.2.1 Reagents and materials

All solutions were prepared with distilled water. Sodium chloride purchased from VWR, and dimethyl sulfoxide (DMSO) purchased from Anachemica. BioPerformance certified 4-(2-hydroxyethyl)-1-piperazineethanesulfonic acid (HEPES) tris (2-carboxyethyl) phosphine hydrochloride (TCEP), mercaptohexanol, gold etchant, and chromium etchant from Sigma-Aldrich. Gold-sputtered glass slides (100 nm Au with 5 nm Cr adhesion layer) were purchased from Deposition Research Lab (St. Charles, MO), with dimensions of 1.0 in. × 3.0 in. × 0.44 in. (width, length, thickness). AZ 40XT (positive photoresist) and AZ 300 MIF developer was obtained from MicroChem. Polydimethylsiloxane (PDMS) was purchased from Dow Corn-ing. Methylene blue-conjugated DNA (MB-DNA) and was purchased from Biosearch Technologies (Novato, CA), purified by RP-HPLC. Oligonucleotides were obtained from Integrated DNA Technologies (IDT; Coralville, Iowa), with purity and yield confirmed by mass spectrometry and HPLC, respectively. Ctrl_Loop sequence was PAGE purified due to the length of the oligonucleotide. Sequences (listed 5′ to 3′) for the Modified ECPA assay are listed in **Table 5.1**. LabVIEW system design software was used to operate our in-house built temperature controller.

Table 5.1	Modified ECPA
Thiol_MB1	Thiol-AAAACGTTAGG-MB
Thiol_MB2	MB-TTTCCTAAAAA-Thiol
Ctrl_Arm1	CCCACTTAAACCTCAATCCACGCGGATTTGAACCCTAACG
Ctrl_Arm2	TAGGAAAAGGAGGAGGGTGGCCCACTTAAACCTCAATCCA
Ctrl_Loop	TGAGGTTTAAGTGGGTACCTATTATCATTGTGAGCTGGATTGAGGTT TAA

Table 5.1 Oligonucleotide Sequences used in Modified ECPA

5.2.2 Preparation of Gold on Glass electrodes and EC Cells

The preparation of SAMs and EC cell preparation were consistent with that of chapter 4.

5.2.3 Preparation of mECPA Monolayer

Dithiol was reduced to a monothiol with TCEP at a 1:1, V: V ratio. 10 μM of thiolated DNA and 10 mM TCEP were mixed and placed in the dark for 1 hour. The solution was then diluted with HEPES buffer (pH 7.4) as needed, typically to 50 μM for both thiol_MB DNA strands. Before plasma bonding of the PDMS wells onto the glass slides, the electrodes were cleaned with piranha solution (H_2SO_4:H_2O_2, 3:1, V: V), which was freshly prepared and placed on the surface of the electrode for 1 minute, then rinsed with deionized water. Once the PDMS was plasma oxidized and bonded to the GoG slide, 100 μL of the reduced thiolated DNA solution was introduced into the electrochemical cell and placed in the dark for 1 hour.

Following this, the electrodes were covered with 3 mM mercaptohexanol solution that was incubated for 40 minutes, to prevent non-specific binding. After rinsing, buffer was added to these modified electrodes, and they were ready to use within in 30 minutes.

5.2.4 Baseline Measurements

To evaluate the baseline of the assay, i.e. the Signal-ON state (**Figure 5.3**), measurements were taken after 1 hour of incubation in HEPES buffer (only) with SWV at frequencies (f_{SWV}) of 4, 6, 8, 10, 15, 20, 30, 40, 50, 70, 100, 150, 200, 250, 400, 500, 650, and 900 Hz. The temperature was held constant at 25 °C by the in-house built temperature controller.

5.2.5 Signal Measurements

To evaluate background currents using DNA arms and the loop model (**Figure 5.3**) an addition of various concentrations of Ctrl_Arm1 and Ctrl_Arm2 were added to the SAM of an electrode and incubated for 2 hours, and various concentrations of Ctrl_Arm1, Ctrl_Loop, and Ctrl_Arm2 were added to the SAM of another electrode and incubated for 2 hours. Measurements were taken via SWV at the frequencies listed above. The temperature was held constant at 25 °C by the in-house built temperature controller.

5.3 Results and Discussion

Baseline, Background, and Target signals with mECPA

The principle of the mECPA is depicted in **figure 5.3**. In this modified system, we have created a “Signal-OFF” based assay, where target introduction is intended to reduce the signal specifically. The *baseline* measurement was defined by two independent 11-nucleotide probe

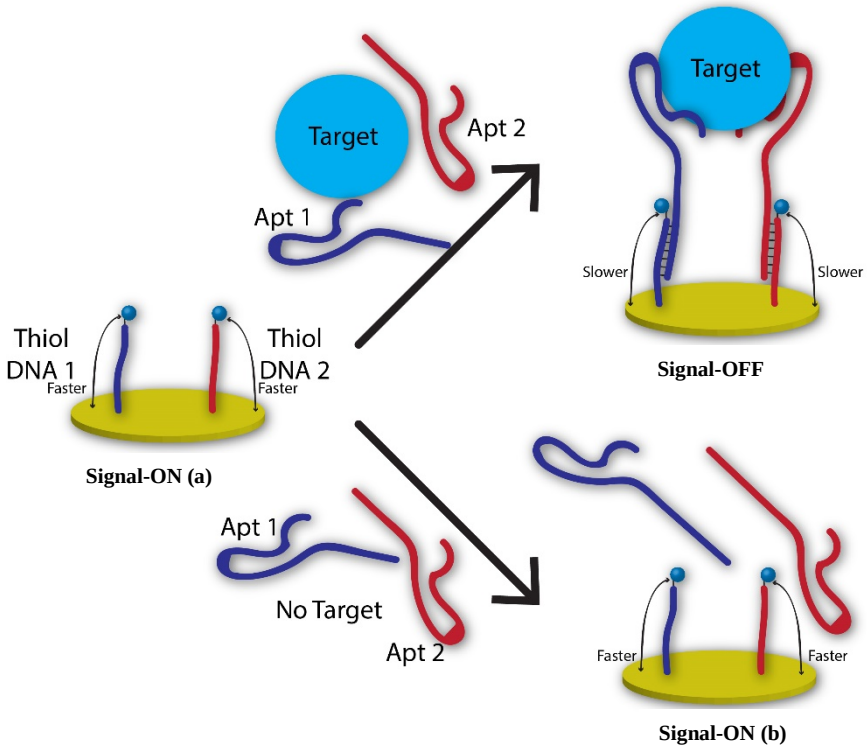

Figure 5.3 Scheme of Modified ECPA. Where Signal-OFF (a/b) give rapid electron transfer and higher current. With the addition of aptamers or antibodies in the presence of a target protein, the Signal-ON complex will give a slower electron transfer due to molecular weight, and a lower output signal.

sequences bound to the surface by a thiol group and an MB redox tag [Signal-ON (a)]. These independent probes were tested using various concentrations, with the optimal target response found at 50 nM. The electron transfer rate of the baseline measurement was expected to be most rapid considering the ssDNA probes were fairly flexible and close to the surface with little hindrance.

The second important measurement in this system was the *background*. An important goal in this work was to reduce the background to reach almost zero, in order to have a more sensitive assay for protein quantification. The *background* [Signal-ON (b)] was measured with the aptamers or antibody-oligos present without the target molecule. Ctrl_Arm1 and Ctrl_Arm2 were designed to hybridize to Thiol_MB 1 and Thiol_MB 2 with only 7 base pairs, to limit background formation as in our prior ECPA work [2]. We hypothesized that this would result in minimal or very weak binding to the electrode surface, where the arm sequences would remain in

bulk solution rather than hybridizing with the surface structure. If confirmed, neither the electron transfer rate nor the current output would be changed.

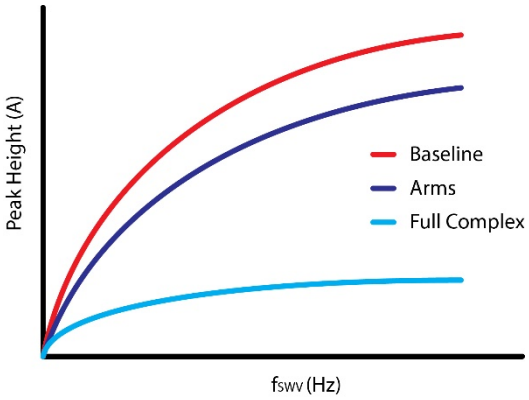

Figure 5.4 Hypothesis of mECPA. Baseline should have the highest overall current with all frequencies, and Arms would minimally decrease, whereas the full complex (Target) would drastically decrease due to the proximity effect.

The last important measurement in mECPA was the *Target*. Theoretically, the target of should be quantifiable or its presence detected due to the proximity effect [Signal-OFF], which would significantly stabilize the 7-base pair arms to bind to the MB-labeled surface DNA. As a model of the proximity complex during optimization (to save expensive reagents), we used a 50-nucleotide oligo that could hybridize to both Ctrl_Arm1 and Ctrl_Arm2 with 15 bp on each side. In turn, the electron transfer rate of MB-DNA should measurably decrease (by SWV) due to the increase in molecular weight and/or steric hindrances. The SWV current should also decrease versus frequency in a manner associated with the amount of target protein added, making this a Signal-OFF assay. A depiction of our hypothesized assay response is given in **figure 5.4**.

Background versus Target signals with mECPA

The calculated hybridization energies (using NUPACK) of 7 base pairs without the presence of target were ΔG = -15.26 kcal/mol for Thiol_MB1 with Ctrl_Arm1 and ΔG = -14.43 kcal/mol for Thiol_MB2 with Ctrl_Arm2 (1:1 ratios). This binding is relatively weak in comparison to the Arms and the loop, where ΔG = -50 kcal/mol (1:1). However, these

calculations assume free-solution interactions, while our system was defined by surface-bound MB-DNA sequences that bound to free-solution arm sequences. Instead of developing a surface binding energy model, we conducted experiments to attempt to empirically optimize the background (as in our prior work). Interestingly, experiments showed background [Signal-ON (b)] at 50 nM arms with the 50 nM probe (Thiol_MBs) to give a large decrease in current with respect to the frequency, as well as a shift in the characteristic reaction time in comparison to the baseline of the same electrode. Once the target (50 nM) was added into the complex, the signal was almost the same as the arms, meaning there was no decrease in current for the addition of the target (**Figure 5.5**). With further optimization, we noticed by adding the Ctrl_Arms in excess (1 µM) to the probe (50 nM) and target (50 nM), although arms are still binding, there was a noticeable decrease when the Ctrl_Loop was added, in comparison to its baseline (**Figure 5.6**). The overall current did not change as much as expected for target, but we did observe a 47% signal suppression at f_{SWV} = 900 Hz once the target was added, while addition of arms showed only a 35% drop at the same frequency, in comparison to its baseline shown in **Figure 5.6**. Lastly, further confirmation was provided using the characteristic electrochemical reaction time, suggesting that the structural changes happening on the surface were proportional to the electron transfer rate as hypothesized (**Figure 5.7**)

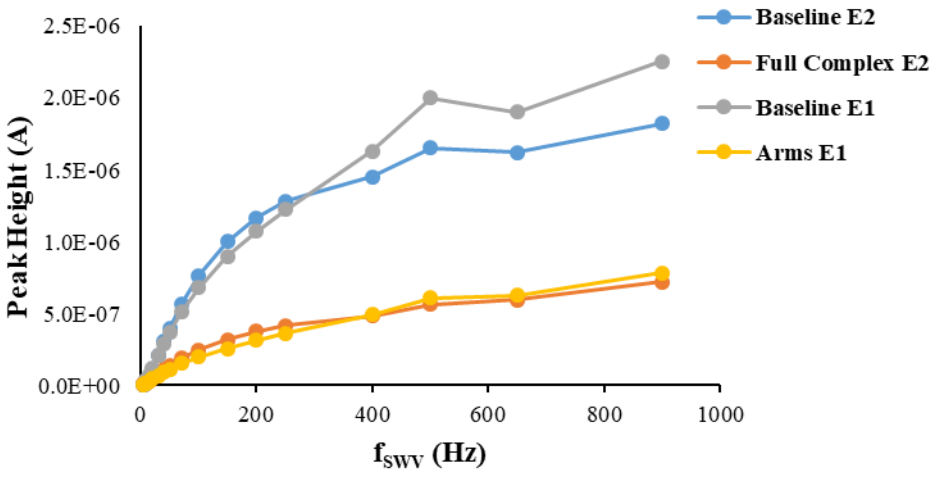

Figure 5.5 1:1:1 distribution of Probe/Arm/Target, there is a drastic decrease in the Arm current v hybridiz without

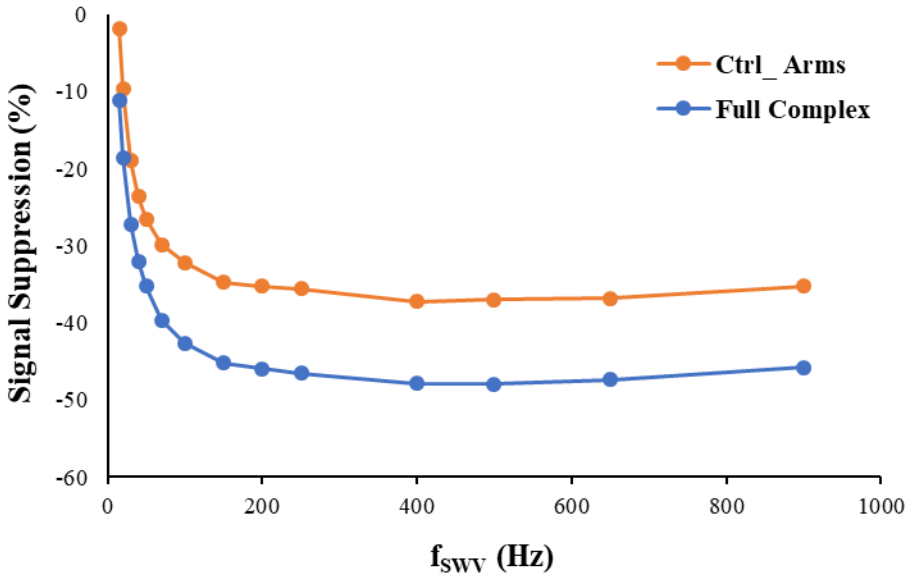

Figure 5.6 Signal Suppression of the Ctrl_Arms and the Full Complex in comparison to their individual baselines.

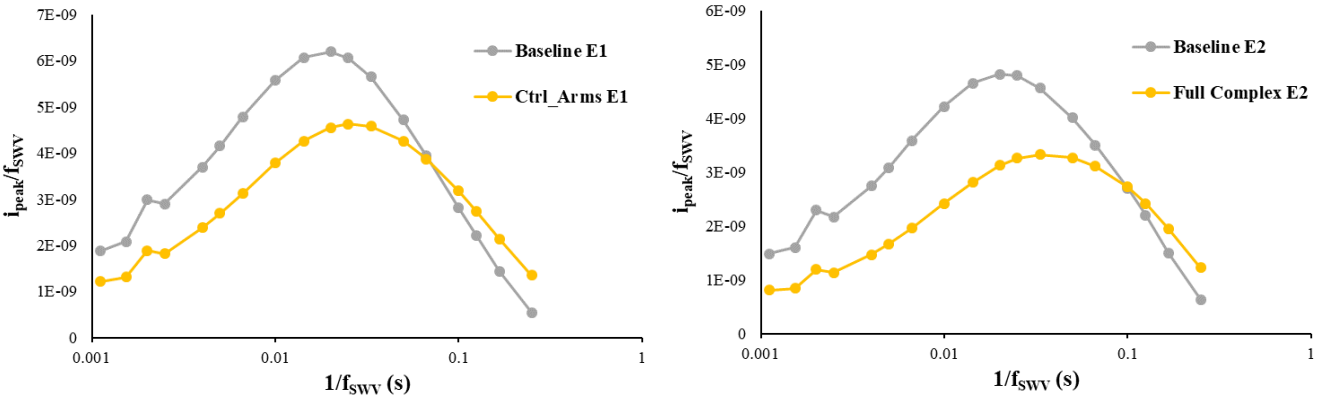

Figure 5.7 Electrochemical characteristic reaction time (ECRT). Both baselines (Grey) have an ECRT of 0.02 seconds. Ctrl_Arms have an ECRT of 0.025s and Full complex 0.033s. The shifts indicated the rate at which the electrons transfer which is proportional to the structural makeup.

5.4 Conclusions

Traditional ECPA, which has potential to be a generalizable point-of-care method, still falls short of the desired workflow and cost due to the need to add expensive reagents into the solution of the electrochemical cell. In this chapter, the initial development of mECPA was presented. This format of the assay has several potential advantages, such as simplified workflow and less expensive reagents. Although quantitative protein detection has not yet been achieved, we have validated the proof-of-concept of mECPA through a target-dependent signal suppression and a decrease in characteristic electrochemical reaction rate upon target binding. With further optimization, mECPA should serve as a simplified alternative to ECPA and provide an important step forward toward generalizable, point-of-care protein quantification.

5.5 References

(1) Schoukroun-Barnes, L. R.; Macazo, F. C.; Gutierrez, B.; Lottermoser, J.; Liu, J.; White, R. J. *Annu. Rev. Anal. Chem* 2016, *9*, 163–181.

(2) Hu, J.; Wang, T.; Kim, J.; Shannon, C.; Easley, C. J. *J. Am. Chem. Soc.* 2012, *134* (16), 7066–7072.

(3) Hu, J.; Yu, Y.; Brooks, J. C.; Godwin, L. A.; Somasundaram, S.; Torabinejad, F.; Kim, J.; Shannon, C.; Easley, C. J. *J. Am. Chem. Soc.* 2014, *136* (23), 8467–8474.

(4) Ren, K.; Wu, J.; Yan, F.; Ju, H.; Zong, C.; Wu, J.; Wang, C.; Ju, H. X.; Yan, F.; Rusling, J. F.; et al. *Sci. Rep.* 2014, *4*, 2410–2415.

(5) Zani, A.; Laschi, S.; Mascini , M.; Marrazza, G. *Electroanalysis* 2011, *23* (1), 91–99.

(6) Yu, X.; Munge, B.; Patel, V.; Jensen, G.; Bhirde, A.; Gong, J. D.; Kim, S. N.; Gillespie, J.; Gutkind, J. S.; Papadimitrakopoulos, F.; et al.. *J. Am. Chem. Soc.* 2006, *128* (34), 11199–11205.

Chapter 6

Conclusions and Future Directions

6.1 Conclusions

The research presented in this dissertation was aimed at developing nucleic acid based, proximity dependent DNA, RNA, and protein assays using electrochemical detection (SWV). Major benefits of these assays are sensitivity, selectivity, and small volume compatibility. For the proximity ligation assay presented in Chapter 2, we set out to quantify adiponectin multimers in small volumes to assist diabetes and obesity research without sacrificing low detection limits. qPCR showed a significant shift in $C_{(t)}$ values that were linear with adiponectin concentration, yet the values changed in the reverse direction compared to our expectations. Since the adiponectin hormone forms various multimer complexes in serum (approximate MW of 30 kDa per monomer), we hypothesized that the DNA tails were insufficiently long to allow hybridization with the connectors, and it is feasible that the single binding sites on each monomer were far enough apart to exclude connector formation and subsequent ligation. For the SWV distance dependence study, we took a closer look at the electrochemical characteristic reaction times and observed slower reaction times as we increased the poly adenines spacers from 0A to 19A, which in turn helped us select the conditions needed for the bistable switch sensor in Chapter 4. Within Chapter 4, we developed the bistable nucleic acid switch that exhibited limits of detection of 3.5 nM for Target DNA and 7.5 nM for miRNA.

The obvious response of the sensor toward NAs, along with its increasingly linear dependence on f_{SWV} at higher target concentrations, and square root dependence without the presence of target, all suggest that the sensor is behaving as predicted. Due to its simplified workflow, this method can potentially be employed for cost-effective, on-site analysis of DNA/RNA in a wide range of samples in the future. Lastly, mECPA was validated as a proof-of-concept in Chapter 5 in hopes of finding a more sensible and readily available point-of-care system. This assay shows promise of quantification and structural conformation changes on the surface, but further optimization and studies of this assay are required.

6.2 Future directions

6.2.1 Reusable electrochemical bistable switch sensor

With an improved understanding of the bistable assay, one could advance the workability of the system to be more cost-effective. Making this loop structure all one strand by bridging the DNA with T4 ligase, the cost should decrease, and limits of detection should improve, giving a more sensitive DNA/miRNA assay. Also in making the assay one independent strand, we could reuse the electrode and the highly concentrated thiol bound to the surface just by adding a denaturing solution between runs. This method would be more cost effective on the reproduction of electrodes and save time with cleaning and fabrication.

6.2.2 Modified ECPA

In chapter 5, we showed that the mEPCA design can undergo structural changes on the surface upon target binding. In future work, this assay should be fully optimized to satisfy key electrochemical factors, such as surface density, temperature, time (diffusion layer), stoichiometry, salt concentration (double layer), and hybridization. Once these optimization

studies are successfully completed, mECPA could feasibly be used with any aptamer or antibody pair readily available, providing a more simplified, generalizable protein detection technique.